THE UNIVERSITY OF HULL

ELECTRO-CATALYTIC REACTIONS

Being a Thesis submitted for the Degree of

Doctor of Philosophy

THE UNIVERSITY OF HULL

by

Carlos Lledo-Fernandez

(June 2009)

Declaration

The work described in this thesis was carried out in the Department of Chemistry, University of Hull under the supervision of Professor G.M. Greenway and Dr. J. Wadhawan between October 2004 and September 2008. Except where indicated by references, the work is original and has not been submitted for any other degree.

Carlos Lledo-Fernandez

June 2009

Table of Contents

ACKNOWLEDGEMENTS

I would like to express my gratitude to my supervisors Prof. Gillian Greenway and Dr. Jay Wadhawan for their continuous guidance and supervision throughout this project. I would like to thank them for their helpful suggestions and useful discussions that enabled me to complete my work successfully, and which made me enjoy my project.

Special thanks to my fellow electrochemists Evangelia Christoforou and Imrem Hatay with whom I worked. I also like to thank Dr Charlotte Wiles and Dr Gary Nicholson for their helpful suggestions. Thanks also to Ryan Mewis and Graham MacRobie for their helpful and funny comments during the big hunt for cyclohexene. I thank Por for her help and friendship. Dr Anthony Walmsley and Dr Tom Mc Creedy were particularly helpful, providing me with useful pointers during my first and second year.
Finally I would like to thank Steve Clark for the microfabrication of the microfluidic devices and Tony Sinclair for his help with SEM.

I wish to express my thanks to the University of Hull for their funding, the technical staff and the Analytical group, past and present, for their help and their group meetings.
A special mention must go to all members of staff of the GRI (K. Atkinson, S.Locke, R. Thompson, and L. Thomas) for their help and their smiles.

I would like to thank my Professor from Almeria, Antonio Manuel Romerosa Nievas for his encouragement when I finished my degree and for his continued interest in my career.

I would like to thank my special friend Pablo Jessop for his talks and for his strength to see the future more clearly.

I would also like to thank my whole family: Dad, Mum, Ione and Iris for their continued support, love, care, and the good times we have shared…(I will stop otherwise I will write another thesis mentioning their good qualities). Especially for my Dad, whose English is not very strong, as I know that he will read the whole thesis. A special mention of course for my grand parents Manolo and Poli for their love. An important

mention for those no longer with us - but I believe that they will be excited for me - my Granddad, Vicente, Grandma, Emilia and my Uncle Juan Antonio.

I would like to thank Robert and Dorothy Beddoes for their support, smile, interest in my career and the amazing trip to Wales in a difficult moment for me.

Finally, I would like to acknowledge my special *peque*, Susie, for her love, taking care of me, her smile, believing in me and for listening to me talking about Chemistry (when she is a teacher of *Languages!*).

I dedicate this thesis to all of the above - without whom I would have never completed this work.

ABSTRACT

This thesis discusses and demonstrates the utility and advantages of redox catalytic reactions and small scale synthetic applications. In particular electro-catalytic reactions are investigated along with electrogenerated chemiluminescence (ECL). ECL is used both as a probe for investigating the redox reactions and as an analytical method. The first chapter reviews the current techniques and achievements found in the area of dynamic electrochemistry and electrogenerated chemiluminescence and discusses occurrence, mechanism and potentially useful reactions worthy of further investigation for analytical applications.

In Chapter 3 the electrocatalytic ECL reaction of $Ru(bpy)_3^{2+}$ with tertiary amines in particular with codeine as a model compound was investigated. The aim of the work was to develop a portable drug testing device, that gave good sensitivity and reproducibility. The $Ru(bpy)_3^{2+}$ was immobilized within the sol-gel matrix to develop a sensor which could be used directly for measuring tertiary amine containing drugs in buffer solution without the need to add reagents. A system of three electrodes was used in which $Ru(bpy)_3^{2+}$was immobilised on to a glassy carbon working electrode. Initial work involved physical entrapment of the $Ru(bpy)_3^{2+}$ within the sol-gel matrix however, problems occurred with leaching of the reagent from this matrix. This problem was overcome by the covalent attachment of a novel $Ru(bpy)_3^{2+}$ derivative to the sol-gel matrix. Using this approach a calibration was obtained using ECL for the determination of codeine over the range 1 $x10^{-3}$ to 1 $x10^{-7}$ M in aqueous buffer with a limit of detection of 2.65 x 10^{-6} M for codeine. Covalent attachment, as compared to the physical entrapment of CL reagent, was advantageous as it ensured homogeneous distribution of the reagent within the matrix and prevented leaching. This reduced analysis costs, extended sensor lifetime and gave a reproducible analyte responses. This method was, however, only suitable for drugs that were soluble in aqueous solution and an alternative approach was needed for insoluble compounds.

Chapter 4 describes an alternative approach for ECL reaction of tris(2,2'-bipyridyl)ruthenium(II) with tertiary amine compounds. In this approach the electrode was modified using microdroplets of a highly hydrophobic tertiary amine (trioctyamine). As well as allowing for the analysis of compounds that were insoluble in

aqueous solution, this setup allowed the investigation of the electron transfer reaction occurring on liquid|liquid interfaces. This mechanism was studied in fully protonated and deprotonated conditions. The extent of the electrochemiluminescence production was shown to be dependent on the degree of the interfacial protonation. Moreover, the data obtained enabled the estimation of the biphasic pKa, which was found to be approximately 10.8. Furthermore, the mechanism was studied in fully deuterated and dedeuterated conditions, in order to investigate the effect of the deuterium on the biphasic pKa. Results suggest that the pKa increases to 13.18 when deuterium is used instead of protons.

In Chapter 5 a further electrocatalytic reaction was investigated. The reaction was that of vitamin B_{12a} with *trans* 1,2-dibromocyclohexane (DBCH) in a homogeneous dimethylformamide media. The reaction was studied by cyclic voltammetry. Four peaks were seen due to the two chemically reversible redox (two electron process) couples for vitamin B_{12a}/B_{12r} (Co(III)/CO(II)L) and B_{12r}/B_{12s} (Co(II)L/Co(I)). When the bulk electrocatalytic reaction was tried in a "one pot" system, the reduction could not, however, be achieved; the cathodically synthesised Co(I)L was thought to be reoxidised at the anode. A "two pot" system did not have sufficient potential control and, therefore, chemical reduction was investigated instead.

Four reducing agents (Na/amalgam, $NaBH_4$/NaOH, DL-cysteine/alkali solution and Zn dust/NH_4CL) were studied to reduce B_{12} to B_{12s} for a simple biphasic batch reaction of vitamin B_{12s} with DBCH. The mild reducing agent Na/amalgam was not successful but the other three methods were shown to give 100% yield if the reaction vials were rigorously shaken. This simple type of green, surfactant free reaction has not been previously reported.

The reaction was then investigated in a microfluidic system. For this work the vitamin B_{12} was reduced before being introduced into the microfluidic device. $NaBH_4$/NaOH and DL-cysteine/alkali solution were selected as the most compatible reducing agents for the microfluidic device. Two types of microfluidic device were employed, one with a T-shape channel, and one with a serpentine channel. The conversions obtained with the microfluidic device were much lower (approximately 10%) than for the simple batch reactions (100%). The yield increased as the flow rate decreased, and the residence time increased. Using the serpentine channel made no noticeable difference to the conversion

rate. Problems were also seen due to the use of excess reducing agent prior to introduction of the reduced vitamin B_{12} into the microfluidic device, as this could cause blockages and bubbles. The main problem was, however, the lack of mixing in the device. One way to overcome this would be to use an ultrasonic transducer with the microfluidic device but although preliminary experiments were carried out, there was not time to fully investigate this approach.

Chapter 1

Introduction

1. 0 Aims of Thesis

The aim of this thesis is to study a series of redox catalytic reactions for analytical and synthetic applications, in particular, the amount of electrogenerated chemiluminescence (ECL) produced via reaction of tris(2,2'-bipyridyl)ruthenium(II) with tertiary amine compounds. This is used both for the detection of tertiary amine analytes as well as to study biphasic electron transfer (ET).

The objectives of the work are as follows:-

1 To utilise sol-gel modified glassy carbon electrodes to develop a portable analytical system, using ECL for the analysis of drugs such as codeine.

2 To use microdroplet modified electrodes with the ECL reaction of tris(2,2'-bipyridyl)ruthenium(II) with the trioctylamine, to study biphasic electron transfer reactions.

3 To study the redox catalytic reaction of vitamin B_{12} trans-1,2-dibromocyclohexane for the synthesis of cyclohexene and investigate the reaction in a microfluidic system.

The remainder of this chapter seeks to detail the basic electrochemical principles underpinning subsequent chapters.

1.1 Dynamic Electrochemistry

1.1.1 Introduction

Dynamic electrochemistry is the study of electron transfer reactions between electrodes (typically, but not always, metallic) and reactant molecules, the latter usually in a located solution phase.

If a general aqueous, heterogeneous electron transfer reactions is considered:

$$O_{(aq)} + ne^- \underset{k_a}{\overset{k_c}{\rightleftharpoons}} R_{(aq)}$$

Equation 1.1

Where O symbolizes the oxidised species, R represents the reduced species, n is the number of electrons transferred, and k_c and k_a are the reduction and oxidation rate constants, respectively. If k_c and k_a are so fast that the electrolysis is effectively an equilibrium, the concentration of O and R at the electrode surface can be given by the Nernst equation:

$$\frac{[O]_{Surface}}{[R]_{Surface}} = exp\left[\frac{nF}{RT}\left(E - E^0\right)\right]$$

Equation 1.2

where, E^0 is the formal electrode potential when all species have unit concentration, this relates to the standard electrode potential via inclusion of activity coefficient effects.
R is the molar gas constant (8.314 J mol $^{-1}$ K $^{-1}$), T is the absolute temperature (K), n is the number of electrons participating in the reaction per mole of analyte, F is Faraday's constant (96485 C mol^{-1}).

1.1.2 The Interfacial Region and Electrolyte Double Layer

The *interfacial region* is the region between the electrode and solution, where electrode reactions actually occur and where the greatest potential differences across the electrical circuit appear. In dynamic electrochemical experiments, a potential difference is applied between an electrode and a solution containing an electrolyte. The applied potential leads to breakdown in electrochemistry of the solution close to the electrode surface. Stern proposed a model for this region consisting of a Helmholtz double layer in series with a Guay-Clapman diffuse layer (see Figure 1.1). In the double layer, solvated ion arrange themselves along the electrode surface forming a sheet of ionic charge called the Outer Helmholtz Plane (OHP) which is ~ 1nm from the electrode surface. The ions can also discard their solvation shell and adsorb onto the electrode surface forming an

Inner Outer Helmholtz Plane (IHP). The disordering effect of thermal motion is taken into account in the diffuse layer where an ionic atmosphere, similar to that described in the Debye-Huckel theory, is present. The potential drop is shoved across the whole region. Electron transfer occurs via tunnelling over distances no greater than the OHP. Therefore, it is the potential drop across the double layer which influences the redox process.

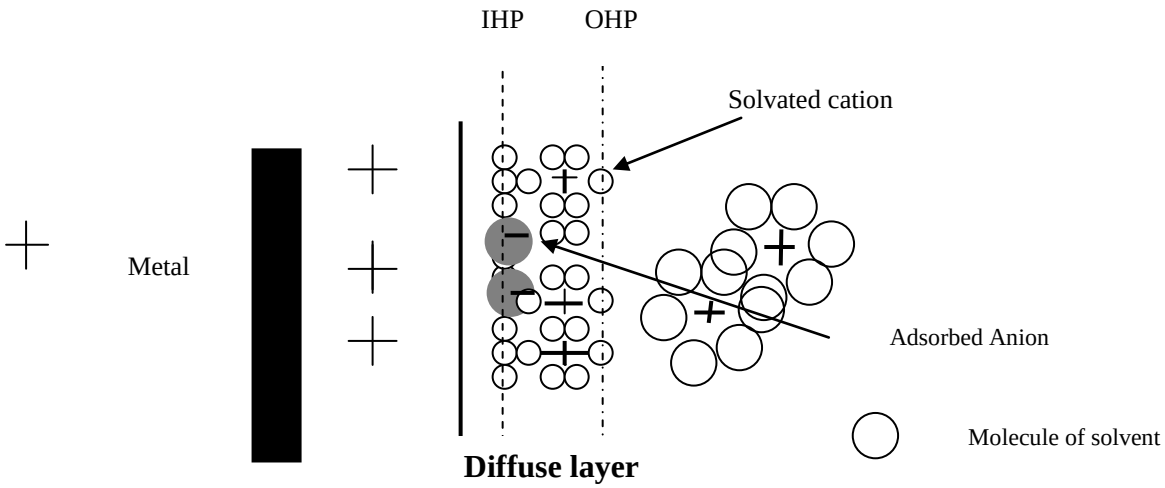

Figure 1.1: The electrical double layer.

1.2 Electrochemical Cells and Reactions

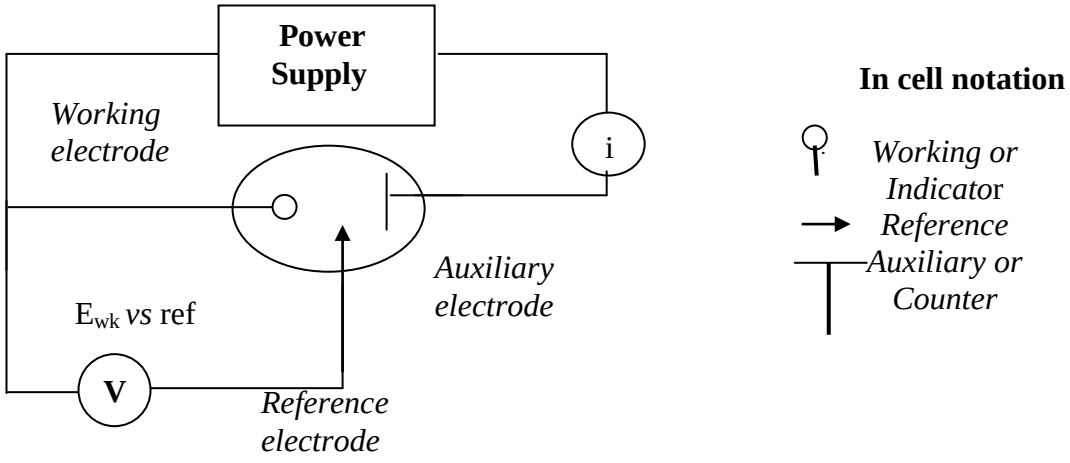

Figure 1.2: Three electrode cell and notation for the different electrodes.

Electrochemical cells can be formed by two or three electrode systems. The two electrode system is the simplest approach to the study of current/voltage characteristics. In the experiments where the iR may be high (*e.g.*, in large-scale electrolytic, galvanic cells or in experiments involving non-aqueous solutions with low conductivities), a three electrode cell is often preferable. In this arrangement, the current is passed between the working electrode (where the reaction takes place) and counter electrode (or auxiliary). The auxiliary electrode can be one of convenience since its electro-chemical properties do not affect the behaviour of the electrode of interest. It is usually chosen to be an electrode that does not produce substances by electrolysis that will reach the working electrode surface and cause interference with the reaction of interest [1].

A net charge separation can be developed between the electrode and the solution, which creates a potential difference at the electrode/surface, $\Delta\phi_{m/s}$ interface given by:

$$\Delta\phi_{m/s} = \phi_m - \phi_s$$

Equation 1.3

where, ϕ_m is the electrical potential at the electrode, ϕ_s is the electrical potential of the solution.

The introduction of a second electrode (reference electrode) and a complete electrical circuit are required to measure the potential difference. As the potential drop at the electrode/solution interface and the voltage remains constant in this electrode,

E (is the difference potential between the working electrode and the reference electrode) Equation 1.3 can be rewritten as:

$$E = \left(\phi_m^{\ test} - \phi_{solution}\right) - \left(\phi_m^{\ ref} - \phi_{solution}\right) = \phi_m^{test} - \phi_m^{ref}$$

Equation 1.4

A potential is applied to the working electrode E_e as it was previously defined by the Nernst equation (Equation 1.2) in order to provoke a current flow into the electrochemical cell. The difference between the applied potential E and the formal electrode potential, E, is termed the operpotential.

$$\eta = E - E^0$$

Equation 1.5

where η is defined as overpotential. The current flowing, (i), is given by:

$$i = \oint nFjdA$$

Equation 1.6

where, n is the number of electrons transferred per mole of reactants. F is Faraday's Constant (96485 C mol^{-1}), A is the electrode area and j is the flux of electroactive species reaching the electrode surface in moles cm^{-2} s^{-1}.

For kinetic limited processes:

$$j = k_o[O]_{surface}$$

Equation 1.7

where, k_0 is the heterogeneous rate constant of the electron transfer reaction. The flux j is a very important factor which will be explained in detail in Section 1.4.

The solution experiences an ohmic drop, iR when a current flow is induced between two electrodes, however this has to be taken into account when the potential E, it is applied to the working electrode:

$$E = (\phi_m - \phi_s) + iR - (\phi_{ref} - \phi_s)$$

Equation 1.8

At systems with a small currents flow between the working and reference electrodes, the ohmic drop in solution is insignificant, therefore iR can be ignored.

Therefore, the potentials applied to the working electrode are directly related to the driving force terms, $(\phi_m - \phi_s)$.

On the other hand, iR will increase when larger currents pass through the system, this therefore, may cause changes in the chemical composition of the reference electrode, so it may no longer be a constant value.

A third electrode, which is more common, is introduced in order to overcome this problem.

The potential of the working electrode is monitored relative to a separate reference electrode, positioned in close proximity. The device used to measure the potential difference between the working electrode and the reference electrode has high input impedance, so that a negligible current is drawn through the reference electrode. Consequently, its potential will remain constant and equal to its open-circuit value.

1.3 Cell Design and Electrode Placement

When a voltage is applied to an electrode as well as the iR drop across the cell, the double layer at the electrode surface needs to be charged. It will take a certain amount of time before the electrode reaches the applied voltage, this is the time constant. This can be reduced in at least three ways.

a) The total resistance can be reduced by increasing the conductivity of the medium through an increase in supporting electrolyte concentration or solvent polarity, or through a decrease in the viscosity.
b) The size of the working electrode reduces the double layer since capacitance is proportional to r_0^2 (although for disc electrodes, solution resistance varies as $1/r_0$).
c) The tip of the reference electrode can be moved as close as possible to the working electrode *e.g.*, using a Luggin capillary.

It is insightful to enquire as to which factors affect the flux of material to an electrode surface. Accordingly the effects due to electrode kinetics and material transport will be studied in turn.

1.3.1 Kinetics of Electrode Reactions

The kinetics of the general electrode reaction in Equation 1.1 are well described by the Butler-Volmer phenomenological formulation.

$$k_a = k_0 \exp\left[\frac{\alpha_a nF\left(E - E^0\right)}{RT}\right]$$

Equation 1.9

$$k_c = k_0 \exp\left[\frac{\alpha_c nF\left(E - E^0\right)}{RT}\right]$$

Equation 1.10

where, k_0 is the standard rate constant cm s^{-1}, α_a and α_c are the anodic and cathodic transfer coefficients; $\alpha_a = 1-\alpha_c$.

These equations are essentially obtained via a linearised free energy transition of O into R, $\alpha_{c/a}$ reflects the position of the transition state along the normalised coordinate. Accordingly, $\alpha_{c/a} \approx 1/2$ for most cases.

The observed rate of reaction at electrode surface, assuming kinetic control, is measured as the total current, *I*,

$$I = i_a + i_c = nFA\left(k_a [R]_{x=0} - k_c [O]_{x=0}\right)$$

Equation 1.11

and the subscript x = 0 refers to the reaction site very close to the electrode surface. Where i_a is anodic current and i_c is cathodic current.
At the equilibrium, the net current is zero, and the concentrations of $[R]_{x=0}$ and $[O]_{x=0}$ are then given by the Nernst equation.

1.4 Material Transport

The rate of reaction can be influenced by the cell potential difference. However, the rate of transport to the surface can also effect or even dominate the overall reaction rate. A typical electrolysis reaction involves the transfer of charge between an electrode and a species in solution. This whole process due to the interfacial nature of the electron transfer reactions typically involves a series of steps (see Figure 1.3) [2].

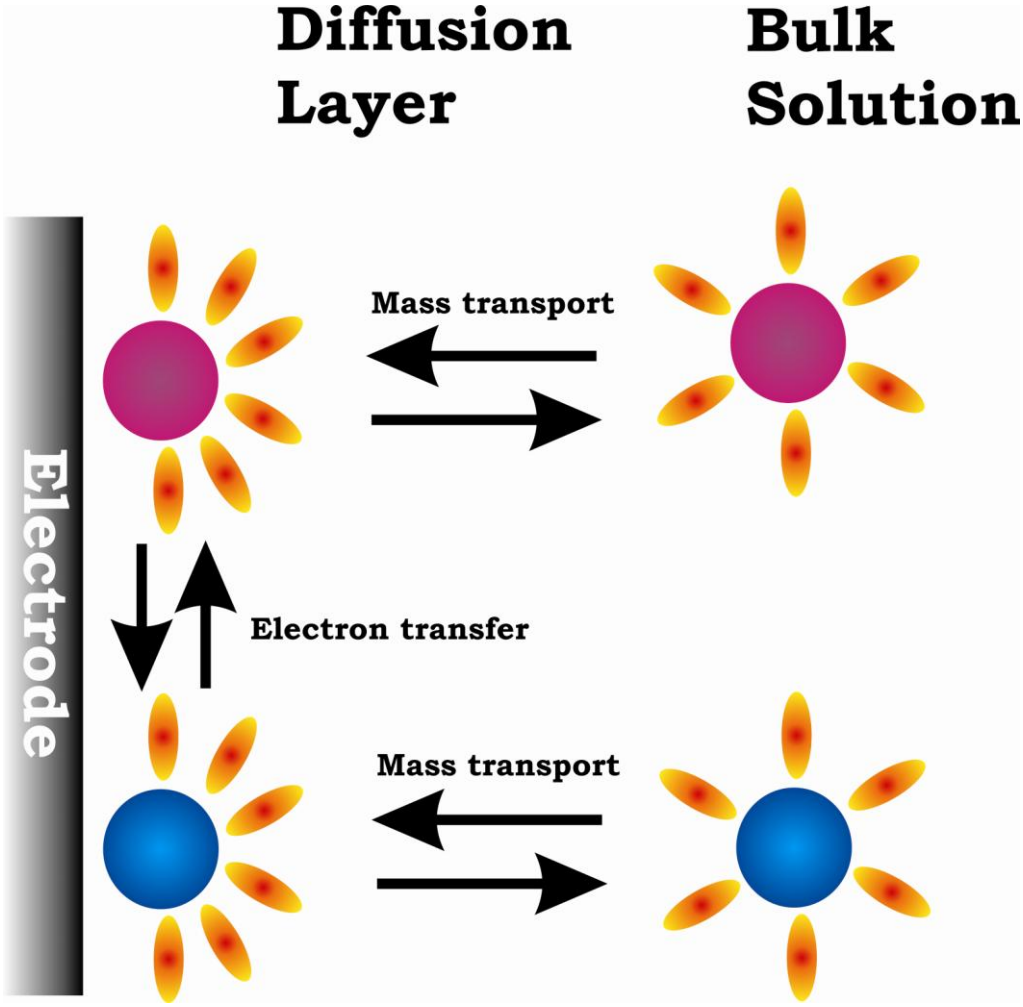

Figure 1.3: Schematic illustration of transport and kinetic phenomena in electrolytic reactions.

The electrode voltage can affect the rate of the electron transfer. This is an exponential relationship, so it would predict from the electron transfer model that as the voltage is increased the reaction rate and therefore the current will increase exponentially. This would mean that it is possible to pass unlimited quantities of current at sufficiently high overpotentials. Of course in reality this does not arise due to mass transport limitations [3-5].

$$i_c = -nFAk_c[O]_{x=0}$$

Equation 1.12

where, A is a fixed electrode area, k_{red} is a rate constant and $[O]_{x=0}$ the surface concentration of the reactant.

If the rate constant for the forward electron transfer process is made large (by for example holding the electrode at a sufficiently negative or positive potentials) then any reactant close to the interface will be immediately converted into products, and the current will be controlled by the amount of fresh reactant reaching the interface from the bulk solution above. Thus movement of reactant in and out of the interface is important in predicting the current flowing. There are three forms of mass transport which can influence an electrolysis reaction: diffusion, convection and migration [6].

1.4.1 Diffusion

This is a process by which different substances mix as a result of the random motions of their component atoms, molecules and ions [7]. Diffusion occurs in all solutions and arises from local uneven concentrations of reagents. The maximisation of entropy causes the smoothing out of these uneven distributions of concentration and are therefore, the main driving force for this process [8]. Diffusion is particularly significant in an electrolysis experiment since the conversion reaction only occurs at the electrode surface. Consequently there will be a lower reactant concentration at the electrode than in bulk solution. Similarly, a higher concentration of product will exist near the electrode than further out into solution.

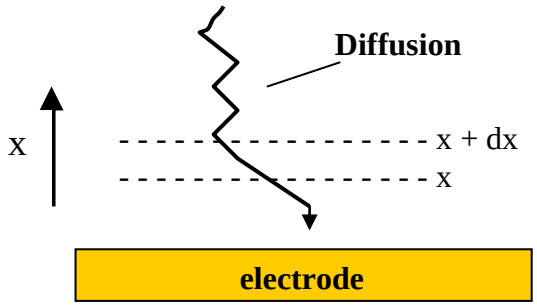

Figure 1.4: Diffusion process [9].

The rate of movement of material by diffusion can be predicted mathematically, Fick proposed two laws to quantify the processes [10]. The first law:

$$J_0 = -D_0\left(\frac{\partial C_0}{\partial x}\right)$$

Equation 1.13

relates the diffusional flux J_o to the concentration gradient and the diffusion coefficient D_o. The negative sign signifies that material moves down a concentration gradient (*i.e.*, from regions of high to low concentration). However, in many measurements it is important to know how the concentration of material varies as a function of time and this can be predicted from the first law. The result is Fick's second law.

$$\frac{\partial C_0}{\partial t} = D_0\left(\frac{\partial^2 C_0}{\partial x^2}\right)$$

Equation 1.14

In this case it considers diffusion normal to an electrode surface (x direction). The rate of change of the concentration (C_0) as a function of time (t) can be seen to be related to the change in the concentration gradient. So the steeper the change in concentration the greater the rate of diffusion [11]. Diffusion is often found to be the most significant transport process for many electrolysis reactions.

Fick's second law permits the prediction of the variation of concentration of different species as a function of time within the electrochemical cell.

1.4.2 Convection

This is a process by which an ensemble of species is transferred from one part of a fluid to another by movement of the fluid itself [12].

This can be via pumping, flowing, stirring, vibrating, etc. There are two forms of convection: natural convection and forced convection. Natural convection is present in any solution and it is generated by small thermal or density differences and acts to mix the solution in a random and therefore unpredictable manner. In the case of electrochemical measurements these effects tend to cause problems if the measurement time for the experiment exceeds 20 seconds. It is possible to drown out the natural convection effects from an electrochemical experiment by deliberately introducing convection into the cell. This form of convection is termed forced convection.

It is typically several orders of magnitude greater than any natural convection effects and therefore effectively removes the random aspect from the experimental measurements.

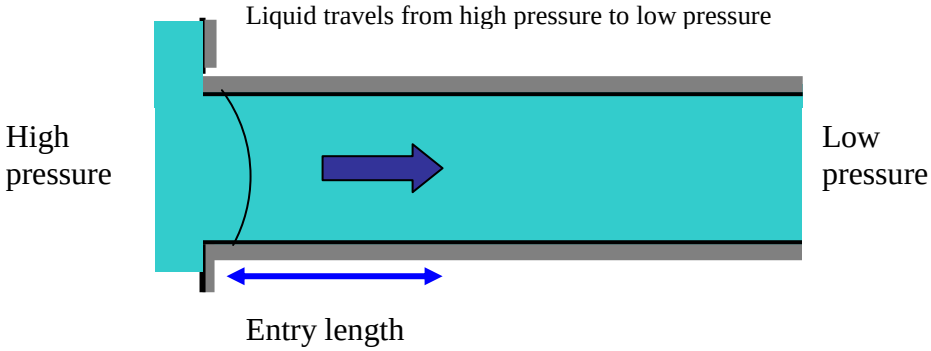

Figure 1.5: The cross section of liquid flowing through a pipe.

If a solution is introduced from the right hand-side and pumped through the pipe and the flow is controlled, after a small lead in length, the profile will become stable with no mixing in the lateral direction, this is termed laminar flow (see Figure 1.6a).

a) Laminar

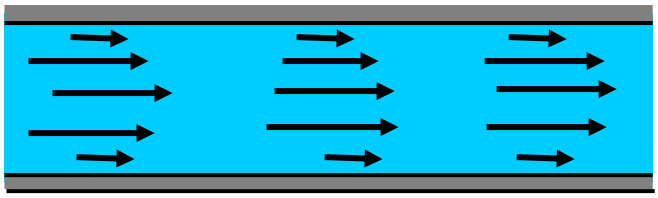

b) Turbulent

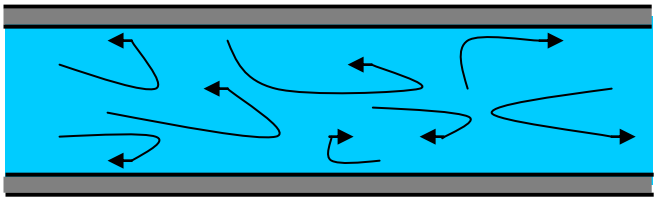

Figure 1.6: Shows flow laminar (a) and turbulent (b).

If however the solution is pumped through the cell at a high rate then the transport can become turbulent, where the solution movement is essentially a random and unpredictable (see Figure 1.6b).

For laminar flow conditions the mass transport equation for (1 dimensional) convection is predicted by

$$\frac{\partial C_0}{\partial t} = -v_x \left(\frac{\partial C_o}{\partial x}\right)$$

Equation 1.15

where, v_x is the velocity of the solution.

When an electrochemical cell possesses forced convection, it must be accounted for the electrode kinetic, diffusion and convection steps, to be able to predict the current flowing.

1.4.3 Migration

This is the movement of ions under the influence of an electric field. In electrochemical systems application of a potential to an electrode creates a charged interface. Any charged species near this interface will either be attracted or repelled from it by an electrostatic force. The migratory flux (j_m) is given by:

$$j_m \alpha - u[B] \frac{\partial \emptyset}{\partial x}$$

Equation 1.16

where [B] is the concentration of species B, $\frac{\partial \emptyset}{\partial x}$ is the electric field, and u the ionic mobility.

The ionic mobility is dependent on the ionic charge and size, as well as on the solution viscosity.

To simplify transport of redox active analytes most voltammetric measurements are performed in solutions which contain an inert background electrolyte in high concentrations compared with the analyte; this material is a salt (*e.g.*, KCl) which does not undergo electrolysis but, migrates, so that the reactants are effectively shielded from migratory effects. The purpose of introducing a background electrolyte into a solution is not however solely to remove migration effects as it also acts to decrease the solution resistivity and its presence in high concentrations enables activity coefficients to be "fixed", so that measurements can be related directly to concentrations.

1.5 Cyclic Voltammetry

Cyclic voltammetry is a very important electrochemical technique it can be used to study the redox behaviour of compounds and probe coupled chemical reactions, in particular to determine mechanisms and rates of oxidation/reduction reactions.

Cyclic voltammetry is a simple extension of the linear sweep technique. Conventional cyclic voltammetry is especially informative about the qualitative aspects of an electrode process however, the response waveforms lend themselves poorly to quantitative equations of parameters.

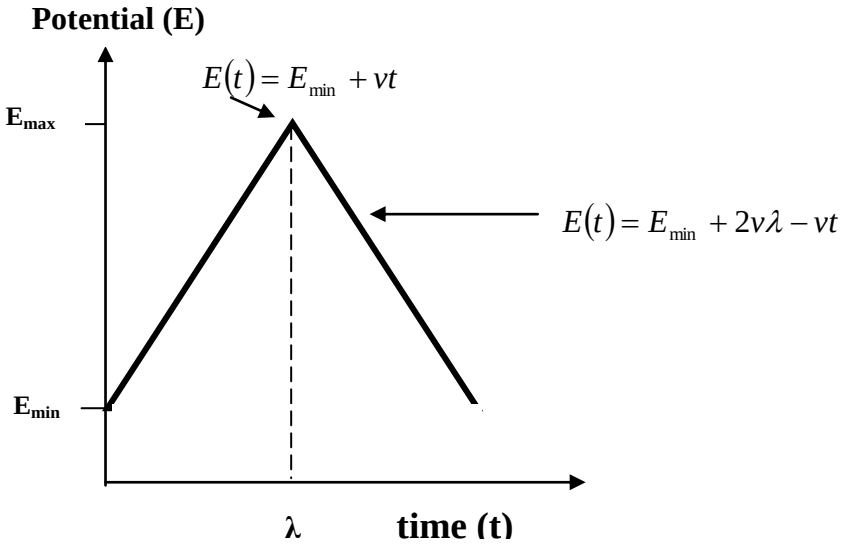

Figure 1.7: Potential dependence on time.

where, λ is the value of t when the potential is inverted, E_{min} is the minimum potential and E_{max} is the maximum potential, and the potential at which the scan direction is switched.

Conventional (dc) cyclic voltammetry probably is the most widely used potential wave perturbative method for studying electrode processes. The use of a triangular waveform at stationary electrodes, allows both the oxidation and reduction pathways to be studied conveniently from the experiment, and quantitative theory has been extensively developed in a readily implemented form [4, 13, 14].

Corrections for charging current, particularly at high scan rates, and data analysis from asymmetric peak-shaped curve, present two of the more important difficulties discouraging more widespread quantitative use of the method.

1.5.1 Theory and Applications of Cyclic Voltammetry for Measurement of Electrode Reactions Kinetics

Cyclic voltammetry has been established as the electrochemical method of choice for the evaluation of the mechanism of charge transfer for more than five decades. During these years a number of methods have been developed for the measurement of electrode reaction kinetics.

Furthermore, the presence of homogeneous reactions in the mechanism is readily detected, and interpretation of results usually is simple. A direct estimate of electrode reversibility is provided, because the potentials at which oxidation and reduction occur are observed directly within range [15]. Advantages of this method include the following:

1. The wide availability of low cost instrumentation.
2. Extensive theory available to guide the experimentalist in the interpretation of the empirical results.

However, this method has two shortcomings:

1. The determination of the mechanism of the second of two or more closely spaced charge transfers reactions (along the potential axis is often difficult). This poor resolution is a result of the current-voltage peak asymmetry.
2. For non-surface confined electroactive material, the concentration of the analyte must be at least 10 μM for the attainment of reliable mechanistic information.

This lower concentration limit is not a reflection of the poor sensitivity of the method, but rather the result of the high capacitance current resulting from sweeping the potential linearly with the time.

1.5.2 Cyclic Voltammetry at Planar Electrodes

Cyclic voltammetry experiments are conducted in quiescent solutions using large (millimetric dimension) electrodes such that diffusion normal to the electrode is the major form of mass transport.

The observed faradaic current depends on the kinetics and transport by diffusion of the electroactive species. It is necessary solve the equations described by Fick's second law of diffusion:

$$\frac{\partial[O]}{\partial t} = D_0 \frac{\partial^2[O]}{\partial x^2}$$

Equation 1.17

$$\frac{\partial[R]}{\partial t} = D_R \frac{\partial^2[R]}{\partial x^2}$$

Equation 1.18

The boundary conditions are:

t = 0	x = 0	$[O]_{x=0} = [O]_{\infty}$	$[R]_{x=0} = 0$
t > 0	$x \to \infty$	$[O] \to [O]_{\infty}$	$[R] \to 0$
t > 0	x = 0	$D_O\left(\frac{\partial[O]}{\partial x}\right) = -D_R\left(\frac{\partial[R]}{\partial x}\right)_0$	
$0 < t \leq \lambda$		$E(t) = E_1 + vt$	
$t \geq \lambda$		$E(t) = E_1 + 2v\lambda - vt$	

Equation 1.19

As there is a fifth boundary condition, it means the kinetic regime of the electrode reaction. This problem was illustrated by first time in 1948 by Randles and Sevick [16, 17] (see Figure 1.8).

1.5.2.1 Cyclic Voltammetry with Reversible Systems

The system is described as "*reversible"* when the electrode kinetics are much faster than the rate of diffusion.

The Nernst equation is the final boundary condition for a reversible system.

$$\frac{[Ox]_{x=0}}{[\mathrm{Re}\,d]_{x=0}} = \exp\left[\frac{nF}{RT}\left(E - E^0\right)\right]$$

Equation 1.20

Rewritten this equation,

$$E = E^0 + \frac{RT}{nF}\ln\frac{[Ox]_{x=0}}{[\mathrm{Re}\,d]_{x=0}}$$

Equation 1.21

where, $[X]_{x=0}$ is the concentration of the species at the electrode surface.

The voltammogram are affected by the reversibility of the electron transfer.
By analysing the Figure 1.8, points to the equation for the peak current in linear sweep voltammetry (at 298 K).

$$i_p = \left(2.69x10^5\right)n^{3/2}AD_0^{1/2}C_0v^{1/2}$$

Equation 1.22

where, A is the area in cm^2, D_0 is the diffusion coefficient in cm^2s^{-1}, C_0 is the concentration in mol cm^{-3}, v is the scan rate in $Vs^{-1}$and i_p peak current in amperes.

The *peak potential*, E_p, is given by,

$$E_p = E^0 - 1.109\frac{RT}{nF}$$

Equation 1.23

As the peak is broad, the peak potential may be difficult to analyse, therefore sometimes it is easier to calculate the potential at $i_{p/2}$, named *half-peak potential,* $E_{p/2}$, which is,

$$E_{p/2} = E^0 + 1.09\frac{RT}{nF}$$

Equation 1.24

Therefore,

$$\left|E_p - E_{p/2}\right| = 2.20\frac{RT}{nF}$$

Equation 1.25

Hence, the peak potential (E_p) is independent of the scan rate (v) and the peak current (i_p) is proportional to $v^{1/2}$.

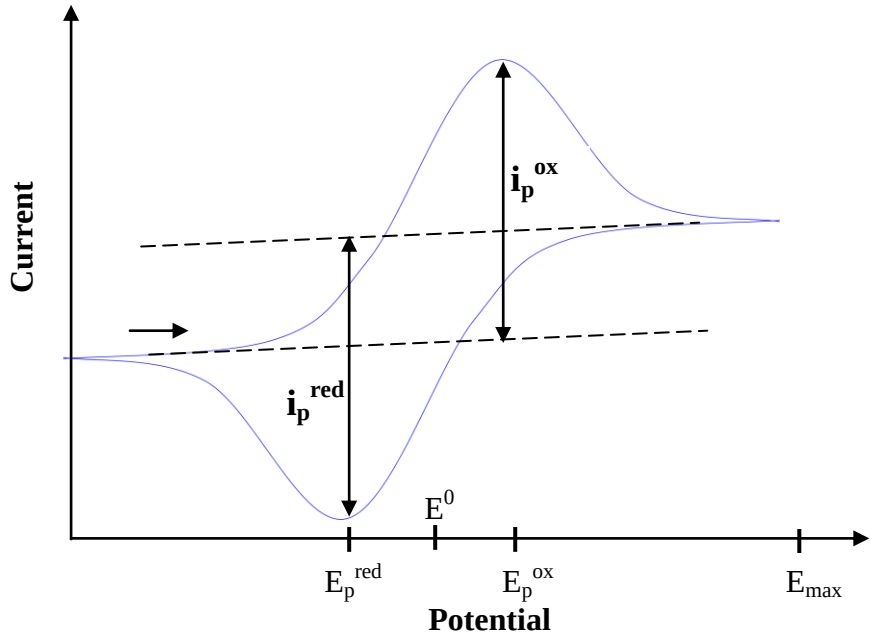

Figure 1.8: Illustrates a reversible system. The arrow shows the direction of the initial scan.

1.5.2.2 Cyclic Voltammetry with Irreversible Systems

The system is described as "*irreversible*" when the electrode kinetics are slower than the rate of diffusion.

For an irreversible reaction of the type one-electron, one-step reaction $\left(Ox + e^- \rightarrow \mathrm{Re}\,d\right)$, linear sweep and cyclic voltammetry give the same voltammetric profile, since no inverse peak emerges on changing the scan direction (see Figure 1.9).

The Nernstian boundary condition is substituted by a kinetic boundary condition when equilibrium is not retained at the electrode surface.

$$\frac{i}{FA} = D_0\left[\frac{\partial C_0(x,t)}{\partial x}\right]_{x=0} = k_f(t)C_0(0,t)$$

Equation 1.26

where, k_f : is the rate constant for the reduction.

In irreversible systems the peak potential appears at higher potentials, exactly beyond E^0 value, due to the small amount or no current flows. Therefore, a bigger overpotential is being requested to lead the reduction.

The peak current for irreversible systems (at 298 K) is given by,

$$i_p = \left(2.99\ x\ 10^5\right)\alpha^{1/2} AC_0 D_0^{1/2} v^{1/2}$$

Equation 1.27

where, A is the area in cm^2, D_0 is the diffusion coefficient in cm^2s^{-1}, C_0 is the concentration in mol cm^{-3}, v is the scan rate in $Vs^{-1}$and i_p is the peak current in amperes.

The peak potential for irreversible system is given by,

$$E_p = E^{0'} - \frac{RT}{\alpha F}\left[0.780 + \ln\left(\frac{D_0^{1/2}}{k_0}\right) + \ln\left(\frac{\alpha F v}{RT}\right)^{1/2}\right]$$

Equation 1.28

$$\left|E_p - E_{p/2}\right| = \frac{1.857RT}{\alpha F}$$

Equation 1.29

Consequently, for a totally irreversible system, E_p depends on the scan rate, variably (for reduction) in a negative direction by 30 mV at 298 K (or 1.15RT/αF) for each ten fold increase in the scan rate (v).

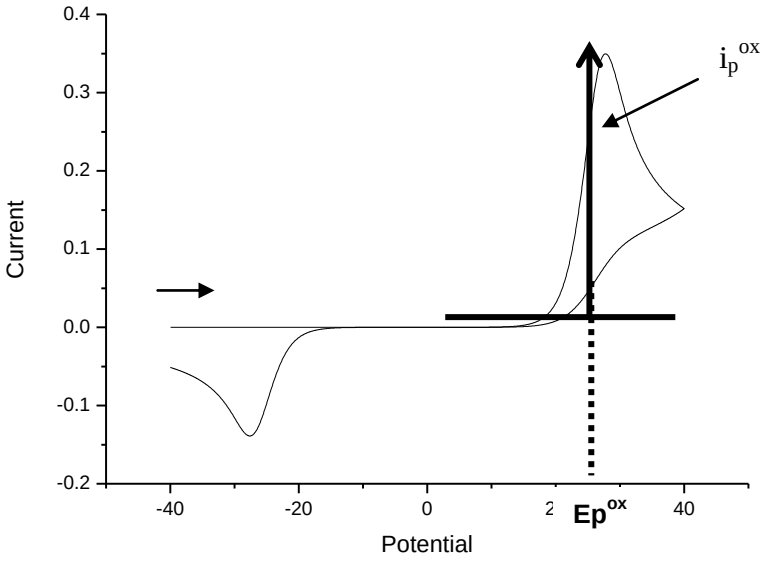

Figure 1.9: Showing an electrochemically-irreversible voltammogram. The numerical values illustrated are dimensionless values of current and potential. The arrow shows the direction of the initial scan.

1.5.2.3 Cyclic Voltammetry with Quasi-reversible Systems

The term *quasi-reversible* was introduced by Matsuda and Aybe [18] for reactions that show electron-transfer kinetic limitations. These systems are intermediate between reversible and irreversible systems.

For the one-step, one electron case,

$$Ox + e \underset{k_b}{\overset{k_f}{\rightleftharpoons}} \mathrm{Re}\, d$$

Equation 1.30

the resultant boundary condition is given by,

$$D_0\left(\frac{\partial C_0(x,t)}{\partial x}\right)_{x=0} = k^0 e^{-\alpha f\left[E(t)-E^0\right]}\left\{ C_0(0,t) - C_R(0,t)e^{f\left[E(t)-E^0\right]} \right\}$$

Equation 1.31

The current is given by,

$$i = FAD_0^{1/2} C_0 f^{1/2} v^{1/2} \Psi(E)$$

Equation 1.32

where, $f = \frac{F}{RT}$, $\Psi(E)$ is a function of quasi-reversible system, A is the area in cm^2, D_0 is the diffusion coefficient in cm^2s^{-1}, C_0 is the concentration in $molcm^{-3}$ and v is the scan rate in Vs^{-1}.

$$\Delta = k^0 / \left[D_0^{1/2} (F/RT)^{1/2} v^{1/2} \right]$$

Equation 1.33

When $\Delta > 10$, the behaviour approaches of a reversible system.

The values of $i_p, E_p, and\ E_{p/2}$ depend on Δ and α. The peak current is given by,

$$i_p = i_p(rev) K(\Delta, \alpha)$$

Equation 1.34

where, $i_p(rev)$: is the reversible i_p value. For a quasi-reversible reaction, i_p is not proportional to $v^{1/2}$. The peak potential is given by an integral equation which is solved using numerical methods. A Nernstian, quasi-reversible, or totally irreversible behaviour depends on the Δ and on the scan rate employed (see Figure 1.10).

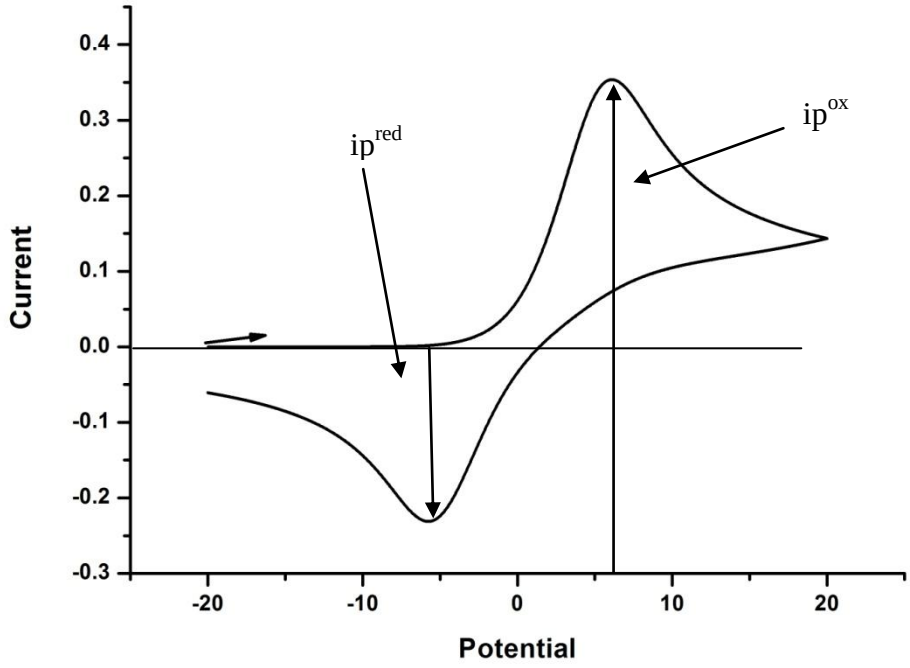

Figure 1.10: Cyclic Voltammogram of a quasi-reversible system. The numerical values illustrated are dimensionless values of current and potential. The arrow shows the direction of the initial scan.

1.5.2.4 Comparison between Reversible and Irreversible Voltammograms

For these systems (reversible and irreversible), the peak current i_p, increases when the scan rate and the concentration of the reactant species increasing. This increase of i_p with increasing scan rate can be explained by looking at Fick's first law, as this law explains that the peak current describes the gradient concentration of Ox close to the electrode surface, which is controlled by the diffusion layer thickness. When faster scan rates are used the potential is swept, less time is available for electrolysis, and therefore there is a reduction on the depletion of Ox close to the electrode. Consequently, the diffusion layer becomes thinner and the concentration gradient steeper.

In order to calculate the reversibility of the electron transfer, the peak potential and the peak size of the reverse sweep can be used.

The separation of the peak potentials, E_{pa}-E_{pc}, it is another important parameter in cyclic voltammetry which can be used to calculate the reversibility of the reaction.

The peak potential separation for a reaction with reversible electron transfer is given by:

$$E_{pa} - E_{pc} = 2.218\frac{RT}{nF}$$

Equation 1.35

The value of the peak potential separation at 298 K is approximately 59mV and is independent of scan rate.

A ratio of the peak currents, i_{pa}/i_{pc} which is one for reversible systems, is another important parameter in these systems. It is independent of the scan rate.

On the other hand in irreversible systems, the ratio of the peak currents, i_{pa}/i_{pc} and the reverse peak are dependent on scan rate. In order to lead the reverse electron transfer, a high overpotential is essential; therefore the peak separation (E_{pa}-E_{pc}) is dependent on the irreversibility of the system.

1.6 Amperometric Detection

Amperometric detection is based on measuring the oxidation or reduction currents of analytes at a working electrode. It has the advantage of incorporating analytes at a working electrode and offers generally good detection limits, however is restricted to the electroactive species concerned [19].

1.7 Potential Step: Chronoamperometry

It is defined as the variation of the current response with time under potentiostatic control. The potential of the working electrode is stepped from a value at which no faradaic reaction occurs or no redox process occurs (E_1) to a potential at which the surface concentration of electroactive species is effectively zero or to a value which the reduction or oxidation is driven (E_2).

Immediately following the step, a large current is detected which falls steadily with time. This current is named as the *Faradaic current, I_f*, therefore, it is only due to a *Faradaic current* electrode process (only electron transfer). Since there has been little time for

any depletion of the electroactive material, the concentration gradients shortly after the step are extremely large. Therefore, the currents flowing are very great at the beginning. Since the depletion occurs, the diffusion layers thickness increases and the current decreases: in the end to zero (see Figure 1.11).

The Cottrell equation shows the current response as function of time

$$|i| = \frac{nFAD_A^{\frac{1}{2}}C_0}{\pi^{\frac{1}{2}}t^{\frac{1}{2}}}$$

Equation 1.36

where, A is the area of the electrode, D_A and C_0 are the diffusion coefficient and concentration of the diffusing material in the bulk of the solution, respectively n is the number of electrons involved in the electrode reaction and F is the Faraday constant 96485 C mol^{-1}.

Potential step experiments can be used to quantify diffusion coefficients by using Equation 1.36.

As can be seen from the Equation 1.36, $t^{1/2}$ is an inverse function and the concentration of the diffusing material (C_0) at the electrode surface decreases, consequently this suggests that the rate at the redox process occurs, is under diffusion control.

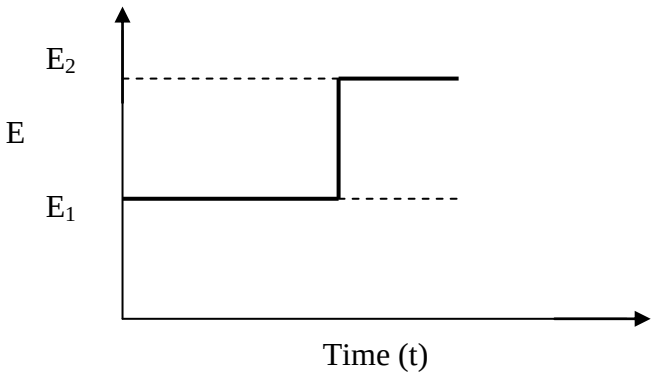

Figure 1.11: Showing the variation of applied potential step chronoamperometry experiment.

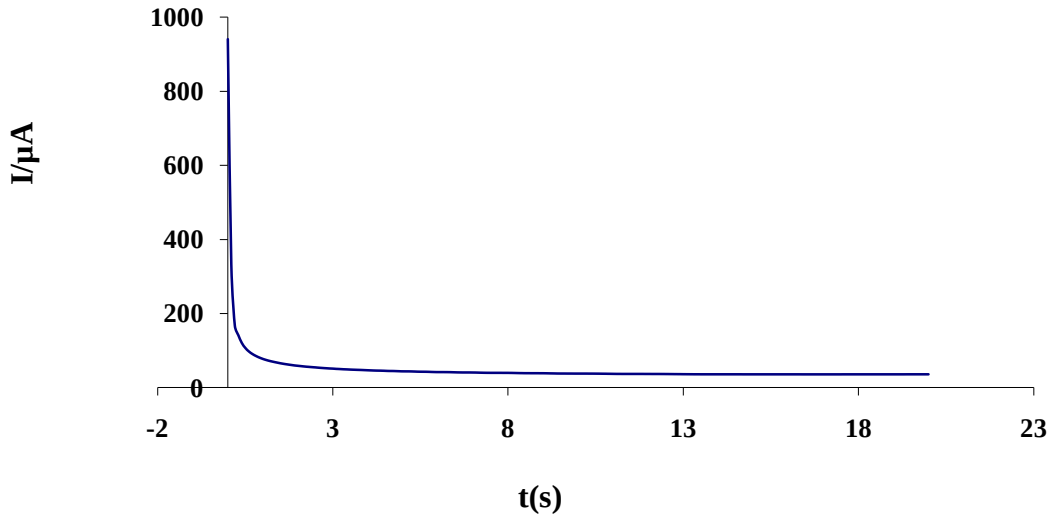

Figure 1.12: Showing the current response in a potential step chronoamperometry experiment. The numerical values illustrated are dimensionless values of current and time.

1.8 Hydrodynamic Electrodes

A hydrodynamic electrode [20] is one in which forced convection is deliberately introduced to dominate transport to the electrode. The main advantage of these electrodes is increased transport of electroactive species to the electrode, leading to higher currents and therefore a greater sensitivity and reproducibility.

The electrode may be fixed or may move (for instance by rotation) forcing convection in the solution and electrolyte solution allowed to flow across the surface.
Prediction of whether flow within an electrochemical cell is laminar or turbulent can be calculated by using the Reynolds number (*Re*). This parameter is dimensionless and it is a function of cell geometry and solution velocity given by,

$$Re = \frac{(length) \times (velocity)}{(kinematic\ viscosity)}$$

Equation 1.37

where, the length and velocity describe the electrode size and the convective flow.

There is a critical value of Re below which the flow change from laminar to turbulent, this is characteristic of each hydrodynamic electrode.

1.8.1 Limiting Currents

The steady-state limiting current (I_L) is one of the most important parameters in order to characterise hydrodynamic electrodes and the region of applied potential which corresponds to greatest sensitivity.

This will be employed for several hydrodynamic electrodes such as the channel electrode and rotating disc electrode. They will be examined in detail in the next section.

1.8.2 Rotating Disc Electrode

This is one of the most well-known hydrodynamic electrodes, which is popular because it is simple to use and easy to make. It consists of a disc electrode inserted in the middle of plane surface that rotates around its axis in a fluid. The disc is located in the centre of the axis.

The working electrode is used a small, metallic disc (*e.g.*, Pt, Au, glassy carbon, etc.) fixed centrally inside a large cylinder made of an insulating material such as Teflon.

The electrode is located into a vessel that contains the solution of interest (see Figure 1.13) and rotated at a constant speed in order to provoke a convective flow.
The solution is spanned out by rotation from the electrode surface in a radial direction (see Figure 1.13) and this in turn draws fresh solution up towards the electrode surface. Therefore, the electrode surface is supplied by a constant flow of electroactive material.

In rotating disc electrode experiments, the Reynolds number is given by,

$$\mathrm{Re} = \frac{w r_c^2}{v}$$

Equation 1.38

where, r_c is the radius of the cylinder, w is the rotation speed in Hz (cycles per second) and v is the viscosity of the solution.

If the Reynolds number does not exceed 1x 10^5 the flow to the electrode remains laminar (see Figure 1.13).

The equation of the velocity component in the z-direction, when is close to electrode surface ($z \to 0$) is given by,

$$v_z = -0.51 w^{3/2} v^{1/2} D^{-1/3} z^2$$

Equation 1.39

As can be seen from the previous equation when the rotation speed (w) is increased the velocity (v_z) also increases.

A sigmoidal curve is obtained when the voltammetry is carried out at steady state; therefore the limiting current can be determined by using the Levich equation for RDE (Rotating disk electrodes),

$$i_L = 0.62 nFA[O]_{bulk} D_B^{2/3} v^{-1/6} w^{1/2}$$

Equation 1.40

which predicts the variation in the transport limited current (i_L) as a function of the rotation speed.

A straight line which passes through the origin is obtained if the transport limited current (i_L) is plotted against the square root of rotation speed ($w^{1/2}$).

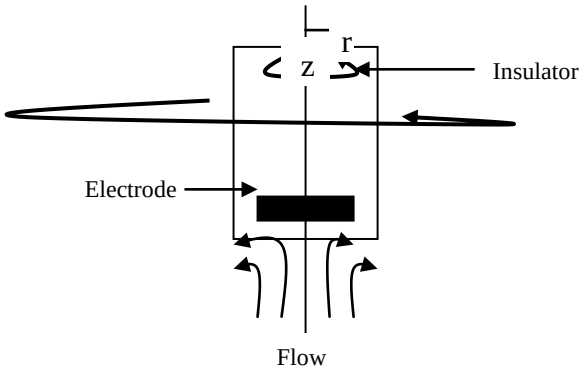

Figure 1.13: The rotating disc electrode.

1.8.3 The Channel Electrode

A channel electrode employs a thin rectangular channel in which the solution is mechanically pumped. The electrode is fixed in one wall of the channel (see Figure 1.14). If laminar flow is observed, the velocity across the channel is parabolic with the maximum velocity taking place at the channel centre (see Figure 1.15). The Reynolds number for the channel can be calculated by using the equation,

$$\mathrm{Re} = \frac{v_0 h}{v}$$

Equation 1.41

where, v_0 is the solution velocity in the centre of the channel, v is the kinematic viscosity of the solution (viscosity/density) and h is the half height of the cell.
Figure 1.15 shows laminar flow, the velocity across the channel has a parabolic shape, with the maximum velocity at the channel centre.

The convective-diffusion equation, for mass transport inside the rectangular channel under termed conditions is given by,

$$D_B \frac{\partial^2 [O]}{\partial y^2} - v_x \frac{\partial [O]}{\partial x} = 0$$

Equation 1.42

The mass transport limited current as a function of the solution volume flow rate (V_f) can be predicted by solving this equation in the same way to the rotating disc electrode (RDE):

$$i_L = 0.925nF[O]_{bulk} D_B^{2/3} V_f^{1/3} \left(h^2 d\right)^{-1/3} w x_e^{2/3}$$

Equation 1.43

where, x_e is the electrode length, h is the cell half-height, d is the width of the cell, w is the electrode width and V_f volume of the flow rate.

This equation predicts that the flow rate (V_f) is sufficiently fast that the diffusion layer thickness is much smaller than the depth of the cell and i_L (limiting current) varies as $V_f^{1/3}$.

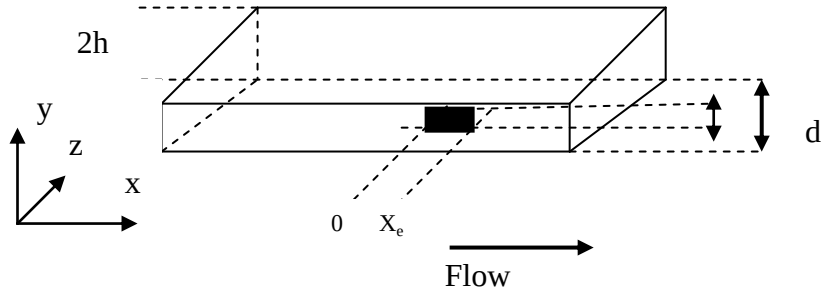

Figure 1.14: Showing channel electrode.

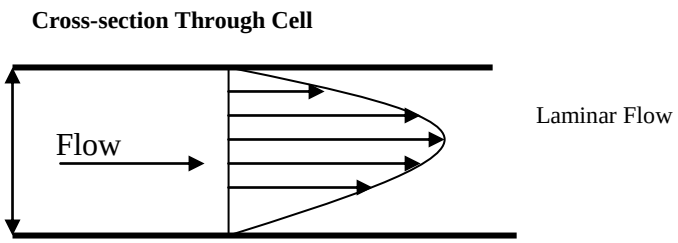

Figure 1.15: Parabolic flow profile in the channel electrode.

1.9 Microelectrodes

Microelectrodes [21, 22] or ultramicroelectrodes, are defined as electrodes which have at least one dimension that is a function of its size (between 0.1 and 50 μm). It is assumed that a microelectrode has dimensions of tens of micrometres or less, below to submicrometre range.

Microelectrode geometry is very diverse; some examples are described in Figure 1.16, which also illustrates very schematically, the way in which diffusion of electroactive species towards the electrode occurs.

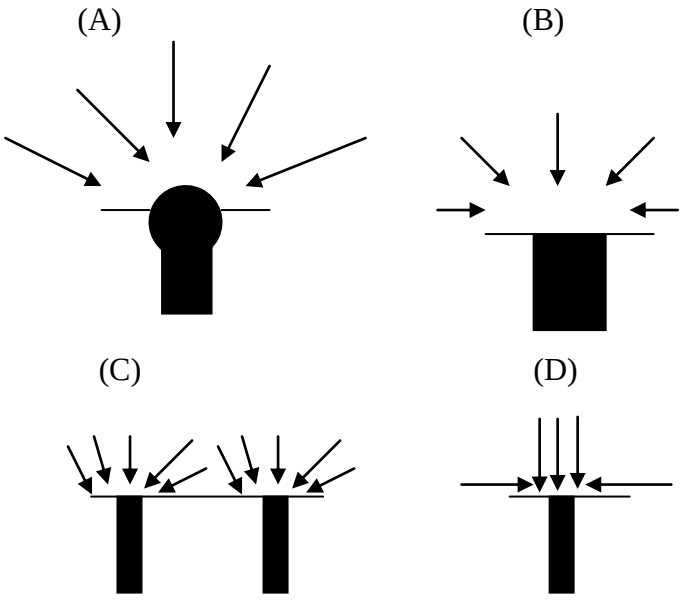

Figure 1.16: Types of microelectrodes: (A) hemispherical, (B) disc, (C) ring, (D) band.

The equation below, shows the variation of current with time when a spherical electrode of radius r_0 is used.

$$I = nFAJ = nFADc_{\infty}\left[\frac{1}{(\pi Dt)^{\frac{1}{2}}} + \frac{1}{r_0}\right]$$

Equation 1.44

This equation is named Cottrell equation with the addition of a spherical term, which is dependent on the reciprocal of the electrode radius. For small time, the first term of the

equation dominates, on the other hand for long time the current becomes independent of the time. The last condition often occurs with microelectrodes ($r_0 \leq 50\ \mu m$).

The reduction of the size of the electrodes provokes a lower capacitance in the total current and steady-state currents could occur in a short time as shown by (Equation 1.44).

In the limiting current region the steady-state at a hemispherical electrode is given by,

$$I = \frac{nFADc_\infty}{r_0} = 2\pi Fr_0 Dc_\infty$$

Equation 1.45

This equation can be rewritten in terms of the surface length, *d*, where $d = \pi r_0$ (it is the distance above the electrode surface from one point at the edge of the hemispherical electrode to the analogous point in the converse side) as,

$$I = 2nFdDc_\infty$$

Equation 1.46

The same equation can be used at a plane disc microelectrode, with only a small error, in this electrode the surface length is given by $d = r_0$.

The critical dimension for band microelectrodes is the width, which differ from disk and hemispherical electrode.

There are some general advantages of microelectrodes, which are listed below.

I. The small size, which allow them to be inserted in places where other electrodes can not be.
II. Low total current, microelectrodes pass tiny amounts of currents therefore, induce small amount of electrolysis. Microelectrode diffusion layers are very thin (of the order of micrometres in size) consequently; the concentration

gradients across the diffusion layer will be high. Therefore, the rate of mass transport to microelectrodes is much higher than for macroelectrode.

III. The high current density leads to good signal resolution and low detection limits.

Some of the applications of microelectrodes are as follows:

1. Electrochemical reaction mechanisms and kinetics.
2. Trace electrochemical analysis.
3. Electrochemical reactions in solutions of very high resistance.
4. Analytical sensing.
5. *In vivo* measurements on biological objects.
6. Detection in flowing liquids.
7. Scanning electrochemical microscopy (SECM).

1.10 Chemiluminescence and Electrogenerated Chemiluminescence

The next section will examine the application and mechanisms of chemiluminescence (CL) and electrochemiluminescence (ECL). In this work only ECL was employed, but both will be examined to give a more comprehensive image of the related process.

1.10.1 Chemiluminescence

Eilhardt Weideman in 1888 was the first to introduce the term chemiluminescence, it is defined as the emission of light from a chemical reaction. It is observed when a chemical reaction produces a species in an electronically excited state that is produced during the course of a chemical reaction. There are two forms of CL, direct CL where the species is promoted to an electronically excited state which emits light when it returns to the ground state and indirect CL, where the species transfers energy to another molecule which then re-emits light. The process is showed in Scheme 1.1.

a) $A+B \longrightarrow [I]^* \rightarrow Products + Light$

b) $A + B \rightarrow [I]^* + F \rightarrow F^* \rightarrow F + Light$

Scheme 1.1: Mechanisms for a) Direct CL, b) Indirect CL, where A & B are reagents, I is an intermediate and F is a fluorophore.

The process that results in the emission step is competing with other deactivation processes; therefore the emission intensity of a chemiluminescent reaction (I_{CL}) is frequently low. I_{CL} is dependent on the rate of the reaction $\left({}^{dC^*}/_{dt}\right)$ and the quantum yield (ϕ_{CL}) of the reaction (where C^* is the excited product).

$$I_{CL} = \phi_{CL}\left({}^{dC^*}/_{dt}\right)$$

Equation 1.47

The quantum yield (ϕ_{CL}) is defined as the product of the excitation quantum yield (ϕE_X) and the emission quantum yield (ϕE_M) with values typically in the range from 0.001 to 0.1 [23].

$$I_{CL} = \phi_{CL}\left({}^{dC^*}/_{dt}\right) = \phi E_X \phi E_M \left({}^{dC^*}/_{dt}\right)$$

Equation 1.48

Where,

$$\phi E_X = \frac{Number\ of\ molecules\ formed\ in\ electronically\ excited\ state}{Number\ of\ molecules\ formed\ reacting}$$

Equation 1.49

And,

$$\phi E_M = \frac{Number\ of\ photons\ emitted}{Number\ of\ molecules\ formed\ in\ electronically\ excited\ state}$$

Equation 1.50

There are several factors that affect chemiluminescence such as: the presence of a catalyst, temperature, pH, ionic strength, hydrophobity of the solvent, solution composition, the presence of energy transfers acceptors, the chemical structure of the chemiluminescence precursor, the nature and concentration of other species that may affect the chemiluminescence pathway.

Chemiluminescence belongs to a larger group of reactions; this group is named as luminescence, where light emission is associated with a transition from one electronic energy level to a lower level. Fluorescence and phosphorescence are included in luminescence, where their excited states are generated through the absorption of photons from a light source, instead of *via* a chemical reaction. Therefore these two processes are known as photoluminescence.

An electron is transferred to a higher energy level when a molecule is promoted to an electronically excited state. The electron will remain spin paired with the electron left behind. When an excited molecule has all the electron spins paired is said to be in an ”excited state”. A pair of electrons is said to be unpaired, when the electron, once excited is realigned parallel to the electron left behind and the excited molecule formed is in an “excited triplet state”.

The species can decay from the excited state to the ground state by different competitive processes (as shown in Figure 1.17).

The species falls to the lowest vibrational level of the excited state (similar to fluorescence)[24] when they looses vibrational energy. The lifetime of fluorescence excites states are between 10^{-5}-10^{-9}s, depending on the molar absorptivity of the molecule[25], the absorption rate is very fast 10^{-14}-10^{-15}s.

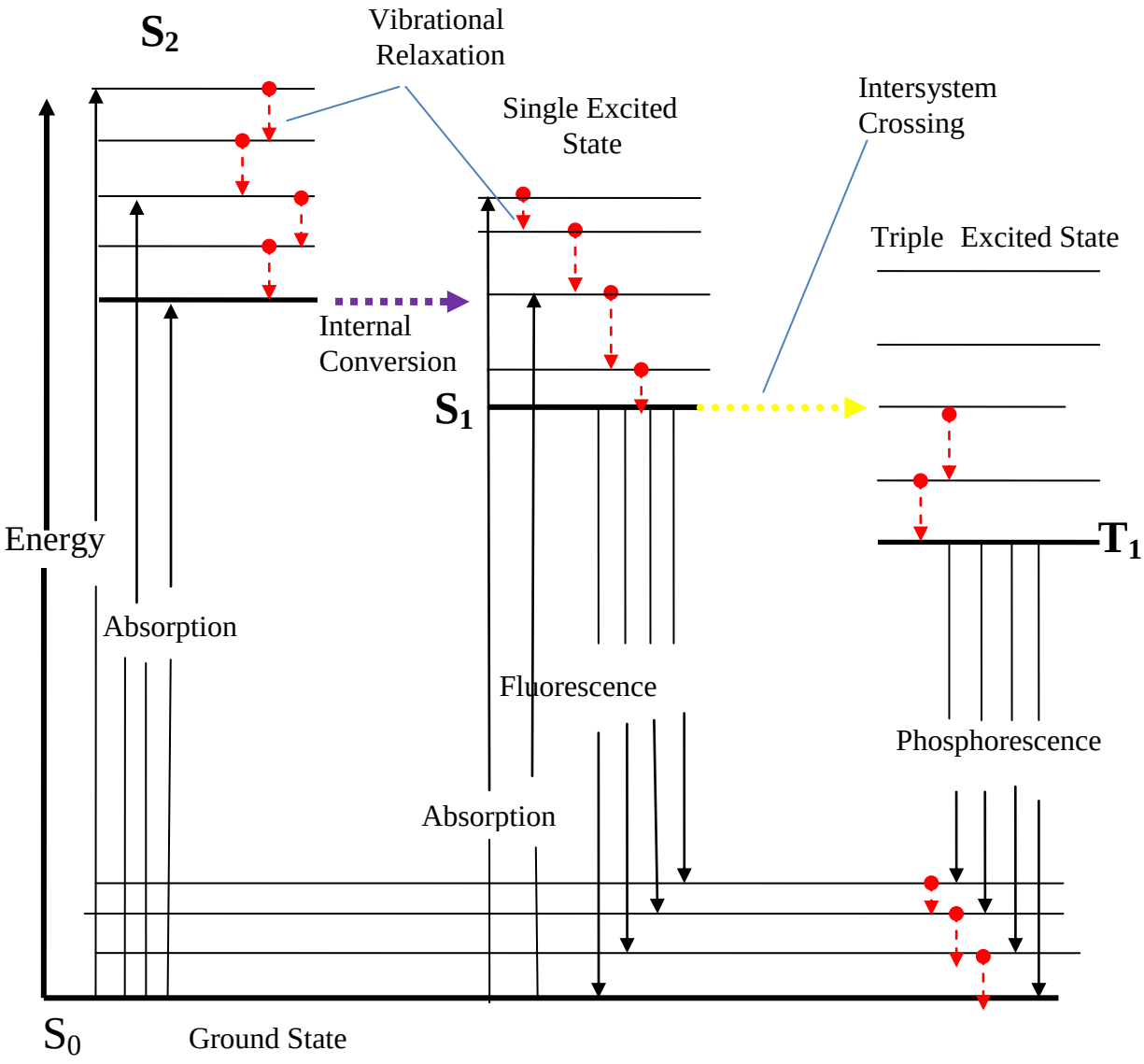

Figure 1.17: Jablonski diagram for a photoluminescent system.

In Figure 1.17 the thick black line shows the quantized energy levels, with S_0 as the ground state containing the majority of molecules in solution at room temperature. The thin lines represent vibrational energy levels associated with a particular electronic state. Internal and external conversion may occur reducing the higher excited state to the lower one when the energy of a higher and lowers excited state overlap (such as S_1 and S_2). Vibrational relaxation (represented by the red arrows) reduces the system energy to lowest vibrational energy level S_1.

When all electron spins are paired and the emission is analogous to fluorescence an excited molecule is normally a singlet. The emission process from a triplet state is similar to phosphorescence. Intersystem crossing occurs when there is a change in electron spin to form an excited triplet state. An intersystem crossing occurs, when there is an overlap of vibrational states between the two of them. Singlet states are normally more energetic than triplet states. Chemiluminescent reactions involving triplet states are unusual because the production of a triplet state by a singlet-triplet transition involves a change of in electron spin. As a result the transition is much slower and the lifetime of the phosphorescence excited states variety from 10^{-4} to a few seconds.

There are several criteria to produce chemiluminescence by light emission, which are listed below.

1) The reaction must generate enough energy to produce an intermediate or product in an excited state (200 kJ mol^{-1}).
2) A reaction pathway must be favourable in order to produce the excited state.
3) A photon of light or transfer energy to an appropriate fluorescent compound must be generated by the excited state, instead of losing the energy by internal or external conversion.

When an electronically excited product is formed by the process of the reaction and it is unable to generate the excess itself, an indirect CL or sensitisation phenomenon occurs.

1.10.2 Chemiluminescence Reactions

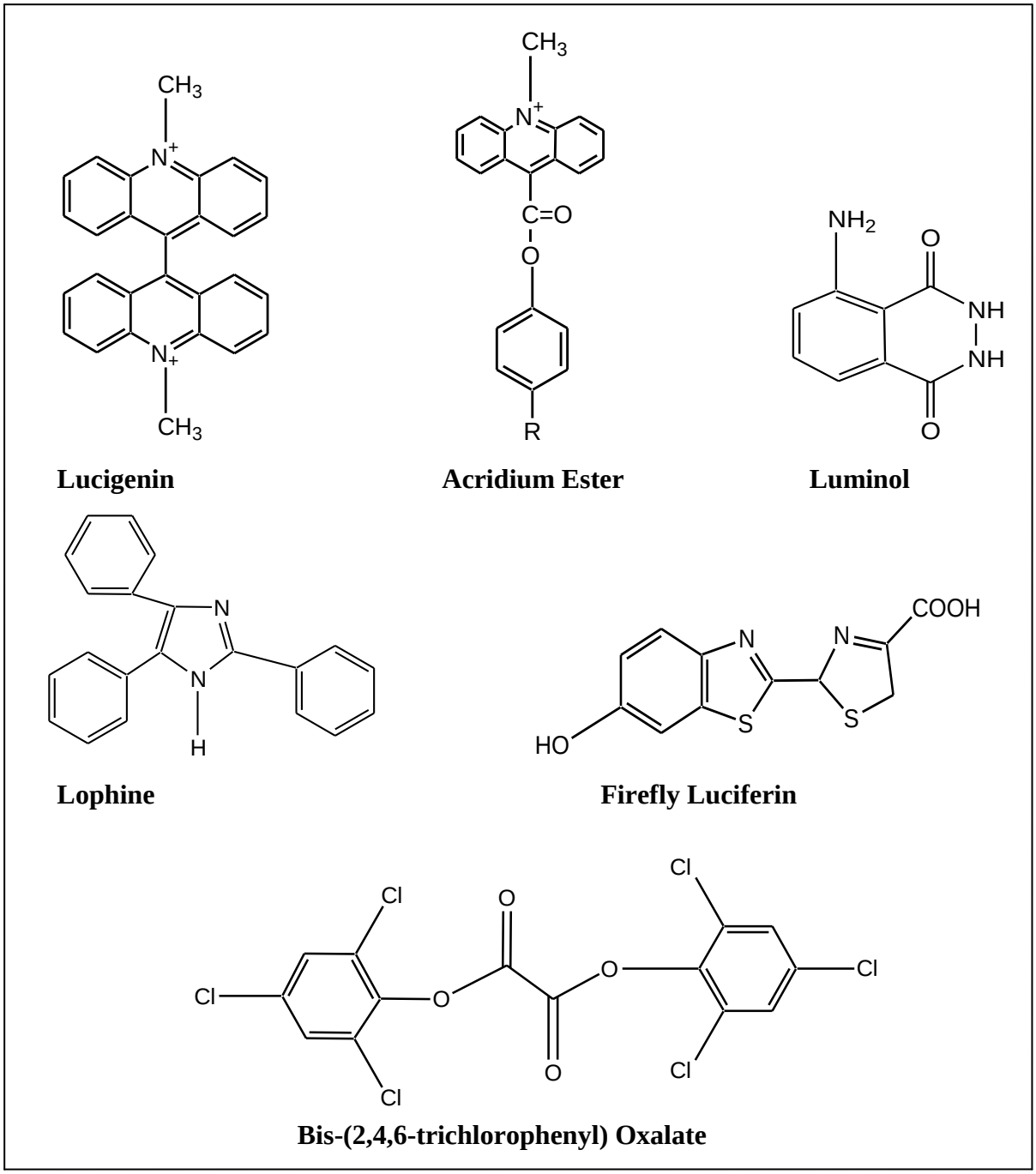

Figure 1.18: Examples of organic chemiluminescent molecules.

Figure 1.18 shows examples of organic molecules that can produce CL upon oxidation. These include cyclophthalhydrazides, of which luminol is the best known example and other systems such as lucigenin, acridium esters, firefly luciferin, bis-(2,4,6-trichlorophenyl)

oxalate and lophine. All of them generate CL when reacted with a range of oxidants in basic solution. These reactions can be exploited for analytical applications to detect:

a) Analytes labelled with CL compound, such as acridium ester labels for immunoassay [26].
b) The oxidant or a reaction producing an oxidant, for example hydrogen peroxide from specific enzymic catalysed reactions with the analyte [27, 28].
c) Species which act as catalysts, such as a variety of metal ions catalysing the luminol CL reaction [29].

Indirect CL is generated by the oxidation of various aromatic oxalate derivatives, typified by bis-(2, 4, 6-trichlorophenyl) oxalate in the presence of a suitable highly fluorescent compound, and the formation of an excited dioexetane like intermediate which transfers its energy to the fluorescer. This reaction is used in the detection of fluorescent analytes such as polyaromatic hydrocarbons [30], or fluorescent labelled analytes [31].

The chemiluminescence of luciferins in living systems, commonly termed as "bioluminescence", is highly efficient due to effective and extremely specific enzyme catalysis by luciferases in the presence of the co-factor ATP (Adeninetriphosphate). Luciferins (see Figure 1.18) have been employed to detect ATP, various enzymes and nucleotides [32]. Finally, it is interesting to mention the use of gas phase CL, and one its example is the reaction of nitrogen monoxide with ozone to generate excited nitrogen dioxide molecules, which has been used for detecting these environmental gaseous pollutants [33].

1.10.2.1 Chemiluminescence Detection for Separation Processes

Chemiluminescence reactions can be used as a detection technique for capillary electrophoresis and immunoassays [34, 35]. Chemiluminescence methodologies also provide a very sensitive and selective means of detection for the analysis of drugs, especially when coupled with the powerful separation technique of high performance liquid chromatography (HPLC). For the ultra-trace analysis of drugs in complex matrices such as biological fluids, the limitations of UV (Ultraviolet) and fluorescence detection are apparent due to the natural absorbance or fluorescence of numerous compounds present in such samples. For CL however, since the excitation of the analyte is *via* chemical reaction, as opposed to other spectroscopic methods, where an excitation light source is used, lower limits of detection can

be achieved, as there is rarely any background signal. This is important in the analysis of potent drugs, for example in a forensic field, where very low levels of the analyte compound are present [36, 37].

1.10.2.2 Tris(2, 2'-bipyridyl)Ruthenium (II)

Another very important CL reagent which is exploited in this thesis is tris(2, 2'-bipyridyl) ruthenium(II) $Ru(bpy)_3^{2+}$.

Hercules *et al.* [38] discovered the phenomenon of chemiluminescence in $Ru(bpy)_3^{2+}$ some 30 years ago. Even though tris(2, 2'-bipyridyl)ruthenium(II) is generally used for electrogenerated chemiluminescence, it can be also excited by chemical means. This reaction will be discussed in detail in Section 1.11.1.

1.11 Electrogenerated Chemiluminescence (ECL)

Electrogenerated chemiluminescence is also known as electrochemiluminescence (ECL), it can be probably best described as chemiluminescence produced directly or indirectly as a consequence of electrochemical reactions. ECL is usually generated by reagents electrochemically produced close to the electrode surface by the application of a selected potential. Electrogenerated chemiluminescence is a general term which has been used to a variety of differing mechanisms and reactions, such as:

- The electrochemical initiation of conventional, usually organic, CL reactions, *i.e.*, the electrochemical oxidation of luminol [39].
- Electrochemical modification of an analyte into a species which can be included in a conventional CL reaction with reagents that they are in the bulk solution.
- High energy electron transfer reactions between organic radicals produced electrochemically at one or more electrodes, *i.e.*, radical ion recombination between polyaromatic hydrocarbons [40].
- High energy electron transfer reactions between inorganic ions, *i.e.*, certain transition metal complexes [41-48].
- Emission from particular oxide covered electrodes, normally named as cathodic luminescence [49].

To make some distinction between the mechanisms explained above, different terms have been used in the literature such as, “electrogenerated chemiluminescence”, ”electrochemiluminescence”, “electroluminescence”, and “ECL”.
In practice these terms have unfortunately been used synonymously and this is because the above lists of ECL mechanisms are not entirely separate; therefore some reactions contain elements of more than one ECL type. It is more convenient, to consider the field of ECL reactions by dividing them into four groups, which have been investigated in detail as follows:

- **Ion annihilation reactions:** Reactions between radical cations and anions produced electrochemically by a single emitter.
- **Electron transfer reactions**: Explaining the electron transfer reactions of inorganic species, such as tris(2, 2’-bipyridine)ruthenium(II). It will be described in detail in Section 1.11.1**.**
- **Electrochemical simulation of conventional CL reactions**: The ECL reaction of common CL reagents such as luminol. It will be described in detail in Section 1.11.2**.**
- **Cathodic luminescence**: The light is emitted during the electrolysis at oxide covered with aluminium electrodes. It will be described in detail in Section 1.11.3.

As previously mentioned, in order to produce emission in the visible range as in conventional CL, the change of free energy of the reaction principal to the emitting species need to be around 200 kJ mol^{-1}. One of the advantages of ECL is that electrolytic processes are able to produce highly energetic and unstable reactants that they are not very easy to generate chemically.

ECL is generally more applicable than CL because in most cases one of the reactants at least can be produced electrochemically. Furthermore ECL is not a destructive technique as ECL emitters maybe re-used; therefore they can continue the analysis without reagent replacement.

1.11.1 ECL in Inorganic Compounds Electron Transfer Reactions of Transition Metal Complexes.

This is the type of ECL reaction used in this thesis.

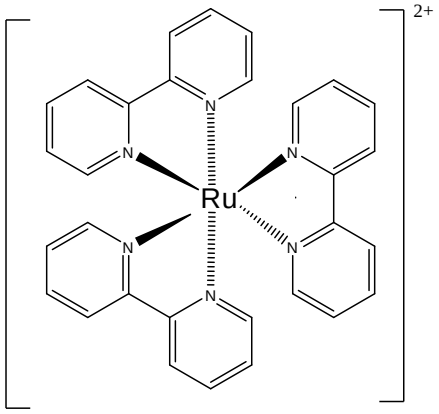

Figure 1.19: Tris(2, 2'-bipyridyl)ruthenium (II).

The emitting state for typical organic systems is formed either directly on electron transfer (S-route), or in energy-deficient systems *via* triplet intermediates (T-route), to yield a fluorescence emission. Singlet excited states, in transition metal complexes, undergo rapid deactivation due to spin-orbital coupling and the luminescence occurs mainly from the lowest energy excited states *via* energy sufficient routes. As the lifetime of these species is too short for them to take part in a subsequent annihilation reaction, the emission is usually phosphorescence from a spin-forbidden excited state [50]. Some of the complexes which posses emissive charge-transfer to ligand excited states are the type of $M(L)_3^{2+}$, where L is a chelating ligand such as 2,2'-bipyridine (bpy), and M is either ruthenium [51-54], osmium [43, 55] or related species. Complexes of rhenium [56, 57] and square planar platinum complexes [47] have also been used.

Other ECL active compounds include platinum and palladium porphyrins with intraligand excited states [58, 59] and multinuclear complexes such as $Pt_2(POP)_4^{4-}$, where POP is diphosphonate, [60, 61] or clusters such as $Mo_6Cl_{14}^{2-}$, where the excited state is thought to involve the metal-metal bonding [62-65]. A great number of analytical applications and investigations have centred on $Ru(bpy)_3^{2+}$or its derivatives due to the intrinsic, and somewhat exceptional properties of such complexes.

ECL emission can be obtained from a solution of $Ru(bpy)_3^{2+}$ through the application of fast cycling alternating between the oxidation and reduction potentials of $Ru(bpy)_3^{2+}$, so as to produce an orange light (λ_{max} = 620nm) by the following reaction mechanism, (see Scheme 1.2):

Bard and Tokel [66] in 1972 described an electrochemical method that resulted in the generation of the excited state $[Ru(bpy)_3^{2+}]^*$ and hence electrochemiluminescence from the interaction between $Ru(bpy)_3^{3+}$ and $Ru(bpy)_3^{+}$ (see Scheme 1.2 below).

$Ru(bpy)_3^{2+} - e^- \longrightarrow Ru(bpy)_3^{3+}$	Electro-oxidation
$Ru(bpy)_3^{2+} + e^- \longrightarrow Ru(bpy)_3^{+}$	Electro-reduction
$Ru(bpy)_3^{+} + Ru(bpy)_3^{3+} \longrightarrow [Ru(bpy)_3^{2+}]^* + Ru(bpy)_3^{2+}$	Electron transfer
$[Ru(bpy)_3^{2+}]^* \longrightarrow Ru(bpy)_3^{2+} + h\nu$	ECL

Scheme 1.2: Formation of $Ru(bpy)_3^{2+}$ via excited state $[Ru(bpy)_3^{2+}]^*$.

To form highly reducing or highly oxidizing intermediates the analytes that can be used with this reaction are usually compounds which can be co-oxidised or co-reduced with $Ru(bpy)_3^{2+}$. Therefore they can react with the ruthenium complex in order to produce the parent complex in an excited state $[Ru(bpy)_3^{2+}]^*$. These compounds are tertiary amines, oxalate and persulfate. The methods for the generation of $Ru(bpy)_3^{2+}$ will be discussed in detail in Section 1.11.1.1**.**

The occurrence of ECL in the reaction of $Ru(bpy)_3^{2+}$ with amines enables the determination of a large number of analytes. Many amine containing analytes such as proteins, drugs of abuse, aliphatic and cyclic amines, antibiotics, amino acids, various pharmaceuticals and pesticides have been determined with high sensitivity using this method. The relationship between ECL behaviour and the structure of the amine containing molecule has been investigated [67]. Tertiary amines produce higher ECL intensities than secondary amines. Primary amines show the lowest ECL intensity.

In 1987, Noffsinger and Danielson [68] proposed a mechanism for the chemiluminescence observed upon reaction of aliphatic amines with $Ru(bpy)_3^{2+}$ (see Scheme 1.3).

$$Ru(bpy)_3^{2+} \longrightarrow Ru(bpy)_3^{3+} + e^- \quad (1)$$

$$Ru(bpy)_3^{3+} + R_3N \longrightarrow [Ru(bpy)_3^{2+}]^* + products \quad (2)$$

$$[Ru(bpy)_3^{2+}]^* \longrightarrow Ru(bpy)_3^{2+} + h\nu \quad (3)$$

Scheme 1.3: Proposed mechanism for the chemiluminescence observed between aliphatic amines with $Ru(bpy)_3^{2+}$

Although Noffsinger and Danielson [68] reported chemiluminescence from $Ru(bpy)_3^{2+}$ and amines, it was, Leland and Powell [69], however who focused on the electrochemical oxidation of tertiary amines to produce chemiluminescence with $Ru(bpy)_3^{2+}$ and discussed in greater detail a possible mechanism. Leland and Powell [69] demonstrated the dependence on the oxidation of the amine to produce a strong reducing intermediate with sufficient energy to generate excited state species $[Ru(bpy)_3^{2+}]^*$ [70, 71].

This reaction can be used for a range of analytical reactions. Firstly by using tertiary, secondary and aliphatic amines. This method has been used for the analysis of drugs [72-74], amino acids [75, 76], antibiotics, [77, 78] , and reduced nicotinamide adenine dinucleotide (NADH) [79]. Secondly, the method has been employed in the determination of oxalate in vegetables [80] and biological samples [81]. Thirdly, this method has been employed in the use of labels based on $Ru(bpy)_3^{2+}$ for polymerase chain reaction (PCR) analysis [82] and immunoassay [83], by reaction of the label with added tripropylamine. Lastly, the selective determination of persulfate (with $Ru(bpy)_3^{2+}$) [84] has been reported.

1.11.1.1 Methods for the Generation of $Ru(bpy)_3^{2+}$

Common to all analytical $Ru(bpy)_3^{2+}$ chemiluminescence applications, is the production of the reactive oxidant, $Ru(bpy)_3^{3+}$ with an analyte species, to generate an emission of light.

The analytical utility of (see Scheme 1.2 in previous section) is obviously dependent upon the emission of light (hυ) being of a measurable intensity and indicative of the concentration of the analyte. There have been a variety of methods used to create the active oxidised reagent $Ru(bpy)_3^{3+}$; these consist of chemical/photochemical, electrochemical oxidation and *in situ* electrochemiluminescence. Each of these methods of generation will be discussed as follows:

1.11.1.2 Chemical and Photochemical Oxidation

Common oxidants such as concentrated nitric acid [85], lead dioxide [38] cerium (IV) [54] and chlorine have been used to produce $Ru(bpy)_3^{3+}$ from $Ru(bpy)_3^{2+}$. The most likely reason for avoiding the chemical generation of $Ru(bpy)_3^{3+}$ is the apparent difficulty in producing a constant, stable supply of the reagent [86].

1.11.1.3 Electrochemical Oxidation

The two types of electrochemical oxidation of $Ru(bpy)_3^{2+}$ to yield $Ru(bpy)_3^{3+}$ are the most popular means of reagent production. In the first type, the reagent is produced in a cell, which is remote from the site of its interaction with the analyte(s). In the other type, both the reagent production and the subsequent chemiluminescent reaction and detection occur within the electrochemical cell.

The first analytical application of electrochemically generated $Ru(bpy)_3^{3+}$ was suggested by Nonidez and Leyden in 1978 [72] . These workers illustrated a steady-state chemiluminescent flow cell which was used to verify the response from several pharmaceutical compounds when reacted with $Ru(bpy)_3^{3+}$. In 1987 Noffsinger and Danielson [70, 75, 87, 88] used a commercially available voltammetric analyser to oxidise the reagent for FIA (Flow Injection Analysis) and LC (Liquid Chromatography) applications.

Analogous work was described by Holeman and Danielson [73], they employed a polarographic analyser to perform the oxidation with a platinum working electrode (maintained at 1.0 V *vs.* Ag) an auxiliary electrodes and a silver wire reference electrode.

1.11.1.4 *In situ* Generated Electrochemiluminescence

In this thesis, *in situ* electrochemiluminescence was used to generate $Ru(bpy)_3^{3+}$. This method will be discussed in detail in Chapter 3. Electrochemiluminescence *in situ* differs from the earlier work described in 1.11.1.3, in that the reagent and analyte, which are both present at the point of oxidation and detection. Consequently, the potential also exist for chemical modification of the analyte(s) *via* oxidation at the electrode surface.

As a result, certain compounds will elicit little or no light emission upon direct with $Ru(bpy)_3^{3+}$ gave analytically useful signals under electrochemiluminescence conditions [89].

These aspects of electrogenerated chemiluminescence using $Ru(bpy)_3^{2+}$, were recently illustrated in a fundamental review by Lee [90].

Ege and co-worker [91] described the determination of $Ru(bpy)_3^{2+}$ in synthetic samples using a previously described [92], conventional three electrode cell with an optically flat bottom that used either glassy carbon or platinum disk working electrodes. An emission was generated by applying a stepping potential over 5-10 s thus, a passivating film was observed on the glassy carbon electrode, as result of the electro reduction of $Ru(bpy)_3^{2+}$. Polishing the electrode to recondition the surface rectified the diminished electrochemiluminescence emission. A platinum electrode, gave a more reproducible electrochemiluminescence signal. It is interesting to note that at the time of these initial studies [54, 81], Bard and co-workers investigated $Ru(bpy)_3^{2+}$ immobilised onto electrode [93-95] .

Greenway and co-workers [89, 96] employed a similar electrochemiluminescence cell configuration using a photomultiplier tube as an alternative of a silicon photodiode for several other analytical applications, due to the lack of sensitivity of the solid state.

1.11.2 ECL Applications of Conventional Chemiluminescence Reactions

One of the most popular CL reactions is with luminol.

In the presence of metal ion catalysts (such as cobalt, copper and nickel) it has been observed that the emission is greatly enhanced. Analytical methods for the determination of these metal ions have been developed [97-100]. Luminol and luminal-labelled species, such as labelled amino acids, has been successfully determined [101, 102]. Scheme 1.4 shows the reaction of luminol.

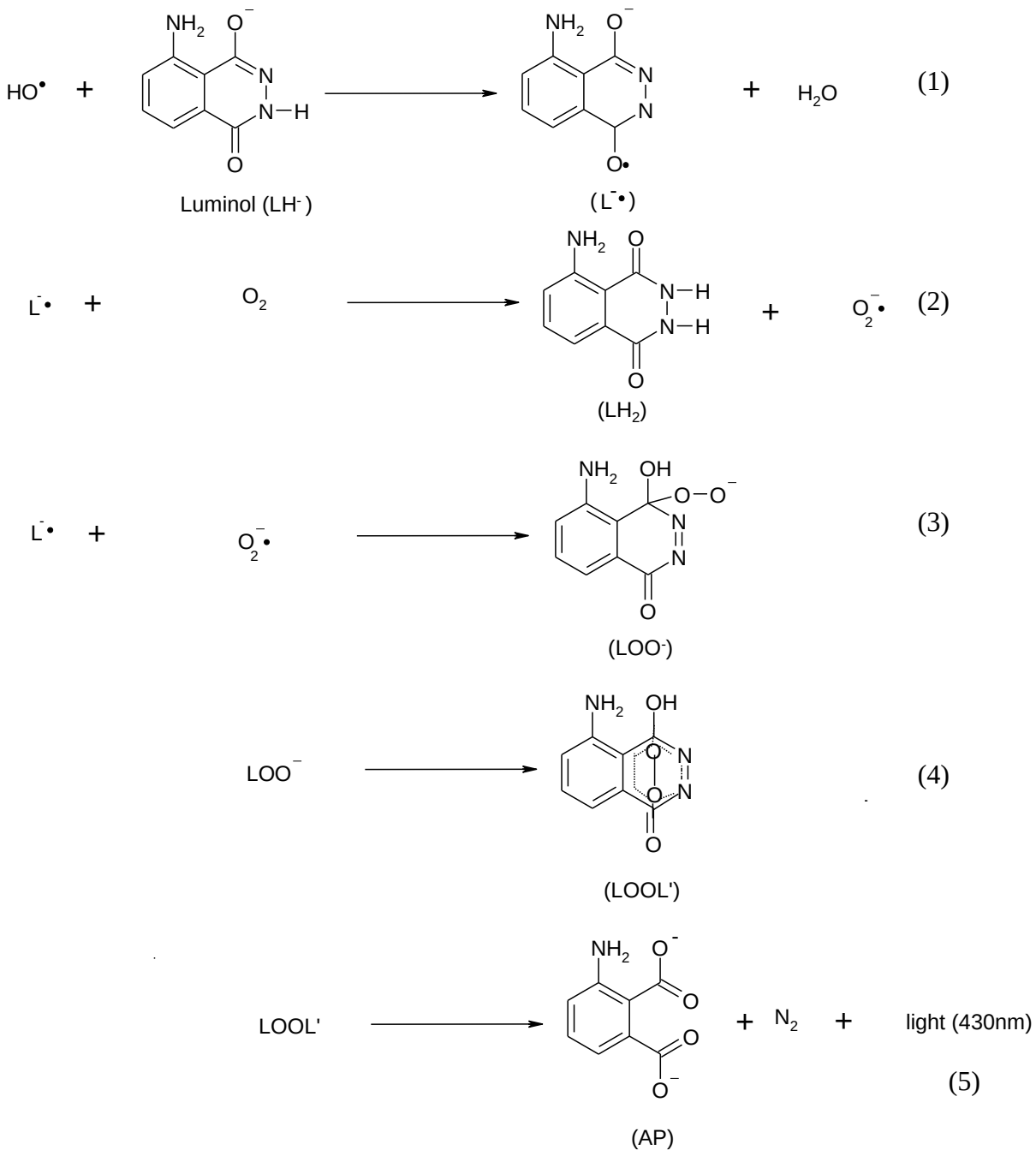

Scheme 1.4: Luminol Pathway (adapted from reference[103]).

The monodissociate luminol, at basic pH (LH^-) reacts with hydroxyl radicals to water and diazamiquinone radical ($L^{-\cdot}$) (reaction (1), see Scheme 1.4). $L^{-\cdot}$ reduces O_2 to superoxide anion ($O_2^{-\cdot}$) and is oxided to 5-aminohyphenthalazine-1,4 dione (LH_2) (reaction (2), Scheme 1.4). $L^{-\cdot}$ and O_2^- yield the carbon-centred hydroperoxide anion (LOO^-) (reaction (3), see Scheme 1.4). LOO^- rearranges to a transient endoperoxide (reaction (4), see Scheme 1.4), which decomposes to give light emission and products, an aminophthalate (AP) and N_2

(reaction (5), see Scheme 1.4). Oxygen centred radicals, such as the hydroxyl and alkoxyl radicals formed by homolytic scission of hydroperoxide, also cause photo-emissive luminol oxidation.

1.11.3 Cathodic Luminescence

Light emitted during the electrolysis at oxide covered metal electrodes in aqueous solution was first observed in 1898 [104]. Electrochemiluminescence, or galvoluminescence as this phenomena is also known, is observed at an anode at sufficiently high voltages (> 30V). The mechanism of this luminescence has been widely investigated and reviewed [49, 105] .

1.12 Analytical Applications of $Ru(bpy)_3^{2+}$ Electrochemiluminescence

Oxalate and organic acids can be examined by this reaction but most analytes have been based on amines.

1.12.1 Amino Acids and Proteins

He and co-worker [75], were the first by using FIA to determine $Ru(bpy)_3^{2+}$ chemiluminescence signal with good detection limits for amino acids peptides and proteins such as proline 1.0 µM, histidine 5.0 µM, hydroxiproline 5.0 µM, tyrosine 5.0 µM and tryptophan 5.0 µM.

1.12.2 Pharmaceuticals

The analytical evaluation of commercially significant pharmaceutical drugs by using $Ru(bpy)_3^{3+}$ chemiluminescence detection has attracted considerable attention.

Other studies described by Greenway's group have focussed on alkaloids [96] local anaesthetics and other pharmaceutical compounds. *In situ* generated $Ru(bpy)_3^{3+}$ was used for the determination of the structurally related alkaloids such as codeine, diacetyl morphine (heroin) and dextromethorphan.

1.12.2.1 Immunoassay and DNA Probe Assay

The application of chemiluminescence for determining analytes specific to human biological activity has received much attention [106]. Clinical applications as well as immunoassay

detection have become increasingly the focus of research over the past decade [107]. The use of chemiluminescent labels is clearly advantageous due to their non-radioactive nature, stability, cost and associated simple analytical instrumentation.

1.13 Comparison of Limits of Detection for ECL Systems

Table 1.1 shows a comparison of limits of detection for tryptophan, 9,10-diphenylanthracene (DPA) and codeine using different ECL systems.

Analytes	**Solvent**	**Limit of Detection (LOD)**	**ECL reaction**	**Reference**
Tryptophan	MeOH-H_2O (15-85)	$2x10^{-13}$ M	Inorganic, HPLC $Ru(bpy)_3^{2+}$	[108]
Tryptophan	$1x10^{-1}$ M NaOH	$1x10^{-5}$ M	Electrochemical enhancement of ECL reaction using a brominating agent	[109]
DPA**	Acetonitrile (MeCN)	$2x10^{-7}$ M	Organic, ED-ET*	[110]
DPA**	Acetate buffer-Brij 35	$1x10^{-8}$ M	Cathodic Luminescence, Al oxide	[111]
Codeine	Polyphosphoric acid present	$3x10^{-7}$ M	Acidic potassium permanganate	[112]
Codeine	Acetate buffer pH 4	$1.5x10^{-8}$ M	Inorganic $Ru(bpy)_3^{2+}$	[96]

Table 1.1: Shows a comparison of limits of detection for tryptophan, DPA and codeine using different ECL systems.

ED-ET* = Energy deficient electron transfer.

DPA = 9,10-diphenylanthracene.**

As can be seen from the Table 1.1 the $Ru(bpy)_3^{2+}$ ECL provides very good limits of detection.

1.14 Reagent Immobilisation

The use of solution based reagents is not easy in portable measurement systems and hence it would be very useful to develop a "reagentless" sensing system. Using ECL already helps to eliminate the need for an oxidising agent with $Ru(bpy)_3^{2+}$ CL, however it would be even better if the $Ru(bpy)_3^{2+}$ could be immobilised onto the electrode surface, making an ECL sensor. The direct immobilization of the chemiluminescent reagent on the electrode surface reduces the consumption of reagents and eliminates the need to incorporate an extra pump to deliver the reagent to the electrochemical cell. In the past $Ru(bpy)_3^{2+}$ has been immobilised at both platinum and glassy carbon electrodes by Collinson *et al*[113, 114].

1.14.1 Sol-Gels

Sol-gel-derived material prepared by the hydrolysis and condensation of alkosilanes (*i.e.*, tetramethoxysilane)(see Scheme 1.5) are an attractive alternative to many polymeric material for solid-state applications. This is due to the ease by which they can be prepared, modified, and doped with various reagents [115-117]. The sol-gel process is a chemical synthesis technique that enables the preparation of porous, high purity, optically transparent and homogeneous glasses. The initial hydrolysis and polycondensation reactions takes place in a localized region lead to formation of colloidal particles. (Sol is a suspension which contains these colloidal particles). The interconnection between these particles increases, and it leads to the formation of a solid gel. While the nature of individual events is random and the geometry and pore-size distribution of the product gel are difficult to determine, the nature of the final polymeric gel can be extended by controlling the rates of the individual steps. Because protons or hydroxide ions are essential for catalysis in silica gel formation, the pH of the reaction medium is an important factor that has an effect on the stochiometry of the final gel.

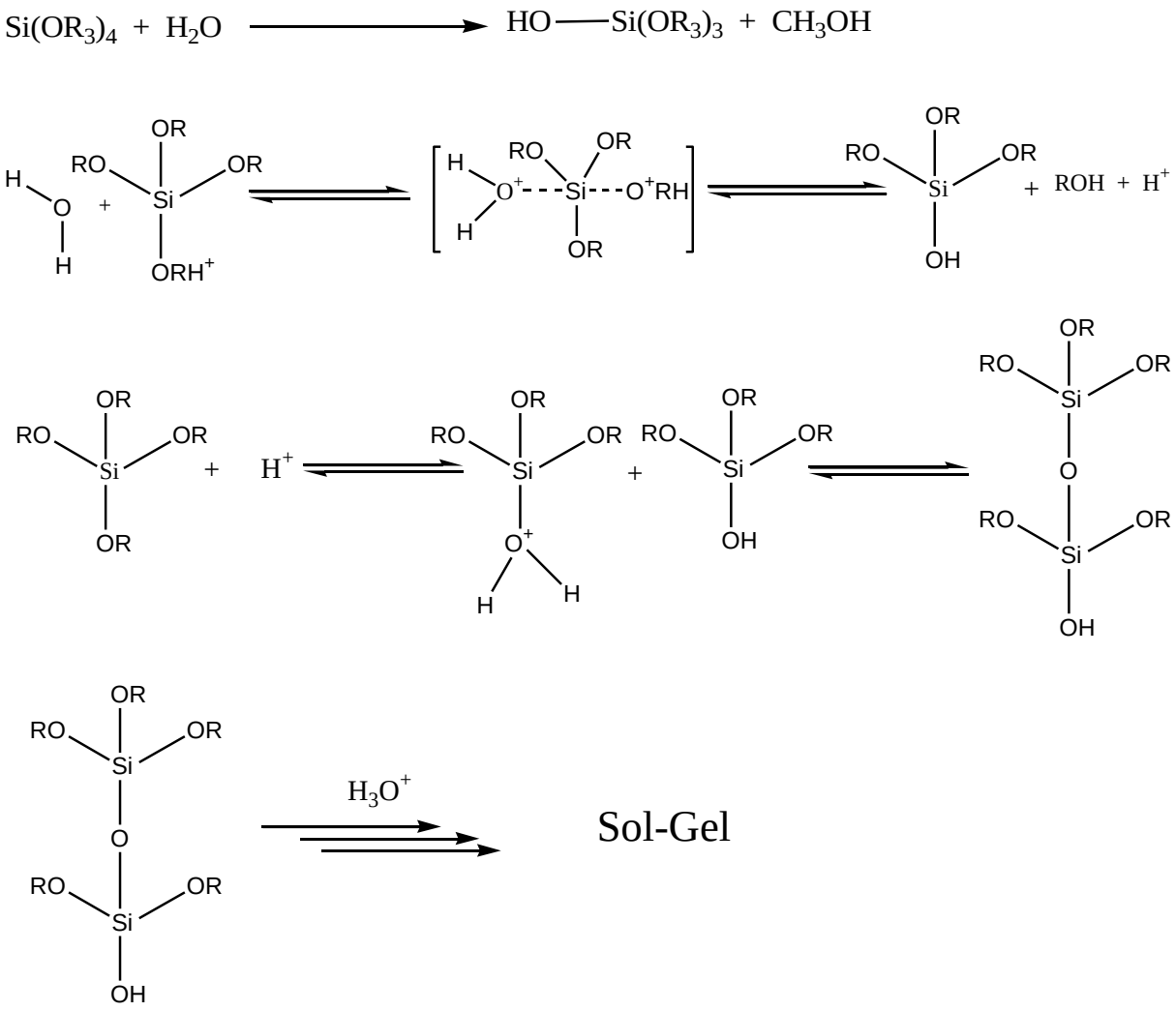

Scheme 1.5: Mechanism of formation of a sol-gel.

The presence of free protons in the medium permits the protonation of the bonded alkoxide and helps its dissociation. The formation of oxo bridges in acidic medium is obstructed resulting from the loss of protons from water or hydroxide ions. Acid catalysis tends to increase the rate of hydrolysis and disfavours condensation reactions; on the other hand basic hydrolysis produces rapid condensation [116] .

1.14.1.1 Sol-Gel Mechanisms

The hydrolysis reaction of tetraalkoxy and organosilanes is influenced by steric and inductive effects and appears to be specific acid (H_3O^+) and specific base (OH^-) catalyzed (see Scheme 1.5). The reaction order with respect to water and silicate is observed to be two and resulting in third- and second-order overall kinetics, respectively. Based on these factors, it is normally agreed that hydrolysis proceeds by bimolecular nucleophilic displacements reactions (SN_2-Si reactions) involving pentacoordinate intermediates or transition states, although by analogy to carbon chemistry siliconium ions, $Si(OR)_3^+$, have also been suggested as possible intermediates [115].

1.14.1.1.1 Acid-Catalized Hydrolysis

The acid-catalyzed mechanism is subjected to both steric and inductive effects. Compared to the SN_2 mechanism, electron-providing substituents should have a greater effect, because the silicon acquires more charge in the transition state.

Under acidic conditions, it is probable that an alkoxide group is protonated in a rapid first step. Electron density is withdrawn from silicon, making it more electrophilic and thus more susceptible to be attacked by water (see Scheme 1.5). The water molecule attacks from the rear and acquires a partial positive charge. The positive charge of the protonated alkoxide is correspondingly reduced, making an alcohol a better leaving group. The transition state decays by displacement of alcohol accompanied by inversion of the silicon tetrahedron.

The hydrolysis rate is increased by substituents that reduce steric crowding around silicon. Electron-donating subsitituents (*e.g.*, alkyl groups) that help to stabilize the developing of the positive charges, should also increase the hydrolysis rate but to a lesser extent, because the silicon acquires little charge in the transition state.
The inversion of the silicon occurs in displacement reactions with good leaving group such as Cl^- or $OCOR^-$ whose conjugate acids (corresponding protonated anions) have pKa< 6. This is the case regardless of the nature of the solvent, provided that the attacking reagent furnishes an entering group more basic than the leaving groups [118] .

For poorer leaving groups such as H or OR whose conjugate acids have pKa> 6, retention or inversion may occur depending on the nature of the catalyst cation and the solvent polarity.

Hydrogen bonding of the solvent may facilitate inversion by activating poor leaving groups [119]. The retention or inversion is further influenced by specific bonding configurations. This mechanism is affected by both steric and inductive factors; however steric factors are more important because silicon acquires little charge in the transition state.

The first stage of the hydrolysis reaction is the rapid protonation of the alkoxide group, as a result the electron density from silicon atom, makes it more electrophilic. The initial hydrolysis and polycondensation reactions are in a localized region, direct to the formation of colloidal particles.

The silanol groups by a condensation reaction forms siloxane bonds, excluding either water or alcohol molecules. Linkage of silanol with siloxane occurs as polymerisation reaction. The rate of condensation is dependent on whether the silanol group is protonated or deprotonated. A minimum in the rate of condensation occurs at pH 2, the isoelectric point of silica. The point of gelation appears when the sol particles combine to form a solid silica network. The resulting amorphous gel contains water and alcohol, therefore, continuously producing sol particles by the hydrolysis condensation of the reactions described earlier.

During this ageing effect, the strength of the gel increases and a reduction in the pore size appears. If the sol-gel is stopped at this stage by surrounding the gel with aqueous medium, the resulting sol-gel is termed as a hydrogel [115].

Finally, in the drying process, the solvents (water and alcohol) are removed from the interconnected pore network by evaporation, resulting in the decrease in pore size and reducing the volume of the sol-gel.

1.14.1.2 Factors Affecting Sol-Gel Properties

One problem with sol-gel is the age, even after the gelation point, the structure and properties of the gel continue to change as long as a solvent remains in its pores and the gel is not allowed to dry. One reason for these changes is that polycondensation reactions are still taking place in the solid amorphous phase therefore cross-linking continues.

The variables solution concentration, film thickness, and equilibration time are all interrelated. Thin film coated electrodes would tend to show greater sensitivity and faster response times as there less distance for the analyte to diffuse through to the electrode; however the amount of reagent in the thin film is less [120]. The rate of diffusion of $Ru(bpy)_3^{2+}$ in polymer films depends on the rate of physical diffusion and the rate of electron self-exchange. Since the self-exchange rate for the $Ru(bpy)_3^{2+}$ couple is large, self-exchange rates can proceed rapidly enough to affect the overall rate of diffusion [121, 122].

A major problem with immobilisation of the Ru complex in sol-gel is the fact that the molecule is small and can leach out. To overcome this, ion exchange material was added to the sol-gel to trap the complex [113, 114]. Another problem that can occur in this work is that sol-gels do not adhere to metals.

In their hydrated state, sol-gel derived material can be quite porous thus providing a good matrix to entrap chemiluminescent reagents that must diffuse together to react [123].

The ECL intensity in the solid-state host was low, therefore to increase the intensity of the ECL it is necessary to understand some of the factors that influence the light production in the porous solids.

For the tertiary amines, the intermediate is believed to be deprotonated one amine radical (see Scheme 1.3) [124, 125].

The diffusion of the molecules trapped within sol-gel derived glasses has been shown highly dependent on the structure of the gel as well as the size and charge of the molecules trapped within [123, 126]. Both surface interactions and surface confinement effects are important [123]. Specific surface interactions between the amine and the walls of the silicate host coupled with their larger size could significantly inhibit their diffusion in this host matrix.

1.14.2 Covalent Attachment

Stronger attachment to the substrate surface can be made by covalent linking of the desired component to surface groups present on, or formed on, the substrate. These covalent linking procedures normally use organosilanes and other linking agents. The substrate surface is

normally pre-treated *e.g.,* by an oxidative reaction, to produce surface groups. The linking agent and the desired component are used to be treated the surface. Favourite components are linked to electrode surfaces in this way such as ferrocenes [127] and $M(bpy)_x^{n+}$ species (M= Ru,Os,Fe) [128-130].

1.15 Conclusions of ECL and CL

From the previous review it can be concluded that ECL has a large potential applications in analytical chemistry and that it warrants further investigation. It could be demonstrated by the observation that apart of having the CL advantages, sensitivity and selectivity, ECL has the following additional advantages:

- The CL reaction can be controlled and manipulated by alterations to the applied potential, allowing better control over the initiation, rate and course of the reaction, since ECL reagents are generated *in situ* at the electrode.
- Since active reagents can be electrochemically generated from passive precursors in the sample, ECL allows existing CL methods to be simplified by using fewer amounts of reagents.
- Facilitating the use of signal modulation and background correction techniques, the production of the light reaction can successfully be switched "on and off ".
- By using voltammetric techniques as well as recording the light output, there is a chance of expanding additional analytical information by monitoring the electrochemical activity of the reaction.
- In order to obtain the maximum sensitivity, the emission is concentrated close to the electrode surface, therefore it can be shaped and accurately positioned in relation to the light measurement device.
- At the electrode surface, unstable intermediates and reagents can be generated and allowed to react *in situ* as soon as they are formed.
- A degree of additional electrochemical selectivity has been introduced into the methodology, since an appropriate potential has been selected to initiate a specific electrochemical reaction.

The construction of instrumentation for the electrogeneration and measurements of chemiluminescence are the main limitations. The need to optimise the experimental conditions such as media composition, to link both the electrochemical and CL reactions is another problem.

1.16 References

1. M.W. Schwarz and S. Irving, *Anal. Chem.*, 1963, **35**, 1770.
2. D.T. Sawyer, A. Sobkowiak, J.L. Roberts, Jr. Sawyer and T. Donald, *Electrochemistry for Chemists, ed. New York: Willey*, 1995.
3. C.M.A. Brett, A.M.O. Brett and M. A. Christopher., *Electrochemistry : Principles, Methods and Applications, Oxford University Press*, 1993.
4. R.S. Nicholson and I. Shain, *Anal. Chem.*, 1964, **36**, 706.
5. R.S. Nicholson and I. Shain, *Anal. Chem.*, 1965, **37,**, 178.
6. A.J. Bard, *J. Electroanal. Chem.*, 1973, **6**, 187.
7. *Oxford dictionary of Chemistry, Oxford University Press*, 2004.
8. C.H. Hamann, A. Hamnett and W. Vielstich, *Electrochemistry, Weinheim: Wiley-VCH*, 1997.
9. S. Thornes, *Principles and Applications of Electrochemistry, Cheltenham*, 1994.
10. A. Fick, *Uber Diffusion, Poggendorff's Annel. Physik. 1855, **94,** 59, in German. In English translation: The London, Edinburgh and Dublin Philosophical Magazine 1855, **10,** 30 and Journal of Science 1855, **16,** 30.*
11. P.H. Rieger, *Electrochemistry, New York : Chapman & Hall*, 1994.
12. C.W. Tobias, M. Eisenberg and C. R. Wilke, *J. Electrochem. Soc.*, 1952, **99**, 359C.
13. M.L. Olmstead, R.G. Hamilton and R. S. Nicholson, *Anal. Chem.*, 1969, **41**, 260.
14. R.S. Nicholson, *Anal. Chem.*, 1965, **37**, 1351.
15. R.J. Klingler and J. K. Kochi, *J. Am. Chem. Soc.*, 1980, **102**, 4790.
16. A. Sevcik, *Collection Czechoslov. Chem. Commun.*, 1948, **13**, 349.
17. J.E.B. Randles, *Trans. Faraday Soc.*, 1948, **44**, 327.
18. H. Matsuda and Y. Ayabe, *Z. Electrochem.*, 1955, **59**, 494.
19. J.M. Mermet, M. Otto and H. M. Widme, *Analytical Chemistry, R. Kellner, Willey-VCH*, 1988.
20. C.M.Brett and A. M. O. Brett, *Comprehensive Chemical Kinetics, Elsevier, Amsterdam*, 1986.
21. J. Heinze, *Angew. Chem. Int. Ed*, 1993, **32**, 1268.
22. K. Stulik, C. Amatore, K. Holub, V. Marecek and W. Klutner, *Pure Appl. Chem.*, 2000, **72**, 1483.
23. D.B. Paul., *Talanta*, 1978, **25**, 377.
24. H.H. Willard, L.L. Merritt Jr, J.A. Dean and F. A. Settle, *Instrumental Methods of Analysis*.
25. D.A. Skoog, F.J. Holler and T. A. Nierman, *Principles of Instrumental Analysis*, Saunders College Publishing, 5th Edition, 1998.
26. I. Weeks, M. Sturgess, R.C. Brown and J. S. Woodhead, *Methods Enzymol*, 1986, **366**, 133.
27. D.T. Bostick and D. M. Hercules, *Anal. Chem.*, 1975, **47**, 447.
28. C. Ridder, E.H. Hansen and J. Ruzicka, *Anal. Lett.*, 1982, **15**, 1751.
29. R. Abbot, University of Hull, 1986.
30. B. Yan, S.W. Lewis, P.J. Worsfold, J.S. Lancaster and A. Gachanja., *Anal.Chim. Acta*, 1991, **250**, 145.
31. N.G.F.M. Lammers, J.H.M. Van der Berg, M. Verzele and C. Dewaele, *J. Chromatogr.*, 1990, **499**, 541.
32. W.R. Seitz, *CRC Crit. Rev. Anal. Chem.*, 1981, **13**, 1.
33. A. Fontijn, A. J. Sabadel and R. J. Ronco, *Anal. Chem.*, 1970, **42**, 575.
34. I. Weeks, *Chemiluminescence Immunoassay*, Elsevier. UK, 1991.

35. H.A.H. Rongen, R.M.W. Hoetelmans, A. Bult and W.P. Van Bennekom, *J. Pharm. Biomed. Anal.*, 1994, **12**, 433.
36. Y. Huanga, C. Zhanga, X. Zhanga and Z. Zhang, *J. Pharm. Biomed. Anal.*, 1999, **21**, 817.
37. F.A. Alya, N.A. Alarfaffja and A.A. Alwarthanb, *Talanta*, 1998, **47**, 471.
38. N.W. Barnett, B.J. Hindson, P. Jones and T. A. Smith, *Anal. Chim. Acta*, 2002, **451**, 181.
39. J. J. K. K.E. Haapakka, *Anal. Chim. Acta.*, 1982, **138**, 253.
40. B. Fleet, G. F. Kirkbright and C. J. Pickford, *Talanta*, 1968, **15**, 566.
41. R.G. Gerardi, N.W. Barnett and S. W. Lewis, *Anal. Chim. Acta*, 1999, **378**, 1.
42. M.M. Richter, J.D. Debad, D.R. Striplin, G.A. Crosby and A. J. Bard, *Anal. Chem.*, 1996, **68**, 4370.
43. H.D. Abruna, *J. Electrochem. Soc.*, 1985, **132**, 842.
44. G. Xu and S. Dong, *Anal. Chim. Acta*, 2000, **12**, 235.
45. P.J. Taverna, H. Mayfield and A. R. J. Andrews, *Anal. Chim. Acta*, 1998, **373**, 111.
46. N.E. Tokel-Takoryan and A. J. Bard, *Chem. Phys. Lett.*, 1974, **25**, 235.
47. S. Bonafede, M. Ciano, F. Bolletta, V. Balzani, L. Chassot and A. V. Zelewsky, *J. Phys. Chem.*, 1986, **90**, 3386.
48. A. Vogler and H. Kunkely, *Am. Chem. Soc. Symp. Ser.*, 1987, **333**, 155.
49. S. Tajima, *Electrochim. Acta*, 1977, **22**, 995.
50. F. Bolletta and S. Bonafede, *Pure Appl. Chem.*, 1986, **58**, 1229.
51. R.S. Glass and L. R. Faulkner, *J. Phys.Chem.*, 1981, **85**, 1160.
52. R. Igarashi, Y. Nosoka, H. Miyama, M. Kaneko and M. Yokoyoma, *J. Electrochem. Soc.*, 1988, **135**, 2987.
53. R. Igarashi, Y. Nosoka, N. Fujii and H. Miyama, *Bull. Chem. Soc. Japan.*, 1989, **62**, 1405.
54. I. Rubinstein and A. J. Bard, *J. Am. Chem. Soc.*, 1981, **103**, 512.
55. J. Ouyang and A. J. Bard, *Chem. Soc. Japan*, 1988, **61**, 17.
56. J.C. Luong, L. Nadjo and M. S. Wrighton, *J. Am. Chem. Soc.*, 1978, **100**, 5790.
57. A. Vogler and H. Kunkely, *Angew. Chem.*, 1981, **20**, 469.
58. F. Bolletta, M. Ciano, V. Balzani and N. Serpone, *Inorg. Chim. Acta*, 1982, **62**, 207.
59. N.A.P. Kane-Maguire, J.A. Guckert and P. J. O'neil, *Inorg. Chem.*, 1987, **26**, 2340.
60. A. Vogler and H. Kunkely, *Angew. Chem., Int. Ed. Engl.*, 1984, **23**, 316.
61. J. Kim, F.F. Bard, A.J. Bard, C. Che and H. B. Grey, *Chem. Phys. Lett.*, 1985, **121**, 543.
62. D.G. Nocera and H. B. Grey, *J. Am. Chem. Soc.*, 1984, **106**, 824.
63. R.D. Mussell and D. G. Nocera, *Polyhedron*, 1986, **5**, 47.
64. R.D. Mussell and D. G. Nocera, *J. Am. Chem. Soc.*, 1988, **110**, 2764,.
65. R.D. Mussell and D. G. Nocera, *J. Phys. Chem.*, 1991, **95**, 6919.
66. N.E. Tokel and A. J. Bard, *J. Am. Chem. Soc.*, 1972, **94**, 2862.
67. A.W. Knight and G. M. Greenway, *Analyst*, 1994, **119**, 879.
68. J.B. Noffsinger and N. D. Danielson, *Anal. Chem.*, 1987, **59**, 865.
69. J.K. Leland and M. J. Powell, *J. Electrochem. Soc.*, 1990, **137**, 3127.
70. K. Chandrasekaran and D. G. Whitten, *J. Am. Chem. Soc.*, 1980, **102**, 5119.
71. M. Kirch, J.M. Lehn and J.P. Sauvage, *Helv. Chim. Acta*, 1979, **62**, 1345.
72. W.K. Nonidez and D. E. Leyden, *Anal. Chim. Acta*, 1978, **96**, 401.
73. J.A. Holeman and N. D. Danielson, *Anal. Chim. Acta*, 1993, **277**, 55.
74. J.A. Holeman and N. D. Danielson, *J. Chromatogr.*, 1994, **679**, 277.
75. L. He, K.A. Cox and N. D. Danielson, *Anal. Lett.*, 1990, **23**, 195.

76. W.A. Jackson and D. R. Bobbitt, *Anal. Chim. Acta*, 1994, **285**, 309.
77. N.D. Danielson, L. He, J.B. Noffsinger and L. Trelly, *J. Pharm. Biomed. Anal.*, 1989, **7**, 1281.
78. M.A. Targrove and N. D. Danielson, *J. Chromatogr. Sci.*, 1990, **28**, 505.
79. T.M. Downey and T. A. Nieman, *Anal. Chem.*, 1992, **64**, 621.
80. N. Egashira, H. Kumasako and K. Ohga, *Anal. Sci.*, 1990, **6**, 903.
81. I. Rubinstein, C. R. Martin and A. J. Bard, *Anal. Chem.*, 1983, **55**, 1580.
82. J. Dicesara, B. Grossman, E. Katz, E. Picozza, R. Ragusa and T. Wouldenberg, *BioTechniques*, 1993, **15**, 152.
83. J.H. Kenten, J. Casadei, J. Link, S. Lupold, J. Willey, M.J. Powell, A. Rees and R. J. Massey, *Clin. Chem.*, 1991, **37**, 1626.
84. K. Yamashita, S. Yamazaki-Nishida, Y. Harima and A. Segawa, *Anal. Chem.*, 1991, **63**, 872.
85. D.M. Hercules and F. E. Lytle, *J. Am. Chem. Soc.*, 1966, **88**, 4745.
86. R.D. Gerardi, N.W. Barnett and P. Jones, *Anal. Chim. Acta*, 1999, **388**, 1.
87. A.W. Knight and G. M. Greenway, *Analyst*, 1996, **121**, 101R.
88. P.J. De Laive, B.P. Sullival, T.J. Meyer and J. Whitten, *J. Am. Chem. Soc.*, 1979, **101**, 4007.
89. A.W. Knight and G. M. Greenway, *Analyst*, 1995, **120**, 2543.
90. W.Y. Lee, *Mikrochim. Acta*, 1997, **127**, 19.
91. D. Ege, W.G. Becker and A. J. Bard, *Anal. Chem.*, 1984, **56**, 2413.
92. H.S. White and A. J. Bard, *J. Am. Chem. Soc.*, 1982, **104**, 6891.
93. I. Rubinstein and A. J. Bard, *J. Am. Chem. Soc.*, 1980, **102**, 6641.
94. C.R. Martin, I. Rubinstein and A. J. Bard, *J. Am. Chem. Soc.*, 1982, **104**, 4817.
95. I. Rubinstein and A. J. Bard, *J. Am. Chem. Soc.*, 1981, **103**, 5007.
96. G.M. Greenway, A.W. Knight and P. J. Knight, *Analyst*, 1995, **120**, 2549.
97. K.E. Haapakka, *Anal. Chim. Acta.*, 1982, **139**, 229.
98. K.E. Haapakka and J. J. Kankare, *Anal. Chim. Acta.*, 1980, **118**, 333.
99. J. An, Q. Yao and F. Huaxue, *Chem. Abstr.*, 1980, **18**, 867.
100. J. An, Q. Yao and F. Huaxue, *Chem. Abstr.*, 1991, **114**, 35053u.
101. M. Sato, T. Yamada, M. Horikawa and D. K. O. K. B. Kagaku, *Chem. Abstr.*, 1983, **51**, 111.
102. M. Sato, T. Yamada, M. Horikawa and D. K. O. K. B. Kagaku, *Chem. Abstr.*, 1983, **99**, 15861z.
103. T. Miyazawa, T. Suzuki, K. Fujimoto and K. Yasuda, *J. Lipid Res.*, 1992, **33**, 1051.
104. F. Braun, *Ann. Phys. Chem*, 1898, **65**, 361.
105. S. Ikonopisov, *Electrochim. Acta*, 1975, **20**, 783.
106. A. Mayer and S. Neuenhofer, *Angew. Chem. Int. Ed.*, 1994, **33**, 1044.
107. W. L. Wallace and A. J. Bard, *J. Phys. Chem.*, 1979, **83**, 1350.
108. K. Uchikura and M. Kirisawa, *Anal. Sci.*, 1991, **7**, 971.
109. S. Sakura, *Electrochim. Acta*, 1992, **37**, 2731.
110. M. Sato, T. Yamada and M. Fujino, *Chem. Abstr.*, 1981, **94**, 149742s.
111. K.E. Haapakka, J. Kankare and K. Lipiainen, *Anal. Chim. Acta*, 1988, **215**, 341.
112. T.J. Christie, R.H. Hanway, D.A. Paulls and A. Townshend, *Anal. Proc.* , 1995, **32**, 91.
113. A.N. Khramov and M. M. Collinson, *Anal. Chem.*, 2000, **72**, 2943.
114. M.M. Collinson, B. Novack, S.A. Martin and J. S. Taussig, *Anal. Chem.*, 2000, **72**, 2914.

115. C.J. Brinker and G. W. Scherer, *Sol-Gel Science-The Physics and Chemistry of Sol-Gel Processing*, Academic press, 1990.
116. B.C. Dave, B. Dunn, J.S. Valentine and J. I. Zink, *Anal. Chem.*, 1994, **66**, 1120A.
117. O. Lev, M. Tsionsky, L. Rabinovich, V. Glezer, S. Sampath, I. Pankratov and J. Gun, *Anal. Chem.*, 1995, **67**, 22A.
118. L.H. Sommer, G.A. Parker, N.C. Lloyd, C.L. Frye and K. W. Michael, *J. Am. Soc.*, 1967, **89**, 857.
119. M.G. Voronkov, V.P. Mileshkevich and Y. A. Yuzhelevski, *The Siloxane Bond, Consultants Bureau, New York*, 1978.
120. L.D. Whiteley and C. R. Martin, *Anal. Chem.*, 1987, **59**, 1746.
121. C. Martin, I. Rubinstein and A. J. Bard, *J. Am. Chem. Soc.*, 1982, **104**, 4817.
122. D.A. Buttry and F. C. Anson, *J. Am. Chem. Soc.*, 1983, **105**, 685.
123. M.M. Collinson, P. J. Zambrano, H. Wrang and J. S. Taussig, *Langmuir*, 1999, **15**, 662.
124. A. W. Knight, *Trends Anal. Chem.*, 1999, **18**, 47.
125. R.D. Gerardi, N.W.Barnett and S. W. Lewis, *Anal. Chim. Acta*, 1999, **378**, 1.
126. N. Koone, Y. Shao and T. W. Zerda, *J. Phys. Chem.*, 1995, **99**, 16976.
127. O. Buriez, E. Labbe, P. Pigeon, G. Jaouven and C. Amatore, *J. Electroanal. Chem.*, 2008, **6**, 169.
128. G.M. Greenway, A. Greenwood, P. Watts and C. Wiles, *Chem. Commun.*, 2006, 85.
129. A. Liu, J. Anzai and J. Wang, *Bioelectrochem.*, 2005, **67**, 1.
130. L.M Goldenberg, M.R. Bryce and M. C. Petty, *J. Mater. Chem.*, 1999, **9**, 1957.

Chapter 2

Experimental Section : Instrumentation and Procedures

2.1 Instrumentation

2.1.1 Development of a Electrogenerated Chemiluminescence Detectors

Chemiluminescence can be detected by using any instrumentation that is sensitive to changes in light intensity. The main requirements for the detector are:

- Detect light over a large range of intensities.
- Highly sensitive over the 400-600 nm spectrum range.
- The output signal should be directly related to the light sensitivity.
- The speed of the response of the detector must be greater than the rate of the chemiluminescence reaction to give a true signal [1].

Usually photon transducers are employed to detect photons of light and convert them into electrical signals. Photon transducers can be divided into two main groups, solid state devices and vacuum tubes.

The photomultiplier tube (PMT) is the most common detection device used in chemiluminescence [2] due to its high sensitivity.

Several factors must be considered in order to choose a suitable photo detector such as: the detectors active area, the signal to noise ratio, the wavelength of light to be detected and the intensity.

Others factors are also important such as: the size and cost of the photo detector. PMTs operate at very low light levels and come in a variety of active area sizes. Taking into account these factors a cost effective, commercially available, small and compact PMT (analog mode) was selected as the photo detector for the portable chemiluminescence detector.

2.1.1.1 Experimental Set Up

The experimental set up mainly used in this thesis consisted of a photomultiplier tube (PMT) holder that encased the PMT (explained in detail in Section 2.1.1.3), electrodes

(explained in detail in Section 2.1.1.2), a potentiostat (explained in detail in Section 2.1.1.2), and a chart recorder to quantify and record the signal.
Figure 2.1 shows the overall instrument set up.

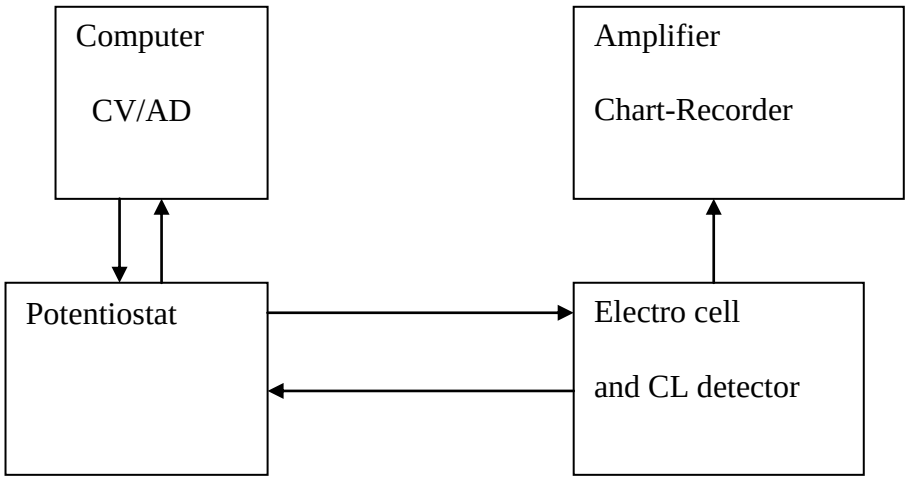

Figure 2.1: Schematic of ECL instrumentation used.

2.1.1.2 Potentiostat and Electrodes

The potentiostat (see Appendix I Figure 1.1) used to generate the electrical potential for this work was a Palm Sens Instruments device controlled by GPES software (Windsor Scientific Ltd, Slough, UK). The potential was applied to a three electrode system. The electrodes were held using 5 amp strip connecters, which were connected to the potentiostat *via* banana plugs both supplied through RS components, Corby, UK.
In experiments where iR may be high as demonstrated in this system a three electrode cell is preferable. The system is composed of the working electrode, auxiliary or counter electrode and reference electrode. Selection of a suitable working electrode is very important in voltammetry.

The first group of experiments (discussed in detail in Chapter 3) were carried out using a glassy carbon rod as a working electrode (i.d 1.0 mm). A platinum wire was used as the auxiliary electrode and a silver wire was employed as a reference electrode, all of them had the same large 2.0 mm i.d, Alfa Aesar, Karlsrühe, Germany, supplied the electrodes (see Appendix I Figure 1.2).

The second group of experiments (is discussed in detail in Chapter 4) were conducted in a conventional three electrode borosilicate glass with a flat bottom, using a 3.0 mm diameter glassy carbon electrode (GC-Typ, Methrom, Switzerland), as a working electrode nickel wire spiral electrode (Ni is a good and cheap substrate for H^+ reduction at the counter electrode when oxidation processes occur at the working electrode) as a counter electrode and a saturated calomel electrode (SCE, Radiometer, Copenhagen, Denmark) as a reference electrode (see Appendix I Figure 1.3).

2.1.1.3 Electrochemiluminescence Detector

The PMT holder (see Appendix I Figure 1.4) was designed and built in-house. It has basically two separated sections, a sample chamber and the PMT holder.

The sample chamber is the wider of the two sections. This section has a zero aperture iris diaphragm with 57 mm internal diameter (Edmund Optics Ltd, York, UK) allow to protect access to the PMT and the chamber in a lit environment. A quartz glass shield protects the diaphragm from liquid spillages (see Figure 2.2).

The PMT is a tube type 9789 (Thorn EMI, Ruslip, UK). The PMT is in turn attached to a power supply and a chart recorder *via* coaxial cables. The power supply for the PMT was a Thorn EMI model 3000R high voltage power supply (Thorn EMI, New York) running at 600 V.

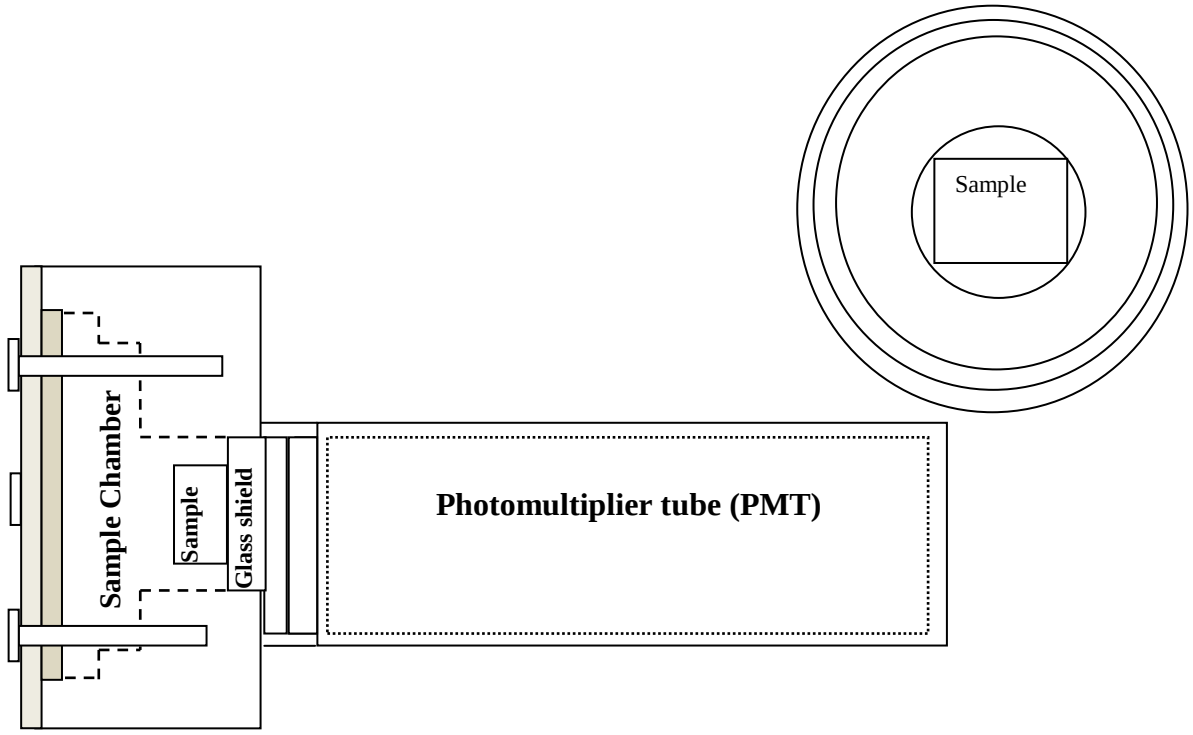

Figure 2.2: Chemiluminescence detector.

2.1.2 Portable Electrogenerated Chemiluminescence Detector

The portable chemiluminescence detection system was made up of a pressed steel box measuring externally 182 x 167 x 105 mm (168 x 140 x 98 mm internal dimensions), that was purchased from RS components (Corby, Northamptonshire, UK). In the absence of 'light background' signal is produced (unwanted output signal) due to thermal emission of electrons at the photo cathode and the dynodes. For the chemiluminescence detector this is 3 mV. The steel box provided a light tight housing for the PMT (Photomultiplier tube) to be situated in and removes interference from external light [3] (see Appendix I Figure 1.5).

The low power consumption photo sensor module (H5784) was obtained from Hamamatsu Photonics Ltd (Hertfordshire). The photo sensor module combines a 'Head-on'PMT (Part number R7400U) with a high voltage supply and signal processing electronics in a metal package (dimensions 22 x 22 x 60 mm). The PMT active area is 8 mm in diameter, providing a spectral response 300-6500 nm, with a peak wavelength of 420 nm. The system was designed with a variable gain dial, allowing the gain of the

PMT and therefore the sensitivity of the PMT to be adjusted. A 15 V power supply is required for the PMT, allowing it to be battery operated (four 9 V batteries). The system could be powered from the mains supply when used in the laboratory; this was used during method development stages of the research to reduce costs. For development purposes in the laboratory a chart recorder was used to record the chemiluminescence signal (Chessel Ltd., Worthing, Sussex). The height of the chemiluminescence response was measured on the chart recorder, which represents the maximum chemiluminescence emission.

To make the system portable and amenable to field use, the system was designed with a protective shutter for the PMT. This allows access to the samples whilst preventing it from being exposed to external light. The shutter was designed in order that it can only be opened when the box is properly shut and when sealed from external light. This is due to the position and configuration of the thread on the closing mechanism, which turns the direction of the shutter. Similarly, when the box is open, the shutter remains closed.

2.2 Reagents

2.2.1 Reagents Used for Electrogenerated Chemiluminescence Detector

The reagents used during these experiments were all analytical grade unless otherwise stated and the water was high purity de-ionised (18MΩ cm^{-1} resistivity) produced by an Elga Elgastat UHQ PS (High Wycombe, UK). Buffer solutions were adjusted using a Hanna instruments PHM2254 pH meter (Hanna Instruments, Kings Langley, UK) which was calibrated prior to use using pH 3.9, 6.4 buffer solutions provided by Aldrich (Gillingham, UK). The reagents used were as follows:

Codeine solution:

The codeine solution was made using a pH 3.9 (1 mM) acetate buffer (unless otherwise stated) as demonstrated by *Greenway et al* [4]. The codeine was obtained from Aldrich

(Gillingham, UK) and the acetate buffer solution was made using acetic acid and sodium acetate both supplied *via* Fisher Chemicals (Loughborough, UK).

Flunitrazepam (Rohypnol) solution:

The flunitrazepam solution was made using pH 3.9 (1 mM) acetate buffer however this proved was unsatisfactory as it will be discussed in Chapter 3. The flunitrazepam was obtained from Aldrich (Gillingham, UK) the buffer was produced using sodium acetate and acetic acid, both supplied from Fisher Chemicals (Loughborough, UK). It was also prepared in methanol/buffer mix, with the methanol obtained from Fisher Chemicals (Loughborough, UK).

Sol-gel fabrication:

The sol-gel solution was prepared by the acid catalysed sol-gel route as described in Chapter 1 where tetramethoxysilane (TMOS), water and 0.1M hydrochloric acid was mixed in an 8:5:0.25 ratio. The tetramethoxysilane (99 + %) was obtained from Aldrich (Gillingham, UK), the hydrochloric acid (37%) was obtained from Fisher Chemicals (Loughborough, UK).

On completion of dip coating (see Section 2.3.2 for the procedure) the electrodes were stored in pH 6.4 (0.1 M) phosphate buffer; this buffer was produced using sodium dihydrogen orthophosphate and disodium hydrogen orthophosphate, both supplied by Fisher Chemicals (Loughborough, UK). The pH 6.4 is the optimum value for keeping the coat electrodes.

Different concentrations of sodium hydroxide and lithium hydroxide (0.1, 0.5 and 1 M) were prepared. Sodium hydroxide was obtained from (Prolabo, France) and lithium hydroxide was obtained from Fisons Scientific (Loughborough, UK).

2.3 Procedures

2.3.1 Electrochemical Measurements

Both cyclic voltammetry and pulsed amperometric detection were used for making measurements. The potentiostat was very flexible and could be programmed to deliver selected voltages at given times. There were certain set voltages that could be applied.

2.3.2 Coating Procedure for a Sol-Gel

The electrode must be polished before and after each experiment. First of all the surface of all the three electrodes was rinsed with high purity water and was carefully dried with a wipe. The working electrode is very important in voltammetry, therefore this electrode was polishing as it follows:

1. The electrode is washing with purified water.
2. A wipe with Kemet Fluid, Type Os (Kemet international ltd., Kent, U.K) was used to polish the electrode.
3. The electrode was rinsed with purified water.
4. Finally, was dried with a wipe.

Glassy carbon rod electrodes were used for the sol-gel coating work. Three separate types of sol-gel were used; a blank sol-gel, one containing $Ru(bpy)_3^{2+}$ and one containing a derivative (it will be discussed in detail in Chapter 3). After at least one hour after preparation of the sol-gel the working electrode was dip coated in the sol-gel solution and allowed to age in pH 6.4 phosphate buffer solution overnight. In the case of the sol-gel containing $Ru(bpy)_3^{2+}$ then it was initially mixed again under stirring to allow for thorough mixing before coating.

With regards to the dip coating (see Figure 2.3) the working electrode was withdrawn from the sol-gel manually with a withdrawal rate of approximately 5cm/min leaving a thin sol-gel coating on the electrode's surface. Small amounts of water and methanol were evaporated from the surface during this process, as the sol-gel continued to hydrolyse and condense. The sol-gel thicknesses was determined using SEM and a micrometer, the thicknesses varied from 30 to 60 μm as discussed in detail in Chapter 3.

The sol-gel is taken place in the small vial and is coated as it shown in the Figure 2.3**.**

The coating procedure is shown to following:

1- Leave for 15 min at room temperature.
2- Just dip coat electrode.
3- If the electrode is left for an hour in the solution, the solution gets sticky as the water and methanol evaporates. When the electrode is then put in contact with buffer solution, the film drops off.
4- Leave the dip coated electrodes overnight in pH = 6.4.

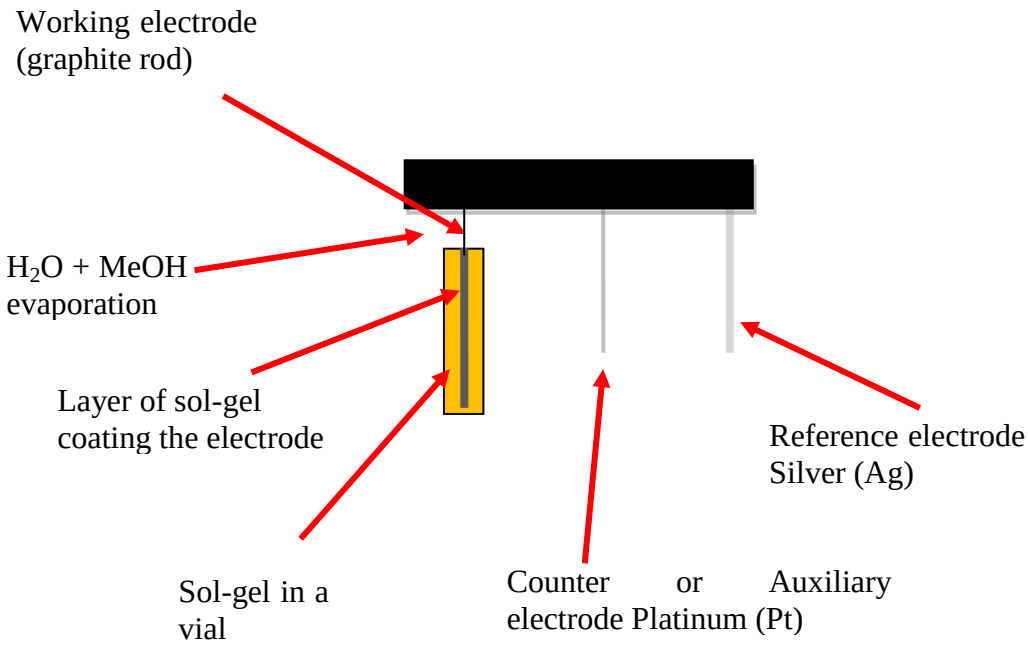

Figure 2.3: Coating procedures.

2.3.3 Electrode Polishing and Coating Procedures for the Formation of Droplets in the Electrode

The electrode must be polished before and after each experiment.

Preparation of droplet-modified electrodes

For the experiments in Chapter 4, the electrode was coated with oil micro droplets.

The glassy carbon working electrode was modified with trioctylamine microdroplets by solvent evaporation of an aliquot of *ca.* 1 mM redox oil dichloromethane solution. Before being immersed, this droplet-modified electrode was inverted and held over the degassing aqueous phase for at least ten minutes (so as to remove oxygen from the oil phase). The electrode was cleaned by rinsing with dichloromethane and polishing on a napped polishing cloth using 0.3 mm alumina slurry (Presi, France) immediately prior to experimentation.

Trioctylamine (TOA) was obtained from Fluka (Loughborough, UK). Dichloromethane was obtained from Fisher Chemicals (Loughborough, UK).

The physical properties of TOA are described as follows:
$C_{24}H_{51}N$, molecular weight = 353.68 g mol^{-1}, density = 0.810 g cm^{-3} and solubility = 0.1 g mol^{-1}

The TOA is oil therefore the surface of the working electrode is hydrophobic modified. (see Figure 2.4).

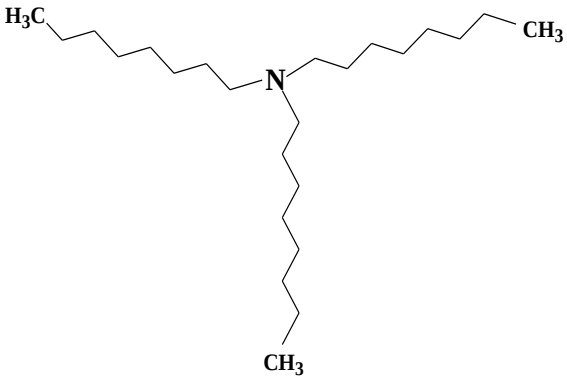

Figure 2.4: Structure of Trioctylamine.

Previous work in both experiments and modelling[5-8] suggests that, the amount of Oc_3N on the electrode, droplets radii are typically 10 µm, affording a global droplets coverage of [9] *ca.* 0.1, and average inter-droplet distances within random distribution[9] of approximately 10 µm.

2.4 Conclusions

This chapter summarises some of the general techniques that have been used in experiments included in this thesis.

Further experimental details are providing in the relevant sections.

2.5 References

1. A. K. Campbell, *Chemiluminescence. Principles and Applications in Biology and Medicine*, Chichester, 1998.
2. *For more information see www.Hamamatsu.com*.
3. L. Marle and G. M. Greenway, *Anal. Chim. Acta*, 2005, **548**, 20.
4. G.M. Greenway and A. W. Knight, *Analyst*, 1995, **120**, 2543.
5. B.A. Brookes, T.J. Davies, A.C. Fisher, R.G. Evans, S.J. Wilkins, K. Yunus, J.D. Wadhawan and R. G. Compton, *J. Phys. Chem. B*, 2003, **107**, 1616.
6. J.D. Wadhawan, R.G. Evans, C.E. Banks, S.J. Wilkins, R.R. France, N.J. Oldham, A.J. Fairbanks, B. Wood, D.J. Walton, U. Schröder and R. G. Compton, *J. Phys. Chem. B.*, 2002, **106**, 9619.
7. T.J. Davies, A.C. Garner, S.G. Davies and R. G. Compton, *J. Electroanal. Chem.*, 2004, **570**, 171.
8. T.J. Davies, A.C. Garner, S.G. Davies and R. G. Compton, *Chem. Phys. Chem.*, 2005, **6**, 2633.
9. T.J. Davies, B.A. Brookes, A.C. Fisher, K. Yunus, S.J. Wilkins, P.R. Greene, J.D. Wadhawan and R.G. Compton, *J. Phys. Chem. B*, 2003, **107**, 6431.

Chapter 3

Development of a reagentless portable system for analysing drugs

3.0 Aims of the Chapter

The application of reagents immobilised within a sol-gel as an electrode coating is investigated, with comparison studies being performed on bare electrodes. These studies were performed for the analysis of drugs using an electrochemically chemiluminescent technique. This was based on the reaction between tris (2,2'-bipyridyl) ruthenium (III) dichloride hexahydrate $Ru(bpy)_3^{3+}$ and tertiary amine containing drugs, a well established reaction that was discussed in detail in Sections 1.12 and 1.13 (Chapter 1).

During the ECL (Electrochemiluminescent) reaction $Ru(bpy)_3^{2+}$ is not consumed but is rather cycled between $Ru(bpy)_3^{2+}$ and $Ru(bpy)_3^{3+}$. To remove the requirement of adding any reagent to the system the $Ru(bpy)_3^{2+}$ can be immobilised onto the working electrode. This creates a sensor that requires the addition of the sample only. Sol-gels were investigated as the immobilisation technique since they allowed the diffusion of molecules through the silica network and reactions could still take place. The sol-gels process involved low temperature hydrolysis of suitable monomeric precursors. The silica matrix was normally formed by hydrolysis of an alkoxide precursor (tetramethyl orthosilicate), catalysed by an acid or base, followed by condensation to yield a polymeric oxobridged SiO_2 network (as was explained in detail in Section 1.14).

3.1 Drugs of Abuse

The drugs of abuse investigated were codeine and rohypnol (flunitrazepam). These compounds were chosen as "drugs of abuse" as they well characterised and are structurally similar to other more hazardous and difficult to obtain drugs (see Figure 3.1) such as cocaine, lysergic acid and morphine all of them having in common a tertiary amine group. Tertiary amine compounds also have other uses apart from pharmaceuticals including pesticides and surfactants, therefore a sensitive analytical method for their detection is obviously desirable.

a) Indole Alkaloids

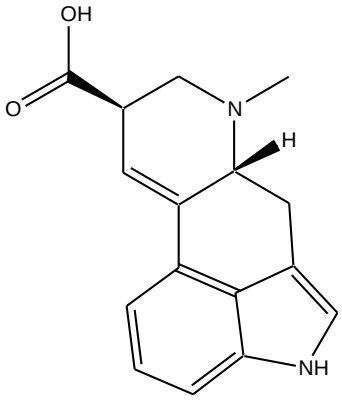

Lysergic acid

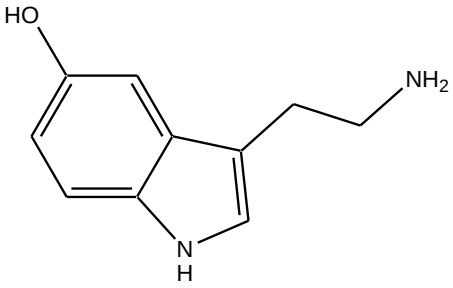

Serotonin

b) Tropane Alkaloids

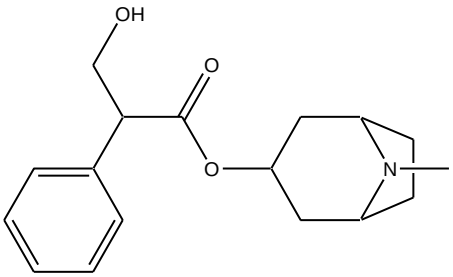

Atropine

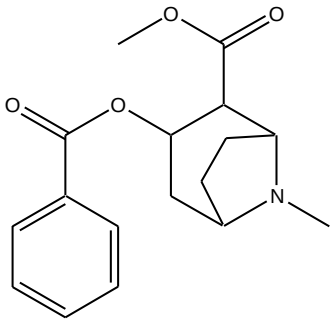

Cocaine

c) Isoquinoline Alkaloids

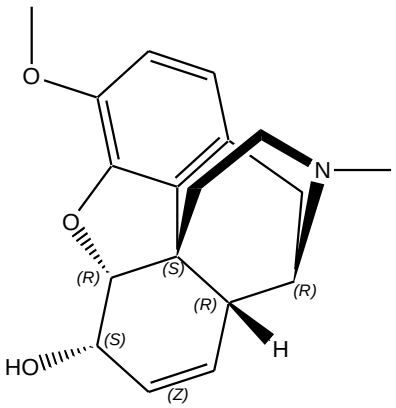

Codeine

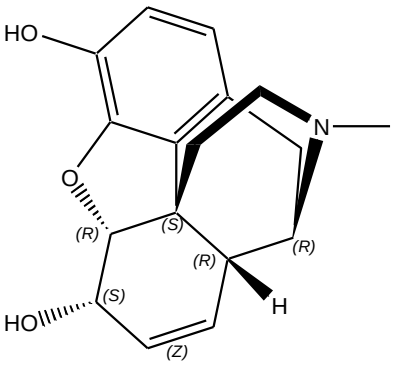

Morphine

Figure 3.1: Molecular structures of a range of alkaloids.

Figure 3.1: shows a range of compounds that can be divided in three separate groups. The first class, the indole alkaloids includes lysergic acid (LSD is the *N,N-diethylamide* of this compound) and serotonin. Other compounds in this group include psilocine (the psychoactive ingredient in magic mushrooms) and bufotenin (the psychoactive ingredient in cahobe beans). In this group serotonin is included, this is an essential neurotransmitter in the central nervous system (CNS), and the other indole alkaloids listed mimic its behaviour due to their structural similarities; hence causing the ill effects such as mental problems (schizophrenia) and hallucinations[1] associated with the compounds.

The second type of compounds are the tropane alkaloids, cocaine and atropine are examples of this group. Their structures are very similar. Cocaine is a stimulant of the central nervous system and also a local anaesthetic.

Atropine is derived from black henbane (*Hyoscynami folium)* and the berries of deadly nightside (*Atropa belladonna).* Historically it has been used as a poison and a pupil dilating agent. It is also employed as an antidote to organophosphate nerve agents.

The third group of compounds are isoquinoline alkaloids. Codeine and morphine have similar structure and both of them are derived from the unripened seed pods of the opium poppy (*Papaver somniferum).* Morphine and codeine are naturally present although codeine is usually present in small amounts, so is normally synthesised from morphine.

Codeine which is used extensively in this work is a methyl ethyl ether of morphine. Codeine is a painkiller like morphine, it is also often used as a cough suppressant. It is normally used in combination with other pharmaceutical pain killers such as paracetamol, ibuprofen and aspirin where it is easily adsorbed through the gastrointestinal tract. However to generate pain relief the human body must convert codeine to morphine using the enzyme cytochrome P4502D6, which typically has a conversion rate of only 10 % [2-4].

The compounds from Figure 3.1 are typically analysed by using the following methods GC-MS[5-9] (Gas Chromatography-Mass Spectrometry), HPLC-UV (High Performance

Liquid Chromatography-Ultraviolet), HPLC-MS (High Performance Liquid Chromatography-Mass Spectrometry), SERS[10-13] (Surface Enhanced Raman Spectroscopy) or LC-MS[14] (Liquid Chromatography-Mass Spectrometry). Some tertiary amines are extremely difficult to derivatise but they can be determined by ECL reaction with Ru $(bpy)_3^{2+}$, without prior derivatisation.

The analysis of flunitrazepam was also investigated. It is an anxiolytic and hypnotic drug know better under the name rohypnol which is normally administered as a short term treatment for sleeping disorders such as insomnia[15].

Rohypnol (flunitrazepam) is used illegally as a "date rape drug" by spiking into alcoholic drinks above the recommended pharmacological dose of 0.5-1 mg in adults[15] to produce a prolonged and extreme intoxication. The sedative effect of the drug is increased by alcohol consumption which creates marked psychomotor impairment and causes the victim to suffer from a "blackout", a type of a short term amnesia that prevents the victim from recalling much if any of the attack. The symptoms generally begin half an hour after ingestion and peak approximately two hours after ingestion. The following day the effects of the drug may be felt and include drowsiness, light-headedness, confusion and ataxia (lack of muscle coordination). Its low dosage and high biotransformation makes its analysis very problematic because it is so rapidly cleared out from the body[16, 17].

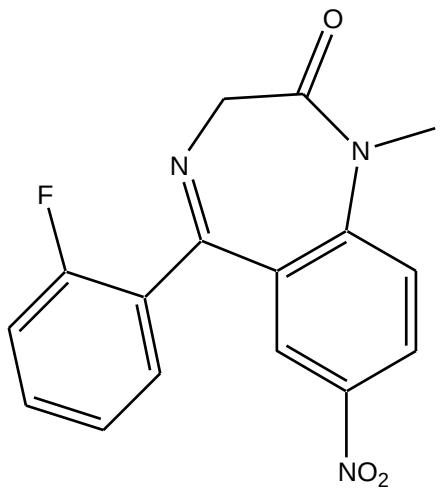

Figure 3.2: Structure of rohypnol (flunitrazepam).

Rohypnol is a benzodiazepine, it is generally analysed by using immunoassays or GC-MS[18-20] methodologies involving blood/serum and urine analysis. Oral fluid analysis has also been performed. Wang *et.al*[19] found that typical benzodiazepine immunoassays have a broad cross reactivity towards widely prescribed benzodiazepines and also found that due to the low dosage of the drug these systems lead to an unacceptable number of false negatives.

A number studies with regards to GC-MS analysis have attempted to analyse rohypnol or its major metabolite 7-aminoflunitrazepam in blood urine, saliva and hair[18-20]. The low dosage and high distribution is one of the problem with the analysis of rohypnol in biological samples by using GC-MS. The limit of detection were determined to be 0.1μg/dL in 1 ml of blood[21] and for saliva 0.05 μg/L[22] when a tablet of 1mg of rohypnol was taken. The drug was detectable, but at extremely low concentrations, for 6 hours after intake of a normal dose of rohypnol, in plasma was not detected.

As can be seen from Figure 3.2, rohypnol has a tertiary amine containing structure and therefore may exhibit ECL like codeine.

3.2 Selection of the Experimental Conditions

3.2.1 Selection of Ru $(bpy)_3^{2+}$ Concentration

Selection of the correct concentration of tris (2,2'-bipyridyl) ruthenium(II) dichloride hexahydrate is an important factor to be considered. A number of factors needed to be considered. The amount of $Ru(bpy)_3^{2+}$ used should be sufficient to produce a good and stable luminescent signal without excessive self-quenching occurring (*i.e.,* external conversion) but it should not be excessive due to reagent cost.

Examining the level of $Ru(bpy)_3^{2+}$ typically used in similar studies by others groups [23-29] it was found that the common concentration of $Ru(bpy)_3^{2+}$ used in these studies was $1x10^{-3}$ M. Obviously a greater concentration of $Ru(bpy)_3^{2+}$ will give a stronger ECL signal until self-quenching becomes an issue. It was decided to use a $Ru(bpy)_3^{2+}$ concentration of $1x10^{-3}$ M in this work.

3.2.2 Designing the Electrochemical Cell

In the next section different aspects that may affect the results of the experiments were carefully studied, such as: polishing of the electrode and ohmic losses (this can be reduced by decreasing the electrode separation and enhancing the ionic conductivity of the electrode).

Ohmic Polarization: Ohmic losses occur because of resistance to the flow of ions in the electrolyte and resistance to flow of electrons through the electrode. The dominant ohmic losses through the electrolyte are reduced by decreasing the electrode separation and enhancing the ionic conductivity of the electrolyte. Because both the electrolyte and fuel cell electrodes obey Ohm's law, the ohmic losses can be expressed by the equation $E_{ohm} = iR$ where i is the current flowing through the cell, and R is the total cell resistance, which includes electronic, ionic, and contact resistance.

Polishing is essential to keep the surfaces of electrodes clean and it also ensures more active surfaces and longer lifetimes for the electrodes. Depending on the variation of usage, methods, and compositions, for maximum results, it is recommended that the electrode is polished regularly especially when the voltammetric data begins to deteriorate. The most common preparation procedure for the preparation of the glassy carbon rod electrode [30-32] is explained in detail in Chapter 2. For example the relatively large surface area of activated carbon (AC) compared to glassy carbon (GC) electrode results in preferential adsorption of solvent or electrode impurities on the activated carbon (AC) rather than the glassy carbon (GC) surface. During the process of developing chemical modifications for polished glassy carbon (GC) surfaces, exposure to organic solvents could clearly be seen to effect electron transfer (ET) kinetics, impurities in reagent grade solvents may adsorb on the glassy carbon.

This is one of the reason why glassy carbon (GC) was used instead of activated carbon (AC) for our experiments.

Preliminary experiments were carried out with the electrode cell shown in Figure 3.3.

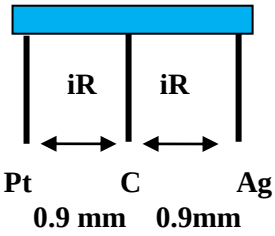

Figure 3.3: Shows the position and distance between the electrodes in a three electrode cell used in this Chapter.

Figure 3.3 illustrates how the electrodes were positioned when the experiment was carried out to obtain a good reproducibility.

As would be expected for reproducible results the electrodes had to be well polished and tightly held in place.

3.2.3 The Selection of the pH

The aim of this section was to study the pH in which is obtained the maximum values of ECL response. The ECL measurements were made using the apparatus described in Section 2.1.1.3.

The applied voltage and pH have been shown to be the most important factors on obtaining ECL response. The applied voltage was studied by Knight *et al*.[29] and it was concluded that the maximum ECL response was obtained between + 0.5 V and + 1.3 V.

With this in mind a linear potential sweep was applied between + 0.5 to + 1.5 V to the working electrode and the emission of chemiluminescent light was detected (see Figure 1.1 with the potentiostat and chart recorder in Appendix I).

Another important factor to be considered is the effect of buffer solutions. Buffer serves two purposes, it provides a means of controlling pH, and allows electrical conductivity between the electrodes in the cell. In order for the ECL reaction to proceed, there must be sufficient electrolyte to allow conductivity at the electrode; however excessive concentrations of electrolyte could inhibit ECL reactions[33, 34]. The relationship between

buffer concentrations and the ECL intensity was previously investigated by Knight *et al.*[29] and it was reported that an enhancement of the ECL response occurred in acetate buffer.

As expected from previous studies the pH of the reagents required to be carefully selected in order to obtain maximum chemiluminescent emission. With this in mind all the solutions were prepared in acetate buffer. A 1 x 10^{-3} M of codeine standard and tris(2,2'-bipyridyl)ruthenium(II) chloride hexahydrate 1x 10^{-3} M was prepared in acetate buffer 1x 10^{-3} M and used to optimise the required pH for the reaction. As can be seen from Figure 3.4 the maximum current intensity was observed at pH 3.9, with a value of 225μA, these values are correlated with the emission of ECL (where it has been observed in Figure 3.5).

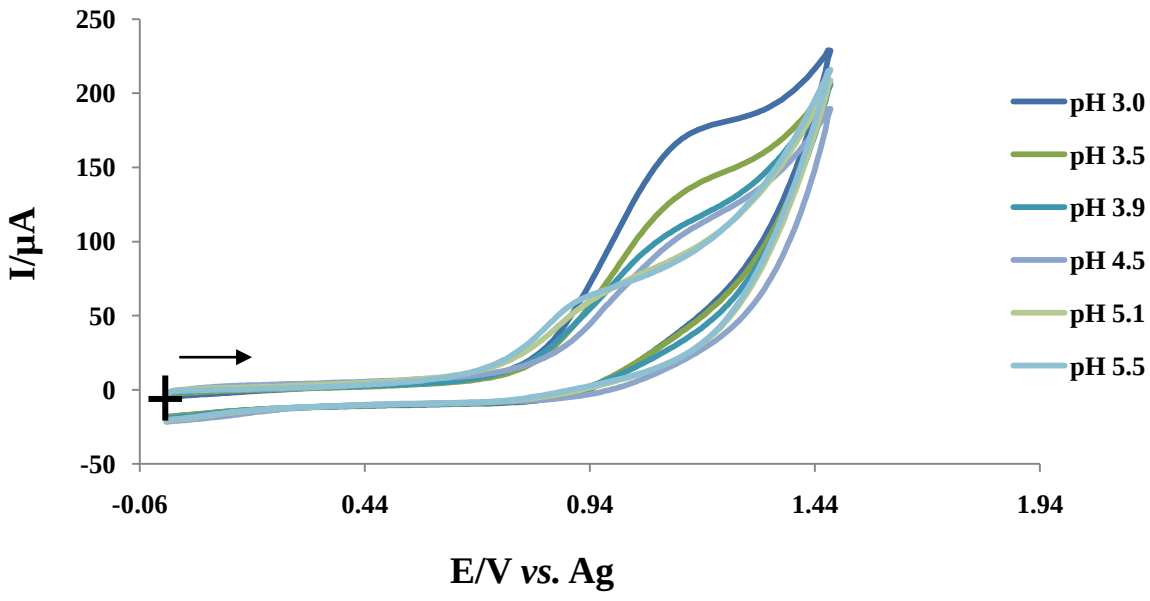

Figure 3.4: Voltammograms in a range of pH between 3.0 and 5.5 in a solution of 1x10^{-3} M codeine, 1x10^{-3} M $Ru(bpy)_3^{2+}$ and 1x10^{-3} M acetate buffer. The cross-lines indicate the point of origin and the arrow shows the direction of the initial potential sweep.

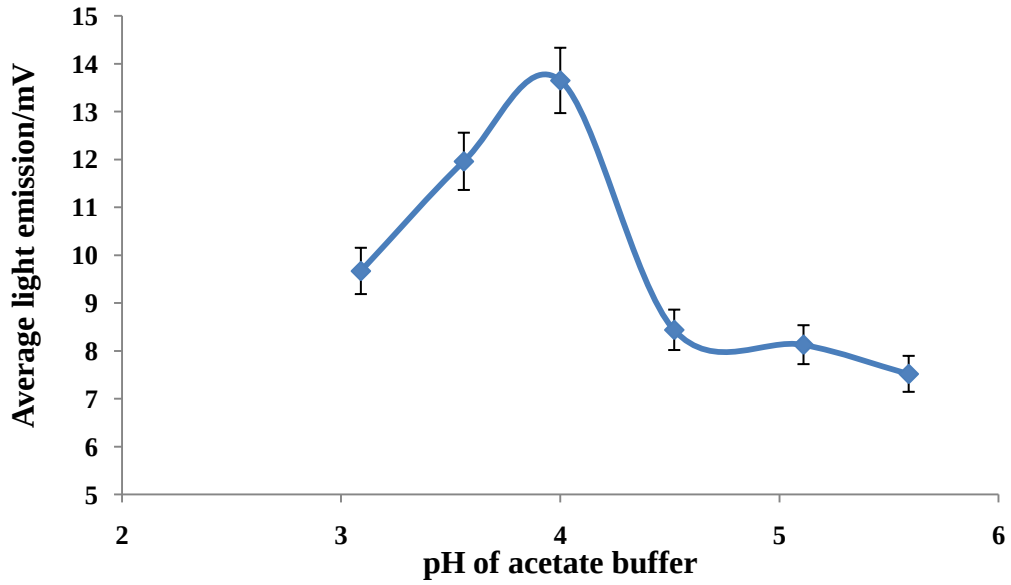

Figure 3.5: pH effect on ECL.

Figure 3.5 shows the effect of pH on the ECL signal for the reaction between 1 x 10^{-3} M codeine and 1 x 10^{-3} M $Ru(bpy)_3^{2+}$ in 1 x 10^{-3} M acetate buffer. This process was replicated three times for each different pH. As can be seen from Figure 3.5, acetate buffer of approximately pH 3.9 was found to produce the highest intensity.

The reason for the pH effect in this reaction is uncertain, however the oxidation of tertiary amines (codeine) has been shown from previous electrochemical studies to produce a short lived radical cation, this is then followed by deprotonation of the α-carbon to form a strongly reducing intermediate [35]. This intermediate is however the source of chemical energy to produce, by reduction of $Ru(bpy)_3^{3+}$, the excited state of $Ru(bpy)_3^{2+}$ in the ECL reaction. There is also evidence of the existence of the highly reactive intermediate due to the light emission.

Therefore, this mechanism is consistent with the observations of the affect of pH on ECL intensity, where the pH must be basic enough to deprotonate the amine radical ion in order for the ECL reaction to proceed.

3.2.4 Effects of the Scan Rate

All the experiments were carried out with a glassy carbon rod electrode (as a working electrode). The solutions tested with $1x10^{-3}$M $Ru(bpy)_3^{2+}$ using $1x10^{-3}$ M of codeine as a model compound in 1 x 10^{-3} M acetate buffer at pH 3.9. During this work the electrode potential was controlled by the Palm Sens computer controlled system as discussed in Chapter 2. The potential levels were initially established using cyclic voltammetry from setting based on literature studies[25, 26]. Figure 3.6 shows voltammograms covering a range of scan rates from 0.005 to 0.25 V/s. The voltammogram observed is one electron process. Two peaks can be detected (oxidation-reduction) due to the reaction between $Ru(bpy)_3^{2+}$ and codeine (explained in detail in Chapter 1). With regards to cyclic voltammetry different scan rates were analysed and correlated against the ECL signal as shown in Figure 3.6. In order to develop the maximum sensitivity the scans were used to evaluate the correct setting for the potentiostat. The ECL results obtained are shown in Table 3.1.

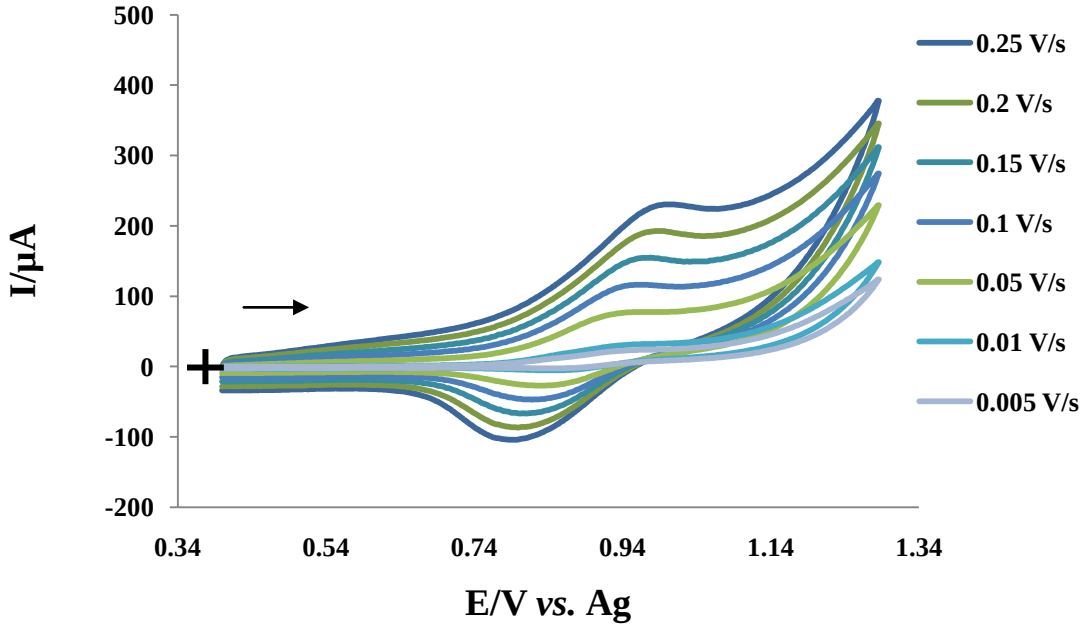

Figure 3.6: Voltammograms for scan rates between 0.005 and 0.25 V/s in a solution of $1x10^{-3}$ M codeine, $1x10^{-3}$ M $Ru(bpy)_3^{2+}$ and $1x10^{-3}$ M acetate buffer at pH 3.9. The cross-lines indicate the point of origin and the arrow shows the direction of the initial potential sweep.

Scan Rate (V/s)	Replicate 1 ECL emission (mV)	Replicate 2 ECL emission (mV)	Replicate 3 ECL emission (mV)	Average ECL emission (mV)	Standard deviation	%Relative standard deviation
0.25	16.85	16.82	16.77	16.81	0.04	0.24
0.20	14.61	14.57	14.54	14.57	0.03	0.24
0.15	11.87	11.84	11.79	11.83	0.04	0.34
0.10	9.70	9.66	9.56	9.64	0.07	0.75
0.05	7.18	7.14	7.12	7.15	0.03	0.43
0.01	4.61	4.53	4.51	4.55	0.05	1.16
0.005	3.98	3.94	3.93	3.95	0.03	0.67

Table 3.1: The change in ECL emission as a function of the scan rates for a single electrode replicated three times.

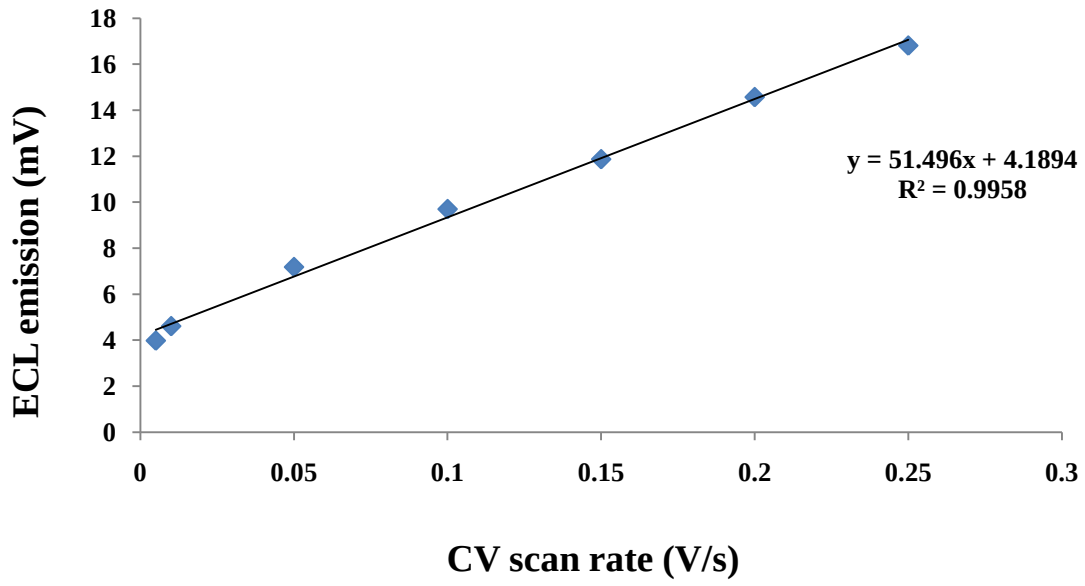

Figure 3.7: The effects of scan rate on ECL intensity. Scan Rate: 0.005, 0.01, 0.05, 0.10, 0.15, 0.20 and 0.25 V/s. Conditions: solution of $1x10^{-3}$ M codeine, $1x10^{-3}$ M $Ru(bpy)_3^{2+}$ and $1x10^{-3}$ M acetate buffer at pH 3.9.

Figure 3.7 shows that as the scan rate (ν) increases the ECL signal increases. When ν increases the flux of material to the surface increase, therefore $sin\frac{dc}{dx}$ increase so i_p increases, thus increasing then ECL signal. A lower scan rate was however chosen to

allow multiple scans at lower concentrations without the signal reducing effects of analyte diffusion. When working with sol-gel coated electrodes it was found by Collinson *et al.*,[36] that at lower analyte concentrations the analyte may not diffuse sufficiently quickly to the electrode surface from the bulk solution before subsequent scans.

With this in mind 0.1 V/s was chosen as a model scan to carry out all our experiments.

3.3 ECL Detection of Rohypnol

It would be very useful to be able to have a portable system for the detection of rohypnol. As mentioned previously rohypnol (flunitrazepam) is a white solid, with a melting point of between 166-167°C, a molecular weight of 313.3 g/mol solubility of 11 µM and pKa is 1.8. The ECL method utilised for codeine was applied to rohypnol using the portable ECL detection system described in Chapter 2. Due to the poor solubility of rohypnol it was dissolved in 60% methanol, 40% acetate buffer pH 3.9 and 5µM Ru $(bpy)_3^{2+}$ but otherwise the same experimental conditions were used as for codeine.

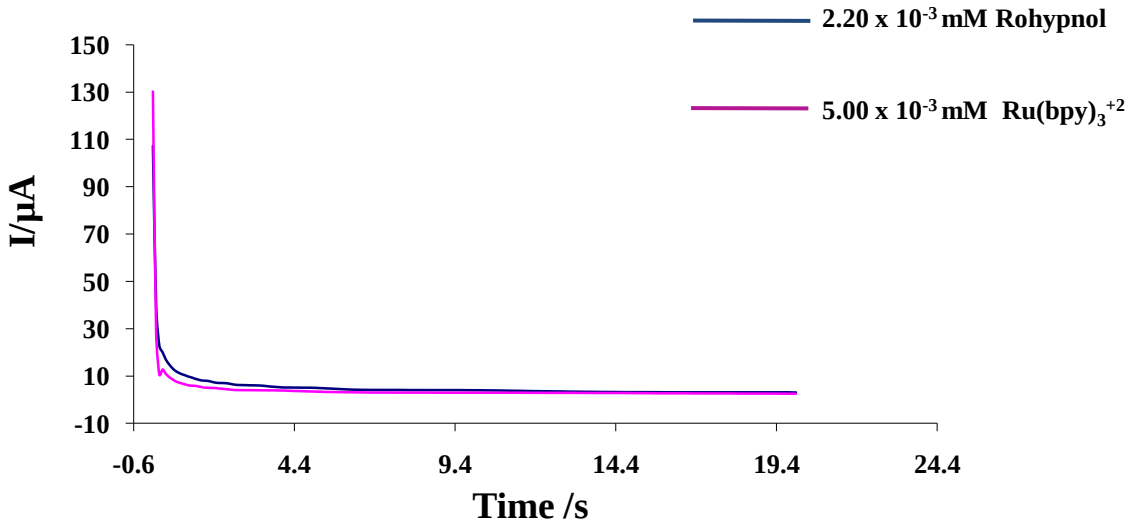

Figure 3.8*:* Comparison between $Ru(bpy)_3^{2+}$ on its own and with the addition of 2.2 µM rohypnol.

From Figure 3.8 it can be seen that an enhancement of the current intensity was obtained in the presence of the tertiary amine (rohypnol).

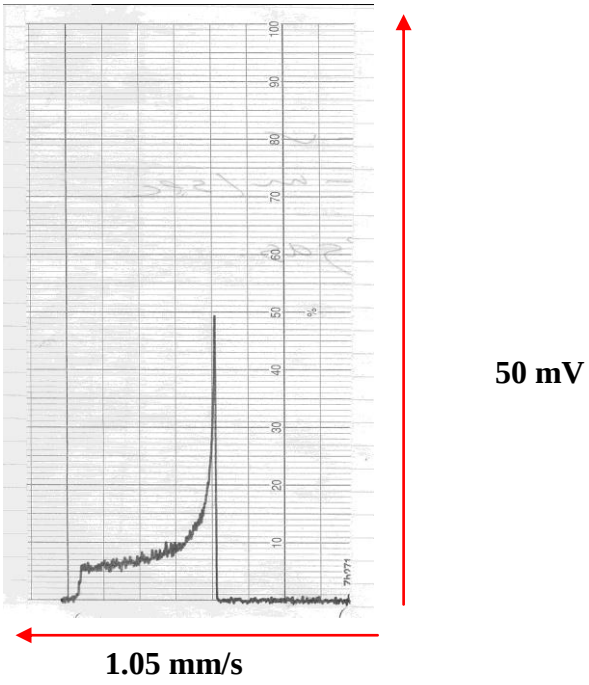

Figure 3.9*:* ECL signal recorded by chart recorder (axis X shows time(s) and axis Y shows signal intensity in (mV)) 2.2 µM. (25.10 mV) (36s).

Figure 3.9 shows when the voltage was applied, the current (t = 0 s) to 19 s there was no signal. After 19 s a signal appears. Therefore this signal can be explained in terms of producing ECL from a redox reaction of $Ru(bpy)_3^{2+}$ and activation of rohypnol. After the application of a voltage the signal decreased dramatically. This can be explained in terms of catalytic response.

Rohypnol (µM)	Replicate 1 ECL emission (mV)	Replicate 2 ECL emission (mV)	Replicate 3 ECL emission (mV)	Average ECL emission (mV)	Standard deviation	%Relative standard deviation
2.2	25.15	25.10	25.05	25.10	0.05	0.20
1.1	16.96	17.00	16.94	16.97	0.03	0.18
0.11	11.94	11.90	11.82	11.89	0.06	0.51
0.011	10.72	10.69	10.63	10.68	0.04	0.43
Blank	5.90	6.01	5.95	5.95	0.05	0.92

Table 3.2: The change in ECL emission as a function of the rohypnol concentration for a single electrode replicated three times.

Table 3.2 shows that the ECL signal increase is proportional to the concentration of rohypnol as can be seen from the Figure 3.10. A blank solution was also studied with 5µM Ru $(bpy)_3^{2+}$ made up in 40% acetate buffer pH 3.9 and 60% methanol.

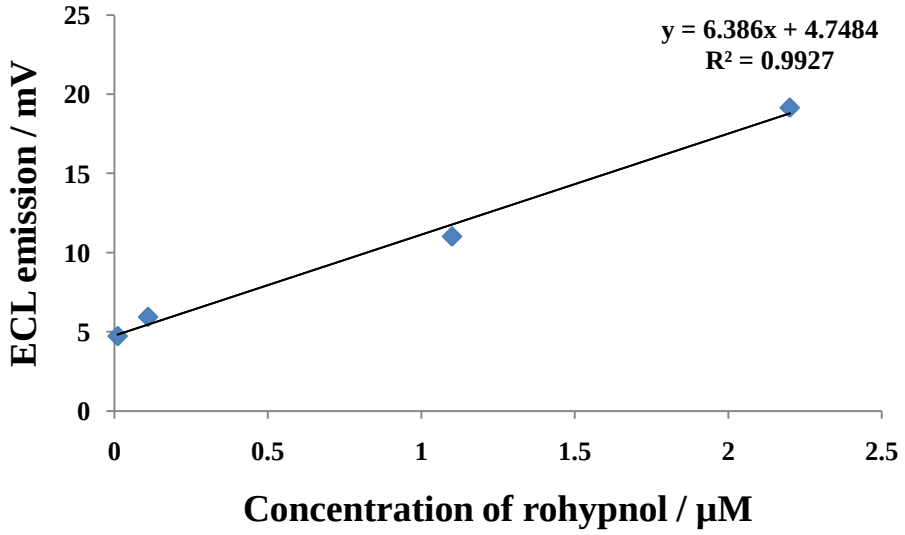

Figure 3.10: The effects of rohypnol concentration on ECL emission (blank was subtracted).

The intensity of the signal obtained was lower than that obtained for codeine. A direct comparison could not be made because methanol depress the ECL signal. Alternative methods need to be found for insoluble drugs and the work described in Chapter 4 begins to address this problem.

3.4 Sol-Gel Coated Electrode

In the next part of the work the effects of sol-gel coating electrodes were investigated. $Ru(bpy)_3^{2+}$ was encapsulated within the sol-gel. In these experiments an electrochemical method (CV) was used to characterize the diffusion coefficient *D* of the redox probes trapped in the hydrated sol-gel derivated materials[37-39]. The gel matrix basically serves as a solid electrolyte, offering a medium for the movement of redox species and ions and provides a simple way to encapsulate in stable host matrix[40, 41]. Interestingly the coatings used for this work had a desirable effect on the sensitivity of the method.

There are many advantages of using a sol-gel coating. Firstly, the surface area of the electrode is effectively increased, due to the porous nature of the sol-gel, which in turn, results in a higher ECL signal than the bare electrode as described in detail in Section 3.4.3. Secondly, sol-gel materials also offer better optical transparency properties, stability and permeability than many organic polymers.

The encapsulation of $Ru(bpy)_3^{2+}$ in a sol-gel and the sol-gel preparation is described in detail in Chapter 2.

To elucidate the electrochemical mechanism occurring at a glassy carbon rod electrode (working electrode), cyclic voltammetry was performed. Between analysis, the electrodes were stored in pH 6.4 (0.1 M) phosphate buffer in order to prevent drying and damage of the sol-gel coating.

3.4.1 Sol-Gel Coating on Metals Electrodes

In this part of the work metal electrodes were initially investigated and the coating of the electrodes is described.

The immobilisation method described by Collinson *et al.*,[42, 43] was investigated on platinum and silver. However, the conditions described in their work could not be repeated as the sol would not go clear and gelation occurred within 5 min of mixing rather than the 1 hour that was stated. This was not surprising considering the high concentration of acid that was described.

Figure 3.11 illustrates the voltammograms for the analysis of codeine $1x10^{-3}$M with the entrapment of $1x10^{-3}$M $Ru(bpy)_3^{2+}$ in a sol-gel with acetate buffer $1x10^{-3}$M at pH 3.9. Platinum and silver electrodes were coated with and employed in this experiment as a working electrode (WE).

A single electron curve was expected with two peaks, an oxidation and reduction peak due to the redox mechanism between $Ru(bpy)_3^{2+}$ and the tertiary amine codeine. The voltammogram observed for silver was straight and no electrochemical behaviour was observed because the sol-gels would not adhere to the metals. Peaks were observed for the voltammogram obtained with the platinum electrode. The peak observed at 0.72 V was very low for an oxidation peak and a reduction peak was not observed. Again the sol-gel did not adhere well to the platinum and although the platinum electrode was slightly better than silver, due to the poor coating of the electrode it was decided not to use metal electrodes. The reason for this effect is not fully understood as the electrodes were prepared using emery paper and diamond paste to remove any oxide layer present and therefore avoid passivation effect.

The coating of glassy carbon rod electrodes was then investigated for the working electrode.

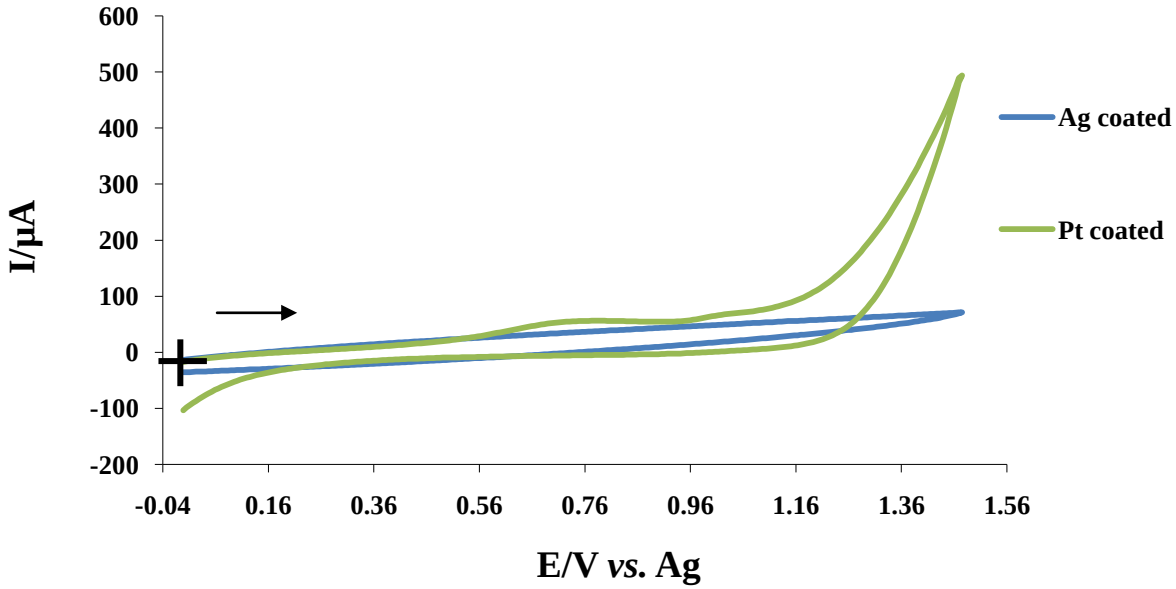

Figure 3.11: Voltammograms using metal electrodes (Ag and Pt) as a working electrodes coated in sol-gel immobilised $Ru(bpy)_3^{2+}$ $1x10^{-3}$ M in a solution of $1x10^{-3}$ M codeine and $1x10^{-3}$ M acetate buffer at pH 3.9 and 0.1V/s. The cross-lines indicate the point of origin and the arrow shows the direction of the initial potential sweep.

3.4.2 Sol-Gel Coating on Glassy Carbon Electrodes

When the glassy carbon rod was coated with a sol-gel as described in Chapter 2, a much more even and reproducible coating could be obtained as compared with the metal electrodes. Only one method of preparation was investigated as Collinson *et al.*,[44] investigated different sol-gel preparations for coating glassy carbon electrodes but no significant difference in the stability of the silica films was observed.

The thickness of the sol-gel coating on the glassy carbon rod electrode, provided by the method utilised, was investigated. Two methods were used to verify the thickness, these were SEM (Scanning Electron Microscopy) and direct measurements with a micrometer gauge.

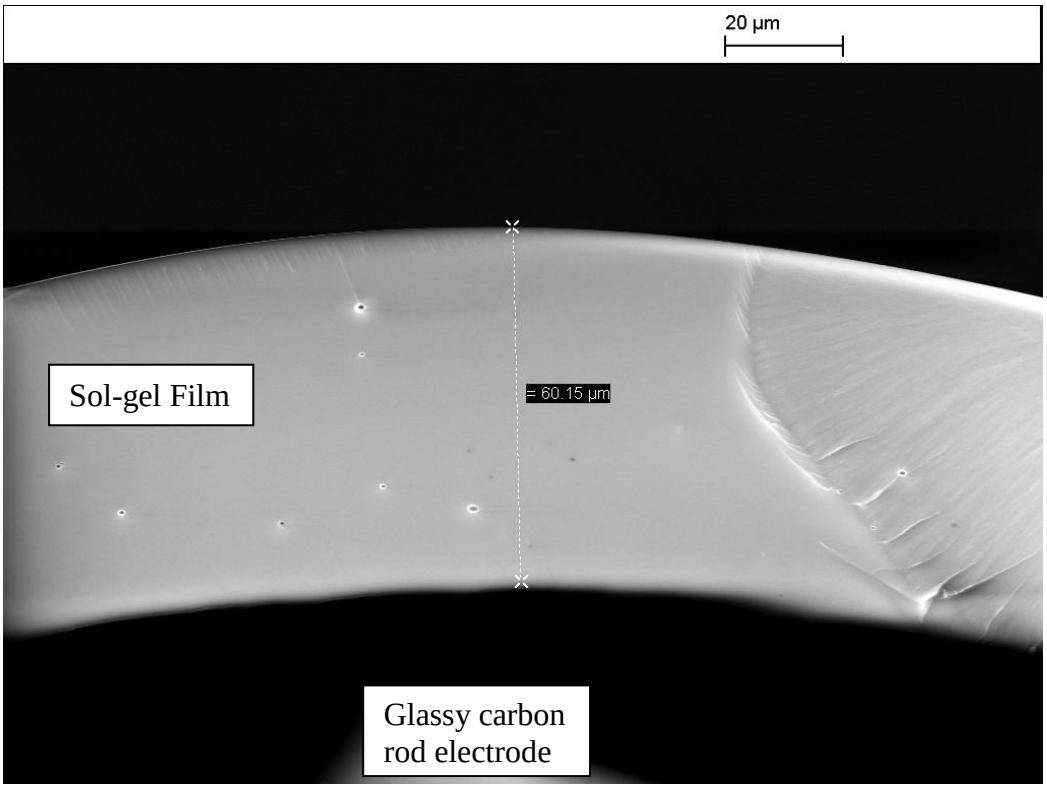

Figure 3.12: A SEM of a glassy carbon electrode coated with the sol-gel used in this work.

Figure 3.12 shows the SEM of a glassy carbon electrode coated with sol-gel. Measurements were taken in several positions and the thickness of the sol-gel was found to vary from approximately 60 µm to less than 1 µm. However, when the coated electrode was introduced into the SEM a vacuum was applied and this lead to some of the sol-gel separating from the electrode surface due to dehydration which made measurement difficult and therefore the SEM measurements were verified using a micrometer gauge.

Accordingly, the thickness of the glassy carbon rod with and without the coating was directly measured. Three measurements were made along the length of the electrode before and after the coating, for four different coatings. The electrode was cleaned and polished in between experiments.

Glassy carbon rod	Replicate 1 (µm)	Replicate 2 (µm)	Replicate 3 (µm)	Mean (µm)	Standard deviation	% Relative Standard deviation
Without coating (1)	960	970	980	970	10	1.03
With coating (1)	990	1000	1010	1000	10	1.00
Without coating (2)	960	970	980	970	10	1.03
With coating (2)	1000	1010	1000	1003	5.77	5.75
Without coating (3)	960	970	980	970	10	1.03
With coating (3)	1000	1000	1010	1003	5.77	5.75
Without coating (4)	960	970	980	970	10	1.03
With coating (4)	1000	1000	1020	1006	11.54	1.15

Table 3.3: Showing different experiments with different thicknesses.

By looking at table 3.3, it can be concluded that the naked electrode had a mean diameter of 970 µm and the coated rod a mean diameter of 1003 ± 3 µm, therefore the mean thickness of the sol-gel was 33 ± 3 µm.

3.4.2.1 Determination of Codeine with $Ru(bpy)_3^{2+}$ Immobilised in Sol-Gels

Subsequent experiments were therefore carried out using a glassy carbon rod as the working electrode. Firstly codeine was analysed electrochemically by using a coated glassy carbon rod working electrode without $Ru(bpy)_3^{2+}$, this was done in order to provide a reference for comparison with the sol-gel coated with $Ru(bpy)_3^{2+}$ electrode.

Figure 3.13: illustrates the voltammograms for the analysis of codeine over a range of concentrations between $1x10^{-3}$M and $1x10^{-7}$M. The shape of the voltammogram are irreversible as $Ru(bpy)_3^{2+}$ was not present neither oxidation potential peaks or reduction

potentials peaks were observed as expected. It can be seen a maximum of intensity current at 50.452 µA for $1x10^{-3}$M and the minimum intensity current at 28.239 µA for $1x10^{-7}$M due to the current intensity is proportional to the concentration of codeine.

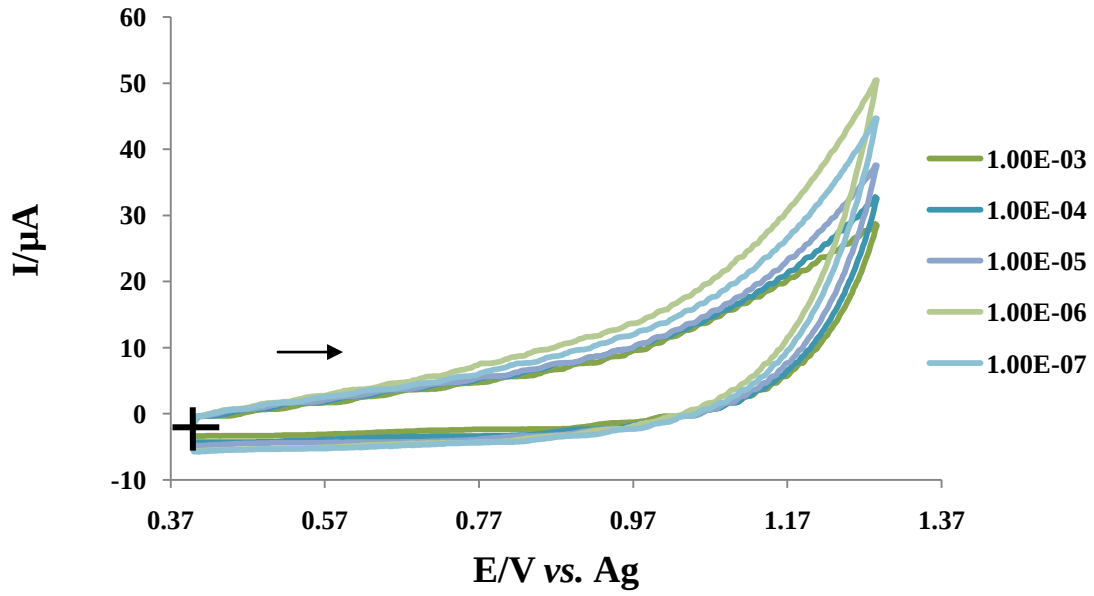

Figure 3.13: Voltammograms of codeine in a range of concentrations between $1x10^{-3}$ and $1x10^{-7}$ M in a solution of $1x10^{-3}$ M acetate buffer at pH 3.9 in a sol-gel coated glassy carbon rod electrode without $Ru(bpy)_3^{2+}$. The cross-lines indicate the point of origin and the arrow shows the direction of the initial potential sweep.

Figure 3.14 shows the voltammogram of a solution of $1x10^{-3}$ M acetate buffer at pH 3.9 $1x10^{-3}$ M $Ru(bpy)_3^{2+}$ immobilised in a sol-gel coated glassy carbon rod at 0.1V/s (No codeine).

Figure 3.15 illustrates the voltammograms for the analysis of codeine with $1x10^{-3}$M $Ru(bpy)_3^{2+}$ encapsulated in a sol-gel, obtained over a range of codeine concentrations in the same way as Figure 3.13. In this work the glassy carbon rod electrode received a sol-gel coating with immobilised $Ru(bpy)_3^{2+}$. In contrast to that observed from Figure 3.13, the CVs are symmetrically reversible (oxidation-reduction) as the reaction described in Section 1.11 (Scheme 1.3) takes place. This is a one electron process. The oxidation peaks are represented by O_1 and the reduction peaks by R_1.

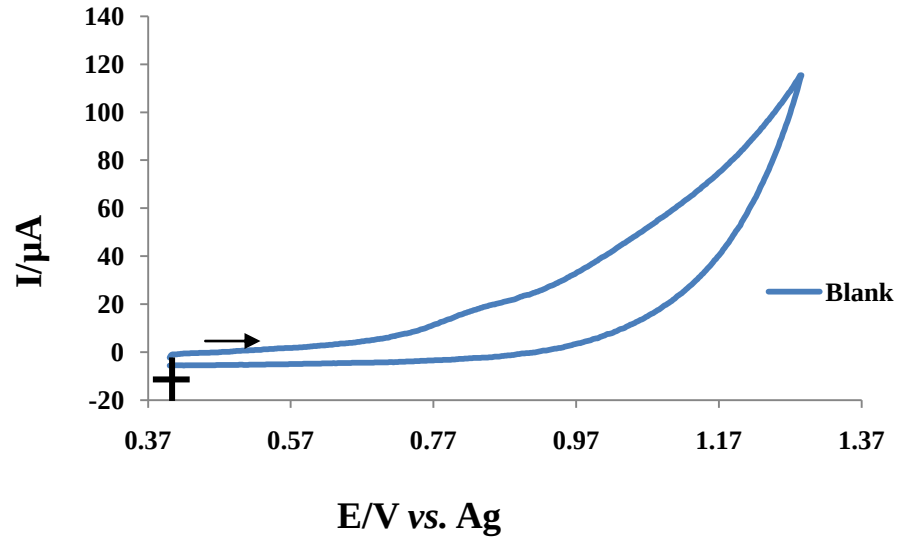

Figure 3.14: Voltammogram of a solution of $1x10^{-3}$ M acetate buffer at pH 3.9 immobilised with $1x10^{-3}$ M $Ru(bpy)_3^{2+}$ in a sol-gel coated glassy carbon rod at 0.1V/s (No codeine). The cross-lines indicate the point of origin and the arrow shows the direction of the initial potential sweep.

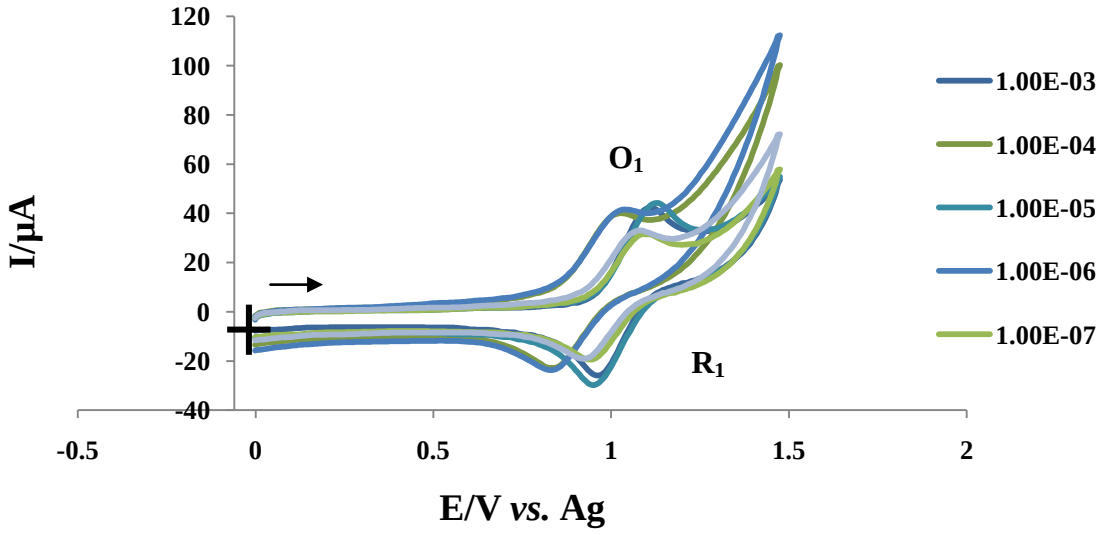

Figure 3.15: Voltammograms of codeine in a range of concentrations between $1x10^{-3}$ and $1x10^{-7}$ M in a solution of $1x10^{-3}$ M acetate buffer at pH 3.9 using $1x10^{-3}$M $Ru(bpy)_3^{2+}$ immobilised in a sol-gel coated glassy carbon rod at 0.1 V/s. The cross-lines indicate the point of origin and the arrow shows the direction of the initial potential sweep.

3.4.3 ECL Emission

The aim of the following section was to demonstrate the effects of sol-gel coated using immobilised $Ru(bpy)_3^{2+}$ by studying ECL emission. ECL provides a way to characterize the diffusion and reactivity of redox probes trapped in silica gels solids. The $Ru(bpy)_3^{2+}$ is encapsulated in the sol-gel coated working electrode.

The ECL emission produced upon the reaction of gel entrapped ruthenium (II) tris (bipyridine) $Ru(bpy)_3^{2+}$ with a tertiary amine such as codeine is related to the concentration of the analyte in solution, as can be observed from Figure 3.16. The abscissa is a logarithm scale to cover a wide calculation range.

Table 3.4 shows the effect that reagent diffusion had on the ECL emission. When the experiment was repeated three times (using the same electrode) a decrease in the ECL signal was observed. The matrix of sol-gel is porous, and through these porous $Ru(bpy)_3^{2+}$ can be leached. $Ru(bpy)_3^{2+}$ is soluble in water therefore it is probably leaching out of the sol-gel matrix into the surrounding aqueous medium. This problem was increased by the fact that each sol-gel was stored in an aqueous buffer solution overnight before use. Later studies based on prevention of leaching supported this hypothesis.

Codeine (M)	**Replicate 1 ECL emission (mV)**	**Replicate 2 ECL emission (mV)**	**Replicate 3 ECL emission (mV)**	**Average ECL emission (mV)**	**Standard deviation**	**%Relative standard deviation**
$1x10^{-3}$	21.10	18.85	16.94	18.96	2.08	10.98
$1x10^{-4}$	18.12	16.02	13.41	15.85	2.36	14.88
$1x10^{-5}$	16.23	13.69	9.62	13.18	3.33	25.29
$1x10^{-6}$	13.78	9.96	7.31	10.35	3.25	31.43
$1x10^{-7}$	11.15	8.47	6.59	8.74	2.29	26.22
Blank	3.34	3.12	2.86	3.11	0.24	7.72

Table 3.4: The change in ECL emission as a function of the codeine concentration for a single electrode replicated three times.

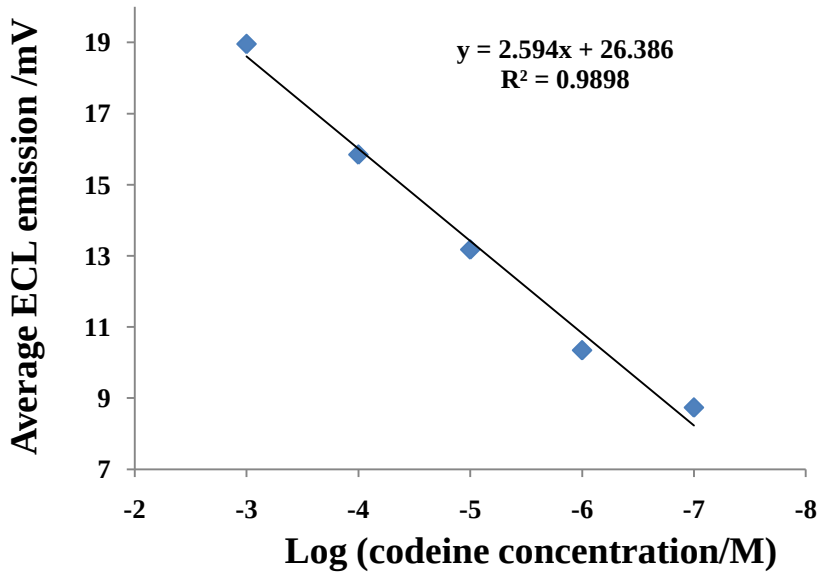

Figure 3.16: Concentration of codeine *vs* ECL (emission). Note the abscissa is a logarithmic scale.

This problem was observed with physical entrapment allowing the leaching of $Ru(bpy)_3^{2+}$ from the coating due to the small size of the molecule. Collinson *et.al*, tried to overcome this problem by incorporating Nafion as an ion exchange reagent in the sol-gel. This helped to prevent the problem of $Ru(bpy)_3^{2+}$ leaching out of the sol-gel coating; but there was a decrease in ECL signal. This decrease could be explained due to a hydrophobic partitioning effect with the Nafion which would reduce the diffusion efficiency of the aqueous based analyte [45].

To overcome the leaching problem covalent immobilisation has been investigated. MacCraith *et al.*,[46] synthesised a derivatised form of $Ru(bpy)_3^{2+}$, 4,4'-bis[(3-triethoxysilypropyl)amide]-2,2'-bipyridine]bis-(2,2'-bipyridine)ruthenium(II) dichloride and incorporated into a fluorescent based oxygen sensor. This was shown to possess good sensitivity and did not suffer from the leaching due to the covalent bonding of the $Ru(bpy)_3^{2+}$. This approach could not however be used for chemiluminescence applications as the residual triethylamine would interfere with the measurement contributing to the ECL signal via reaction with Ru^{III} species.

Barnett *et. al.*,[47] immobilised the ruthenium derivative (4-[4-(dichloromethylsilanyl)-butyl]-4'-methyl-2,2'-bypiridyl)bis(2,2'-bipyridyl)ruthenium(II) on silica particles for

CL but the stability and reproducibility was disappointing for codeine standards in aqueous solution.

3.5 Covalent Attachment of Electrochemiluminescent Reagents in Silicate Sol-Gels

To overcome these problems with the immobilisation techniques it was decided to try covalent attachment of $Ru(bpy)_3^{2+}$ to a sol-gel matrix using a new derivative.

A new compound (Figure 3.17) was therefore synthesised for this work by Dr. Charlotte Wiles (University of Hull). It contained hydrolysable linkers that allowed the covalent attachment of the $Ru(bpy)_3^{2+}$ derivative to the sol-gel matrix. It was envisaged that this derivative, 4,4'-bis[(3-triethoxysilylpropyl)amide-2,2'-biyridine] bis (2,2'-bipyridine) ruthenium (II) dichloride (see Figure 3.17) would prevent leaching and also be able to bond with other silica systems. Such as glass coils, micro channels and optical fibres; that could be used for both chemiluminescence (CL) and electrogenerated chemiluminescent techniques. The design of the material would ensure that the Ru complex was evenly distributed and prevent leaching. An initial communication was published describing the synthesis and showing the possibilities of this approach but the material was not fully evaluated [48]. It was clearly shown in this communication that leaching did not occur with this material. Reproducible ECL signals of 7.7 mV (% RSD = 1.07, n = 24) were obtained [48].

In this thesis the novel material was further evaluated and a calibration obtained.

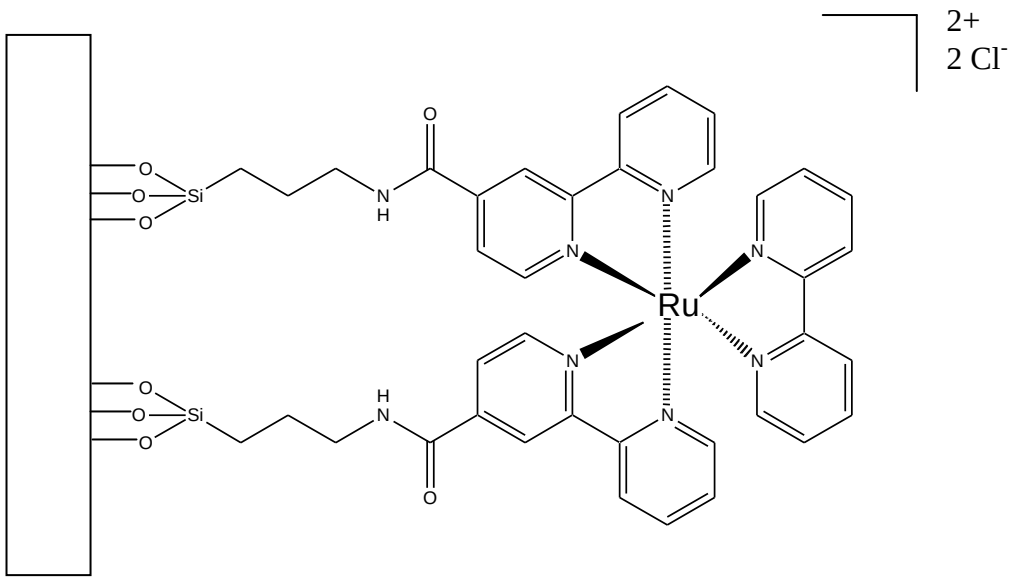

Figure 3.17: Schematic illustrating the covalent immobilisation of tris (2,2'-bipyridyl) ruthenium (II) complex onto a silica surface.

3.5.1 Voltammograms for Covalently Immobilisation

The organosilicate sol-gels was prepared by using a modified method reported by Collinson *et al.*,[49] where a solution of TMOS and the ruthenium derivative (~ 6.5% wrt TMOS) were hydrolysed in the presence of an acid catalyst (0.1M aq. HCl), followed by base catalysed gelation. The electrodes were coated by dipping the working electrode into the hydrolysed solution containing the novel compound (see Figure 3.17). The detailed procedure is described in Chapter 2. Gelation was then induced by placing the electrode in borate buffer (pH 8.5, 0.1 M) for 24 h to age the film. The pH used for the experiments was 3.9 as discussed in the previous section.

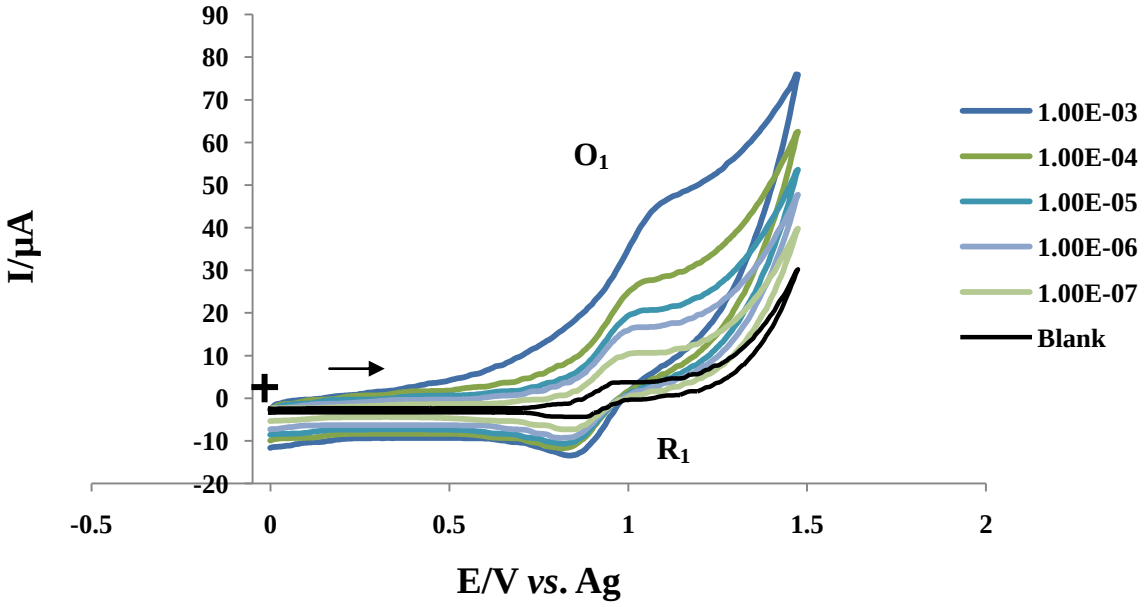

Figure 3.18: Voltammograms of codeine in a range of concentrations between $1x10^{-3}$ and $1x10^{-7}$ M in a solution of $1x10^{-3}$ M acetate buffer at pH 3.9 immobilised with $1x10^{-3}$ M of the derivative in a sol-gel coated glassy carbon rod and the blank (without codeine) at 0.1V/s. The cross-lines indicate the point of origin and the arrow shows the direction of the initial potential sweep.

Using the experimental set up described in Section 3.2.2 with the glassy carbon rod electrode coated with the covalently immobilised $Ru(bpy)_3^{2+}$ the voltammograms seen in Figure 3.18 were obtained for a range of concentrations of codeine. These show a one electron process which is reversible as illustrated by the two peaks (redox) due to the oxidation-reduction mechanism between the tertiary amines and $Ru(bpy)_3^{2+}$ as explained in detail in Chapter 1. A maximum of current of 74.62 µA was observed for a $1x10^{-3}$M codeine solution. The minimum of intensity was detected at 39.36 µA when $1x10^{-7}$M codeine was used. On the first forward scan, a weak oxidation peak appears at potential 1.10 V (O_1) for the strongest concentration of codeine $1x10^{-3}$M. A reduction peak was observed around 0.86 V (R_1).

3.5.2 ECL Emission for Covalently Immobilisation

Table 3.5 shows the ECL emission for a range of concentrations of codeine between $1x10^{-3}$ to $1x10^{-7}$M. Three replicates measurements were made for each concentration and as can been seen although there was a slight decrease in signal this was drastically reduced from previous results (Table 3.4) where leaching had been observed.

Codeine (M)	**Replicate 1 ECL emission (mV)**	**Replicate 2 ECL emission (mV)**	**Replicate 3 ECL emission (mV)**	**Average ECL emission (mV)**	**Standard deviation**	**%Relative Standard deviation**
1.00×10^{-3}	28.08	28.03	27.95	28.02	0.06	0.23
1.00×10^{-4}	24.89	24.83	24.82	24.85	0.04	0.15
1.00×10^{-5}	21.81	21.76	21.70	21.76	0.05	0.25
1.00×10^{-6}	19.06	18.99	18.90	18.98	0.08	0.42
1.00×10^{-7}	16.27	16.24	16.05	16.19	0.12	0.74
Blank	4.56	4.64	4.48	4.56	0.08	1.75

Table 3.5: The change in ECL emission as a function of the codeine concentration for a single electrode replicated three times.

The results were plotted as ECL signal vs log codeine concentration and a linear relationship was observed (Figure 3.19). The limits of detection (3 x blank) were calculated for the lower linear portion of the graph and was found to be 2.65×10^{-6} M. These results were higher than those obtained by Barnett *et al.*,[47] for chemiluminescence in acetonitrile however the stability of the reagent in aqueous solution was superior.

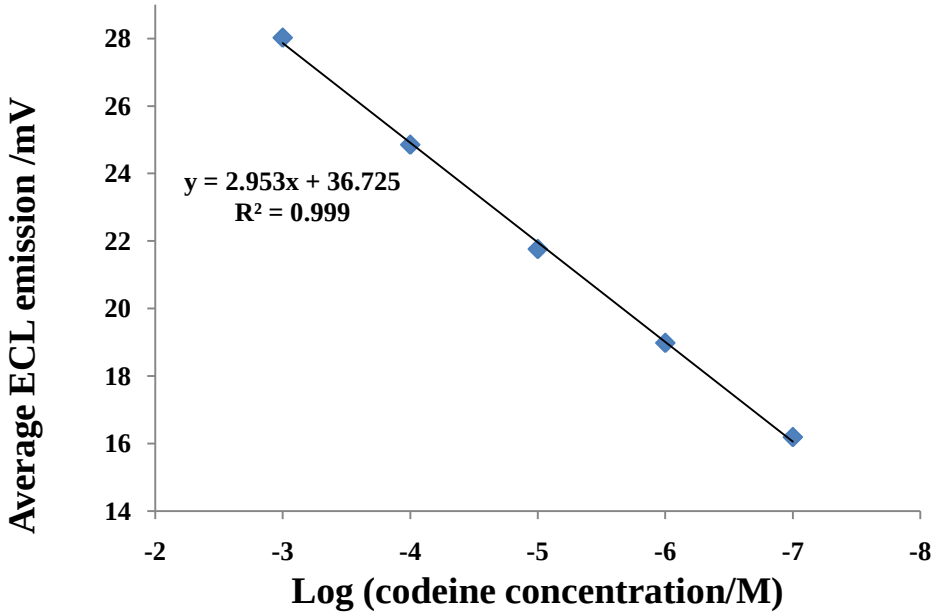

Figure 3.19: ECL calibration for codeine. Note the abscissa is a logarithmic scale.

In summary, when this method using a derivative (covalent attachment) is compared to the physical entrapment of CL in sol-gels, covalent immobilisation is advantageous. Covalent attachment ensures homogeneous distribution of the reagent within the matrix and improves reproducibility and extends sensor lifetime. In addition the prevention of reagent leaching and reduction of the analysis costs were overcome.

3.6 Conclusions

In this chapter $Ru(bpy)_3^{2+}$ was immobilised within the sol-gel matrix to develop a sensor which could be used directly for measuring tertiary amine containing drugs in buffer solution without the need to add reagents. Initially tris (2,2'-bipyridyl) ruthenium (II) dichloride hexahydrate was physically entrapped within the sol-gel matrix. There were however problems with this method because $Ru(bpy)_3^{2+}$ diffuses out of the matrix leading to a continual decrease in the luminescence.

The problem of leaching reagent and signal degradation was overcome by the covalent attachment of a novel $Ru(bpy)_3^{2+}$ derivative to the sol-gel matrix. Using this compound a calibration was obtained using ECL for the determination of codeine over the range 1 $x10^{-3}$ to 1 $x10^{-7}$ M in aqueous buffer, with a limit of detection of 2.65 x 10^{-6} M.

Covalent attachment compared to the physical entrapment of CL reagent was advantageous as it ensured homogeneous distribution of the reagent within the matrix and prevented leaching. This reduced analysis costs, extended sensor lifetime and gave reproducible analyte responses. The method however could not be extended to insoluble drugs such as rohypnol and an alternative approach is required. One such approach would be to use a biphasic system as described in Chapter 4.

3.7 References

1. S. Ege, *Organic Chemistry-Structure and Reactivity*, D.C. Heath and Company, 1994.
2. M.D. Yoseph Caraco, *N. Engl. J. Med.*, 2004, **351**, 2867.
3. A. Harvey and R. Lane, *Eur. Neuropsychopharmacol.*, 1996, **6**, 42.
4. A. Gaedigk, L. Ndjountche, K. Divakaran, L.D. Bradford, I. Zineh, T.F. Oberlander, D.C. Brousseau, D.G. McCarver, J.A. Johnson, S.W. Alexander, K.W. Riggs and J. S. Leeder, *Clin. Pharmacol. Ther.*, 2007, **81**, 242.
5. F. Liu, X.Y. Hu and J. Luo, *J. Chromatogr. B*, 1994, 658.
6. F.R. Song, M. Cue and S. Y. Liu, *Rapid Commun. Mass Spectrom.*, 1999, **13**, 478.
7. U. Staerk and W. R. Kulpman, *J. Chromatogr. B*, 2000, **745**, 399.
8. K. Panganiban, P. Jacob, E.T. Everhart, E.C. Tisdale, S.L. Batki, J.E. Mendelson and R. T. Jones, *J. Anal. Tox.*, 1990, **23**, 581.
9. E.J. Rook, M.J.X. Hillebrand, H. Rosing, J.M. van Ree and J. H. Beijenem, *J. Chromatogr. B*, 2005, **824**, 213.
10. K.M. Clauwaert, J.F. van Bocxlear, W.E. Lambert and A. P. d. Leenhher, *Anal. Chem.*, 1996, **68**, 3021.
11. P.A. Steenkamp, N.M. Harding, F.R. Van Heerden and B. E. V. Wyk, *Forensic Sci. Inter.*, 2004, **145**, 31.
12. C. Kirchhoff, Y. Bitar, S. Ebel and U. Holzgrabe, *J. Chromatogr. A*, 2004, **1046**, 115.
13. G. Trachta, B. Schwarze, B. Sangmuller, G. Brehm and S. Schneider, *J. Mol. Struct.*, 2004, **693**, 175.
14. R. Kronstand, I. Nystrom, J. Strandberg and H. Druid, *Forensic Sci. Inter.*, 2004, **145**, 183.
15. *Brit. Nat. Formulary, Brit. Med. Assoc. & R. Pharma. Soc. G. Brit.*, 2004, **47**, 868.
16. R.H. Schwartz, R. Milteer and M. A. LeBeau, *Southern Med. J.*, 2000, 558.
17. R.H. Schwartz and A. B. Weaver, *Clinical Pediatrics*, 1998, 321.
18. N. Samyn, G. De Boeck, V. Crimele, A. Verstaete and P. Klintz, *J. Anal. Tox.*, 2002, **26**, 211.
19. P.H. Wang, C. Lui, W.I. Tsay, J.H. Li, R.H. Liu, T.G. Wu, W.J. Cheng, D.L. Lin, T.Y. Huang and C. H. Chen, *J. Anal. Tox.*, 2002, **26**, 411.
20. M.A. Elsohly, S. Feng, S.J. Salamone and R. Brenneisen, *J. Anal. Tox.*, 1999, **23**, 486.
21. A. A. Elian, *J. Anal. Tox.*, 1999, **101**, 107.
22. N. Samyn, G.D. Boeck, V. Cirimele, A. Verstraete and P. Kintz, *J. Anal. Tox.*, 2002, **26**, 211.
23. G.M. Greenway, L.J. Nelstrop and S. N. Port, *Anal. Chim. Acta*, 2000, **405**, 43.
24. J.M. Gonzalez, G.M. Greenway, T. McCreedy and Q. Song, *Analyst*, 2000, **1254**, 765.
25. Q. Song, G.M. Greenway and T. McCreedy, *Analyst*, 2001, **126**, 37.
26. G.M. Greenway, A.W. Knight and P. J. Knight, *Analyst*, 1995, **120**, 2549.
27. S.J.L. Dolman and G. M. Greenway, *Anal. Commun.*, 1996, **33**, 139.
28. R.C. Engstrom, K.W. Johnson and S. DesJarlais, *Anal. Chem.*, 1987, **59**, 670.

29. A.W. Knight and G. M. Greenway, *Analyst*, 1995, **120**, 2543.
30. A.J. Wain., A.N. Kirkham., D.J. Walton., B. Wood., R.R. France., S.D. Bull., J.D. Wadhawan and R. G. Compton., *J. Am. Chem. Soc.*, 2003, **125**, 11418.
31. L. Sieminska and T. W. Zerda, *J. Phys. Chem.*, 1996, **100**, 4591.
32. M. T. McDermott, K. R. Kneten and R. L. McCreery, *J. Phys. Chem.*, 1992, **96**, 3124.
33. J. Kanga, H. Weia, W Guoa and E. Wanga, *Electrochem. Commun.*, 2007, **9**, 465.
34. S. Dinga, J. Xua and H. Chen, *Talanta*, 2006, **70**, 403.
35. J.K. Leland and M. J. Powell, *J. Electrochem. Soc.*, 1990, **137**, 3127.
36. M.M. Collinson, H. Wang, R. Markote and A. N. Khramov, *J. Electroanal. Chem.*, 2002, **519**, 65.
37. H. Cattey, P. Audebert, C. Sanchez and P. Hapiot, *J. Mater. Chem.*, 1997, **7**, 1461.
38. M.M. Collinson, P. J. Zambrano, H. Wrang and J. S. Taussig, *Langmuir*, 1999, **15**, 662.
39. H. Cattey, P. Audebert, C. Sanchez and P. Hapiot, *Phys. Chem. B*, 1998, **102**, 1193.
40. C.B. Dave, B. Dunn, J.S. Valentine and J. I. Zink, *Anal. Chem.*, 1994, **66**, 1120a.
41. O. Lev, M. Tsionsky, L. Rabinovich, V. Glezer, S. Sampath, I. Pankratov and J. Gun, *Anal. Chem.*, 1995, **67**, 22A.
42. A.N. Khramov and M. M. Collinson, *Anal. Chem.*, 2000, **72**, 2943.
43. M.M. Collinson, B. Novack, S.A. Martin and J. S. Taussig, *Anal. Chem.*, 2000, **72**, 2914.
44. M.M. Collinson, C.G. Raush and A. Voigt, *Langmuir*, 1997, **13**, 7245.
45. M.N. Szentirmary and C. R. Martin, *Anal. Chem.*, 1984, **56**, 1898.
46. C. Malins, S. Fanni, H.G. Glever, J.G. Vos and B. D. MacCraith, *Anal. Commun.*, 1999, **36(1)**, 3.
47. N.W. Barnett, R. Bos, H. Brand, P. Jones, K.F. Lim, S.D. Purcell and R. A. Russell, *Analyst*, 2002, **127**, 455.
48. G.M. Greenway, A. Greenwood, P. Watts and C. Wiles, *Chem. Commun.*, 2006, 85.
49. M.M. Collinson and B. Novack, *Journal of Sol-Gel Science and Technology*, 2002, **23**, 215.

Chapter 4

Electrogenerated Chemiluminescence at Liquid|Liquid Interface : Evidence Inverted & Proton-Coupled Electron Transfer

4.0 Aims of the Chapter

Microdoplet-modified electrodes have recently come to the fore as a means of assessing the aqueous biphasic redox activity of a plethora of hydrophobic liquids [1], primarily since this technique enables the probing of the redox modulation of micro-structured biometric membranes.

In the case of undiluted redox-switchable liquids, electron transfer is initiated at the base-circumference of each individual droplet with concerted ion transfers (expulsion or insertion), so as maintain overall droplet electro-neutrality. In recent work [2], the possibility of such electron transfer processes causing a biphasic electron transfer coupling has been explored.

This work reports for the first time electrogenerated chemiluminescence (ECL) at droplet modified electrodes. The system involves oxidation of aqueous tris(2,2'-bipyridyl)ruthenium(II) ions at a glassy carbon electrode on which a random array of microdroplets of a highly hydrophobic tertiary amine (trioctylamine) are immobilised. Luminescence, produced via electron transfer over the cupola surface of the droplets from the oil to aqueous tris(2,2'-bipyridyl)ruthenium(III) ions synthesised via electrochemical oxidation at the uncovered parts of the electrode surface, is demonstrated. The extent of ECL production is shown to be dependent on the degree of interfacial protonation, with a proton-coupled biphasic electron transfer reaction occurring when the liquid | liquid interface is fully protonated, changing to a biphasic outer-sphere electron transfer mechanism when the interface is fully deprotonated. The competition and gradual dominance of one of these extreme mechanisms under intermediate interfacial protonation conditions thence enables the sensitive, kinetic estimation of the biphasic pK_a.

This work is then extended to study the case of deuterium-coupled electron transfer.

4.1 Introduction

4.1.1 Factors Affecting Electrode Reaction Rate and Current

Interpreting the rate of an electrode reaction is often more complex than doing the same for a reaction occurring in solution or in the gas phase. The latter is called a homogeneous reaction, because it occurs everywhere within the medium at a uniform rate. In contrast an electrode process is a heterogeneous reaction occurring only at the electrode-electrolyte interface. Its rate depends on mass transfer to the electrode and various surface effects, in addition to the usual kinetic variables. Since electrode reactions are heterogeneous, their reaction rates are usually described in unit of mol s^{-1} per unit area; that is:

$$\text{Rate (mol s}^{-1}\text{ cm}^{-2}) = \frac{i}{nFA} = \frac{j}{nF} \qquad \textbf{Equation 4. 1}$$

where j is the current density.

The factors affecting electrode reaction rate and current are as follows.

1. Mass Transfer (*e.g.*, of oxidised species from the bulk solution to the electrode surface).
2. Electron transfer at the electrode surface.
3. Chemical reactions preceding or following the electron transfer. These might be homogeneous processes (*e.g.*, protonation or dimerization) or heterogeneous ones (*e.g.*, catalytic decomposition on the electrode surfaces.
4. Other surface reaction, such as adsorption, desorption or crystallization (electrodeposition) [3].

4.1.2 Electrochemistry of Immobilised Redox Droplets

A droplet is a small volume of liquid bound completely or almost completely by free surfaces. In our experiment the droplets are bounded by a solid and a liquid phase. The Trioctylamine (TOA) was used as a redox oil.

Since 1976, when Murray and co-workers [4-6] carried out the first experiments, electrodes that have been chemically modified by electroactive substrates have been utilised significantly in the protein film voltammetry and electroanalysis spheres. The respective work by Laviron, Anson and colleagues, and Matsuda *et* co-workers [7-10], on the modification of electrodes with adsorbates, and redox-active monolayers, reveals that there is a plethora of techniques for altering the surface of electrodes [1].

Extensive study to determine simpler methods of immobilising redox-active materials on the surface of electrodes has been carried out over the last ten years. With regards to liquids, immobilisation of redox-active microdroplets may be achieved by evaporating an aliquot of an electroactive [11] solution using a solvent base.

The investigation of electroactive compounds using this method has been a desirable option, due to the minimal amount of material necessary (usually less than *ca.* 10 nmol), and the possibilities it affords for exploring an abundance of compounds with high insolubility, which cannot, therefore, be studied in aqueous solutions. Due to the production of unusual materials of a liquid|liquid like base from electrochemical transformations in aqueous solutions, the electrochemistry of redox-active liquids on electrode surfaces has recently attracted a high level of interest [1].

4.1.2.1 Electrochemistry at the Three-Phase Boundary

This methodology involves electrode modification with liquid microdroplets. The result of the current method is that electron transfer is restricted, at first, to the annular region; that is to say where the oil and aqueous electrolyte phase and electrode meet, unless the electrolyte ions partition into the microdroplets. The term “three phase boundary” is used to define this junction [12-14]

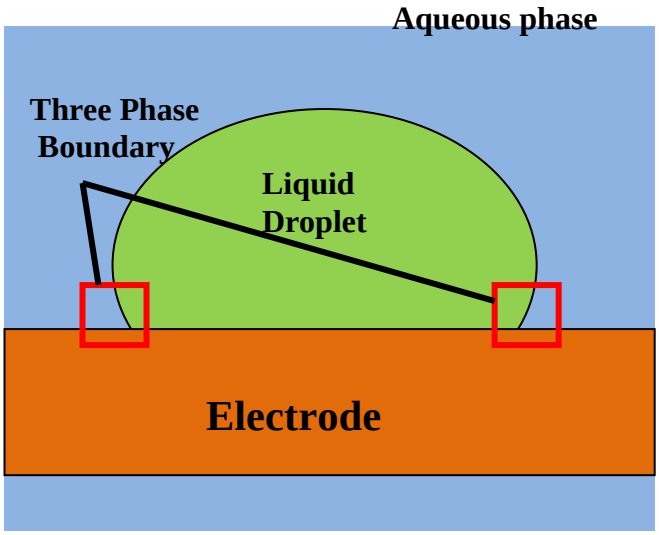

Figure 4.1*:* Electrochemistry at the three-phase boundary (taken from ref [15]).

4.1.2.2 Electron Transfer Processes at the Liquid/Liquid Interface

To be transferred electrons at the liquid|liquid interface, the non-aqueous droplets normally needs to be supported. The liquid|liquid protonation process offers the most customary method of electron transfer.

4.1.2.3 The Current–Voltage Curves in the Case of Hydrophilic Compounds and Electrolyte Counter Ions (Electrochemically Induced Ion Expulsion Process)

Decreasing the hydrophobicity of the oil phase (by, for example, employing a redox oil with a lower degree of substitution or with polar side chains) or increasing the hydrophilicity of the aqueous-based counter ion has a profound effect on the voltammetry [1].

$$A(l) - e^{-} \rightleftarrows A^{+\cdot}(aq)$$

Equation 4.2

Thus, the electro-generated cation is expelled from the oilphase [15] with electron transfer is initiated at the three phase boundary [16-19], although the dissolution may apparently leave from the liquid/liquid interface [16, 18].

On the reverse (second) sweep, the neutral oil is formed either, at the naked electrode surface or droplet three-phase boundary, where it nucleates either as a new microdroplet, or grows into another one. In some cases, the second and third successive oxidation peaks move to slightly more negative potentials, this is due to the partitioning of aqueous electrolytes into the organic deposits, or as a result of the smaller size of there deposited microdroplets [18, 19].

For ‘‘hard ’’anions (such as fluoride or sulfate), the voltammetric signals are narrow, and both oxidation and reduction peak potentials are essentially independent of aqueous anion concentration. This is not the case for ‘‘softer ’’anions (such as bromide and nitrate), which may insert into the oil if it is made more hydrophobic [16, 18].

4.2 Results and Discussion

First considered is the voltammetry of the individual components of the biphasic system.

4.2.1 Voltammetry of Oc_3N (Trioctylamine) Microdroplets

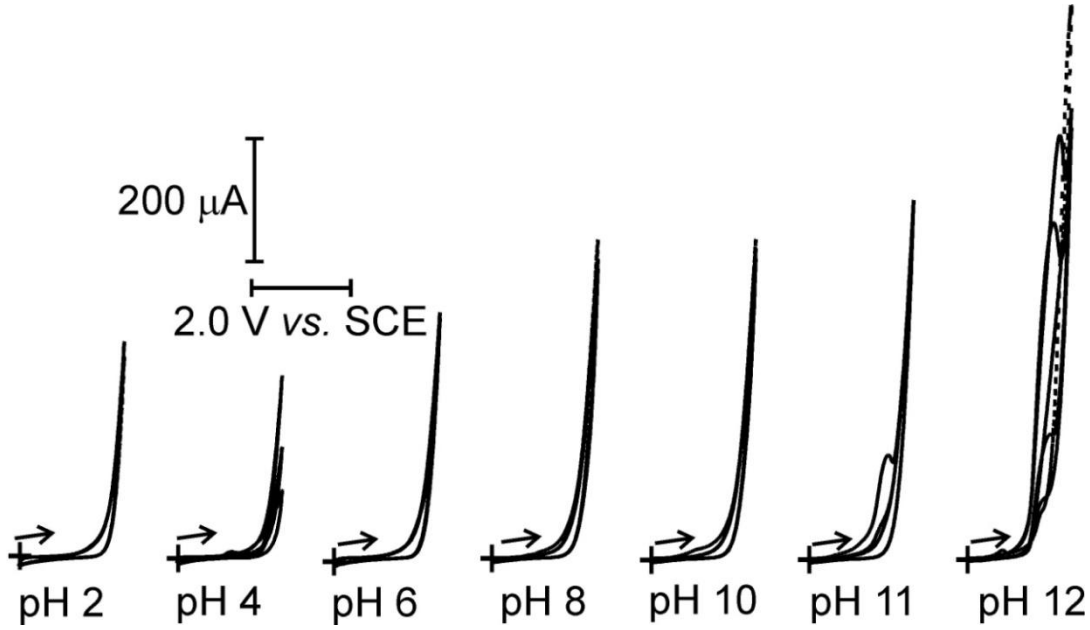

Figure 4.2: **Cyclic voltammograms (0.1 V s^{-1} scan rate) showing the oxidation of 1.0 nmol Oc_3N immobilised as microdroplets on a 3.0 mm diameter glassy carbon disc electrode immersed in an aqueous electrolyte consisting of 0.1 M sodium perchlorate and 0.1 M phosphate buffer solution at various values of solution pH. Three consecutive scans are shown in each voltammogram; the peaks observed when the solution pH is less than 12 are from the third scan. The cross-lines indicate the point of origin, and the arrows show the direction of the initial potential sweep.**

Figure 4.2 illustrates the voltammetry of a glassy carbon electrode coated with microdroplets of trioctylamine at a scan rate of 0.1 V s^{-1} immersed into phosphate buffer solution containing 0.1 M sodium perchlorate at a variety of pH values. It is readily apparent that when the aqueous bathing medium is at pH values of 11 and below, there is no discernable oxidation wave except that corresponding to solvent breakdown within

the potential range studied ($0.0 \leq E/V \leq 2.0$), the latter occurring at higher potentials than expected on glassy carbon due to the nature of the partially-blocked surface. In contrast, at pH values of 12 a single, chemically-irreversible oxidation wave appears at 1.7 V *vs.* SCE. This wave is not due to the solvent breakdown; rather it is due to the oxidation of the tertiary amine [20], presumably at the three-phase boundary of oil | aqueous electrolyte | electrode [1, 21]. A plausible mechanism is as follows.

$Oc_3N(l) + ClO_4^-(aq) - e^- \rightarrow Oc_3N^{+\bullet}ClO_4^-(l)$ (a)

$Oc_3N^{+\bullet}ClO_4^-(l) \rightarrow Oc_2N(^{\bullet}CHCH_2CH_2CH_2CH_2CH_2CH_3)(l) + H^+(aq) + ClO_4^-(aq)$ (b)

$Oc_2N(^{\bullet}CHCH_2CH_2CH_2CH_2CH_2CH_3)(l) + ClO_4^-(aq) - e^- \rightarrow$
$[Oc_2N^+{=}CHCH_2CH_2CH_2CH_2CH_2CH_2CH_3]ClO_4^-(l)$ (c)

$Oc_3N(l) + ClO_4^-(aq) + H^+(aq) \rightleftarrows Oc_3NH^+ClO_4^-(l)$ (d)

Scheme 4.1

The first step in this process (see scheme 4.1) is thought to form the cation radical of trioctylamine (a). However, in order to maintain an electrostatically-neutral oil phase, this is likely to be accompanied with the insertion of aqueous perchlorate ions (the most lipophilic anion in the aqueous medium). The cleavage of an α-carbon-hydrogen bond with expulsion of protons and perchlorate ions from the oil phase (b) enables the irreversible formation of a radical intermediate, which may undergo further heterogeneous oxidation at lower potentials (*viz.* $E^0_{scheme\,4a} > E^0_{scheme.4c}$). The dynamics of the oxidation are complex, as evident by the positively-shifted waves in the second and third scans; the formation of new phases during the electrochemical oxidation cannot be discounted. This suggested oxidative pathway may only occur if the trioctylamine exists in a non-protonated state; below the biphasic pK_a of the oil, protonation of the surface is likely [22], and forms an ionic pair (scheme 4.1 d).

The extent to which the above surfactant-forming process occurs in the oil phase will depend on the diffusivity of protons and perchlorate ions within the hydrophobic bulk phase, and the degree at which this ionic liquid is soluble in water. As the former is

likely to be slow[23], and the ionic liquid is likely water-insoluble[24], this is restricted to an outer "shell"[23]. Accordingly, biphasic voltammetry of this protonated phase (as evidenced by the peaks in the third voltammetric scan, presumably oxidising the products of initial electrolysis) may either be initiated along the same triple phase junction, or at the electrode | protonated oil | non-protonated oil boundary. The former case is likely thermodynamically slow; the latter is kinetically limited by perchlorate ion penetration into the bulk coupled with appropriate ion-adjustment in the outer covering.

It is noteworthy that the above reaction mechanisms involve perchlorate ions to exist within the oil phase as well as in the bathing aqueous medium. The above stepwise processes are suggested, over the alternative of proton-coupled electron transfer, since perchlorate ions are hydrophobic and are known to form tight ion pairs[25]. Moreover, when the voltammetry is undertaken in the absence of perchlorate ions (*viz.* in phosphate buffer solutions only), voltammetric peaks are observed between 1.0 – 1.2 V *vs.* SCE at *every* pH value in the range $2.0 \leq pH \leq 12.0$ (data not shown), with broad peaks observed at pH values less than 4, and two waves above pH 4. At all pH values, the integrated charge reveals that up to up to three electrons can be passed at low scan rates ($0.02\ V\ s^{-1}$), whilst at higher scan rates, only ½ Faraday mol^{-1} can be electrolysed. This more complex voltammetry (which demonstrates an appreciable shift to more negative values as the proton concentration is reduced) can be tentatively understood as being proton release upon electron transfer; quantification is difficult due to the broadness of the waves. Nevertheless, we suggest that since the counter ions are hydrophilic, only the surface of the liquid is protonated, and this charge is countered by the formation of a double layer around the droplets in the aqueous phase. This is perfectly plausible due to the high Gibbs transfer energy for PO_4^{3-}, HPO_4^{2-}, and $H_2PO_4^-$. the perceived droplet structure are given in Figure 4.3.

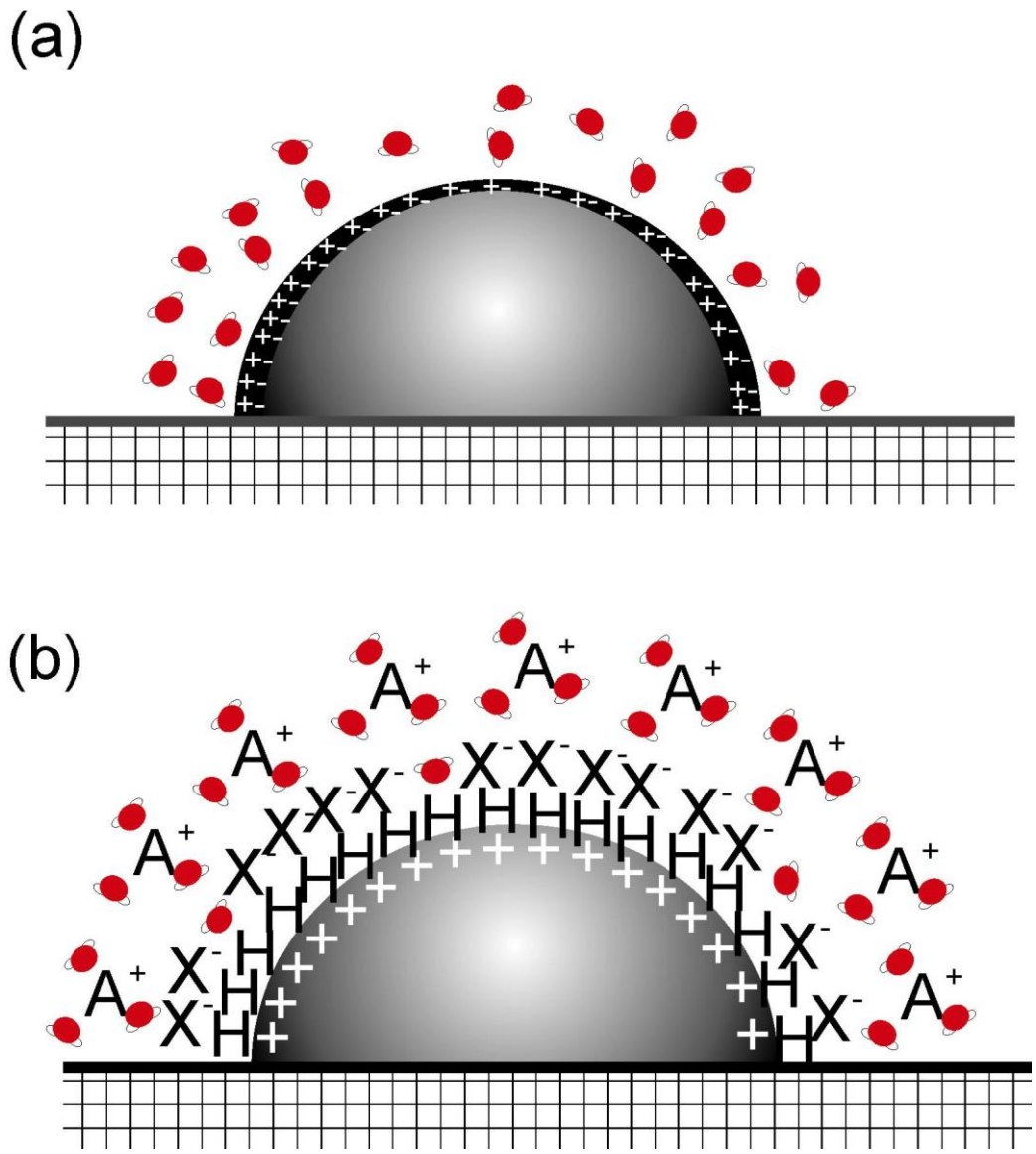

Figure 4.3: **Schematic illustration of the interfacial structure of Oc_3N microdroplet supported on an electrode surface: (a) an extreme case of ion-pairing at a protonated interface causing a new phase "shell" (note that density effects have not been considered); (b) the formation of an electrical double layer around each droplet as a result of interfacial protonation (the electrode double layer has not been considered). Note that the extent to which (a) is appropriate for the case when perchlorate ions are present is difficult to acertain, and it does not necessarily mean that there is no structuring of the aqueous phase in (a).**

4.2.2 Voltammetry of $Ru(bpy)_3^{2+}$ at Glassy Carbon Electrodes

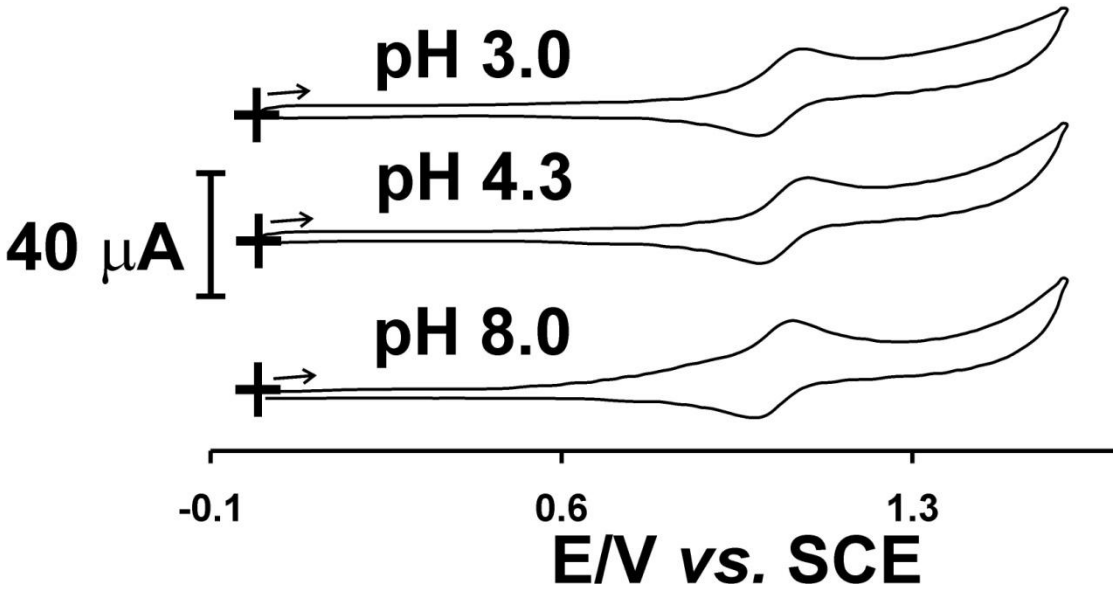

Figure 4.4: Cyclic voltammograms (0.1 V s^{-1} scan rate) for the oxidation of 1.0 mM $Ru(bpy)_3^{2+}$ at a 3.0 mm diameter glassy carbon electrode immersed in 0.1 M aqueous phosphate buffer solution. Only one voltammetric scan is shown. The cross-lines indicate the point of origin, and the arrows show the direction of the initial potential sweep.

Figure 4.4 illustrates cyclic voltammograms (at a scan rate of 0.1 V s^{-1}) for the oxidation of 1.0 mM tris(2,2'-bipyridyl)ruthenium(II) in aqueous solution at a "naked" glassy carbon electrode at various solution pH values.

It is evident that at low pH, a single, electrochemically quasi-reversible wave at $E_{mid} = ½(E_p^{Ox} + E_p^{Red}) = 1.03 \pm 0.01$ V *vs.* SCE (ΔE_{pp} = 83 + 7 mV; $i_p^{Ox}/i_p^{Red} = 1.2 \pm 0.1$) is present. This one-electron wave is due to the following redox process

$Ru(bpy)_3^{2+}(aq) - e^- \leftrightarrows Ru(bpy)_3^{3+}(aq)$ **Equation4.3**

A Randles-Sevcík analysis of the peak oxidative current furnished a diffusion coefficient of $Ru(bpy)_3^{2+}$ of $5.7 \pm 1.4 \times 10^{-6}$ cm^2 s^{-1}. When the solution pH is larger than *ca.* pH 5, a voltammetric pre-wave at E_p^{Ox} = 0.83 V *vs.* SCE becomes discernable. This feature dominates the voltammetry at high scan rates, and increases in magnitude with prolonged immersion of the electrode in the aqueous solution (data not shown). It has been demonstrated [26] that this wave is due to the voltammetry of adsorbed $Ru(bpy)_3^{2+}$ which is irreversibly "stripped" off the electrode during oxidation.

In the next section is considered the electrochemistry when both oil and chemical oxidant are present in the investigated system.

4.2.3 Biphasic Electron Transfer

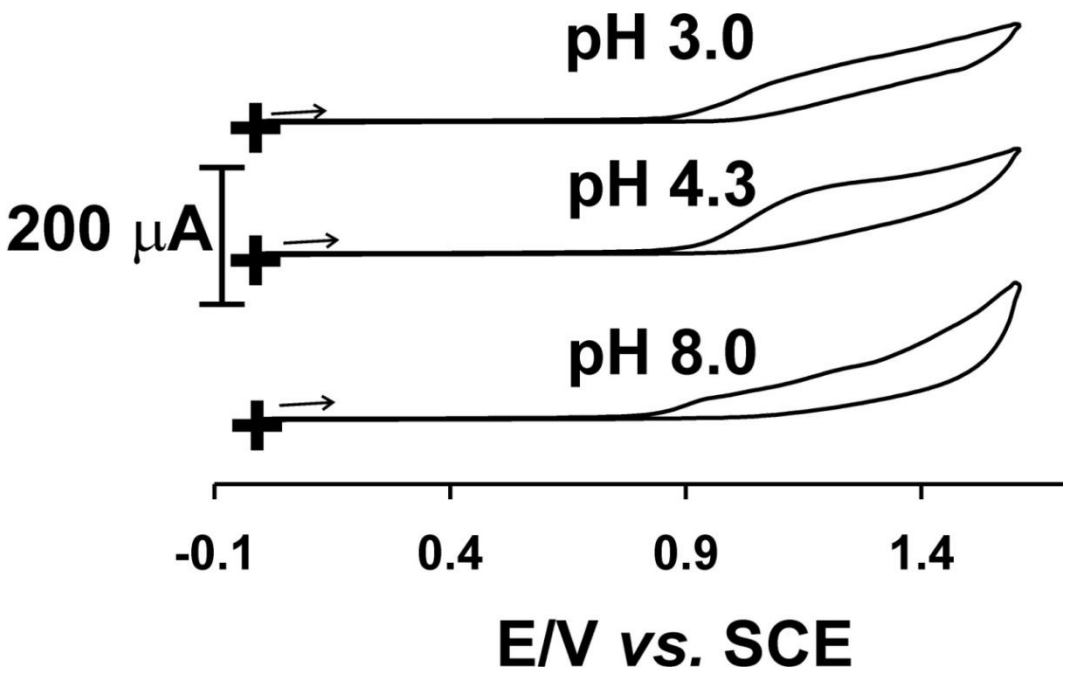

Figure 4.5: Cyclic voltammograms (0.1 V s^{-1} scan rate) for the oxidation of 1.0 mM $Ru(bpy)_3^{2+}$ at a 3.0 mm diameter glassy carbon electrode on which 1.0 nmol Oc_3N are immobilised in the form of microdroplets, and immersed in 0.1 M aqueous phosphate buffer solution. Only one voltammetric scan is shown. The cross-lines indicate the point of origin, and the arrows show the direction of the initial potential sweep.

Note that the scale bar is an order of magnitude larger in Figure 4.5 compared with Figure 4.4.

The presence of microdroplets of Oc_3N on the surface of the glassy carbon electrode causes the oxidation peak of $Ru(bpy)_3^{2+}$ to increase in magnitude compared with bare electrode despite the reduced electrode area for the oxidation – see Figure 4.5 for representative voltammograms. Strikingly, these cyclic voltammograms do not exhibit reverse waves for the reduction of electrogenerated $Ru(bpy)_3^{3+}$, suggestive of its reduction at the oil | aqueous interface:

$$Ru(bpy)_3^{3+}(aq) + oil^{Red}(l) \rightarrow Ru(bpy)_3^{2+}(aq) + oil^{Ox}(l) \qquad \textbf{Equation 4.4}$$

This amperometric augmentation of the oxidation wave of the aqueous complex occurs at every value of the solution pH within the range tested. However, it observes a pH dependence similar to that reported for the voltammetry of the oil see Figure 4.5.

In order to determine whether this liquid | liquid redox catalysis is accompanied with luminescence, the electrochemical oxidation perturbation was limited as a pulse by potentiostatting the droplet-modified electrode at 1.2 V *vs.* SCE for 20 s. This potential allows for the formation of $Ru(bpy)_3^{3+}$ under mass-transport-limited conditions. Figure 4.6 illustrates typical ECL responses.

Figure 4.6A

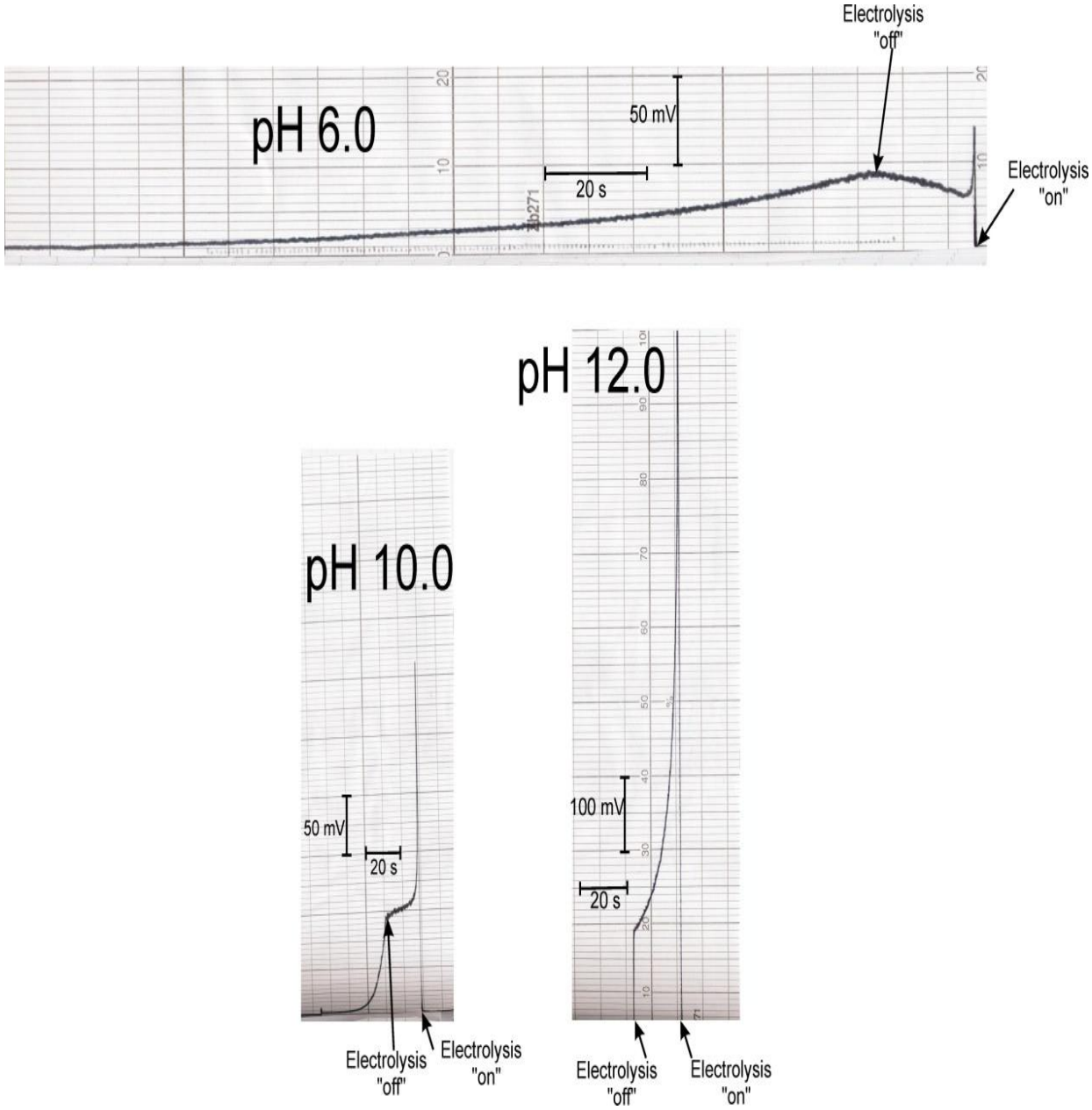
pH 6.0
50 mV
20 s
Electrolysis
"off"
Electrolysis
"on"
pH 10.0
50 mV
20 s
Electrolysis
"off"
Electrolysis
"on"
pH 12.0
100 mV
20 s
Electrolysis
"off"
Electrolysis
"on"

Figure 4.6B

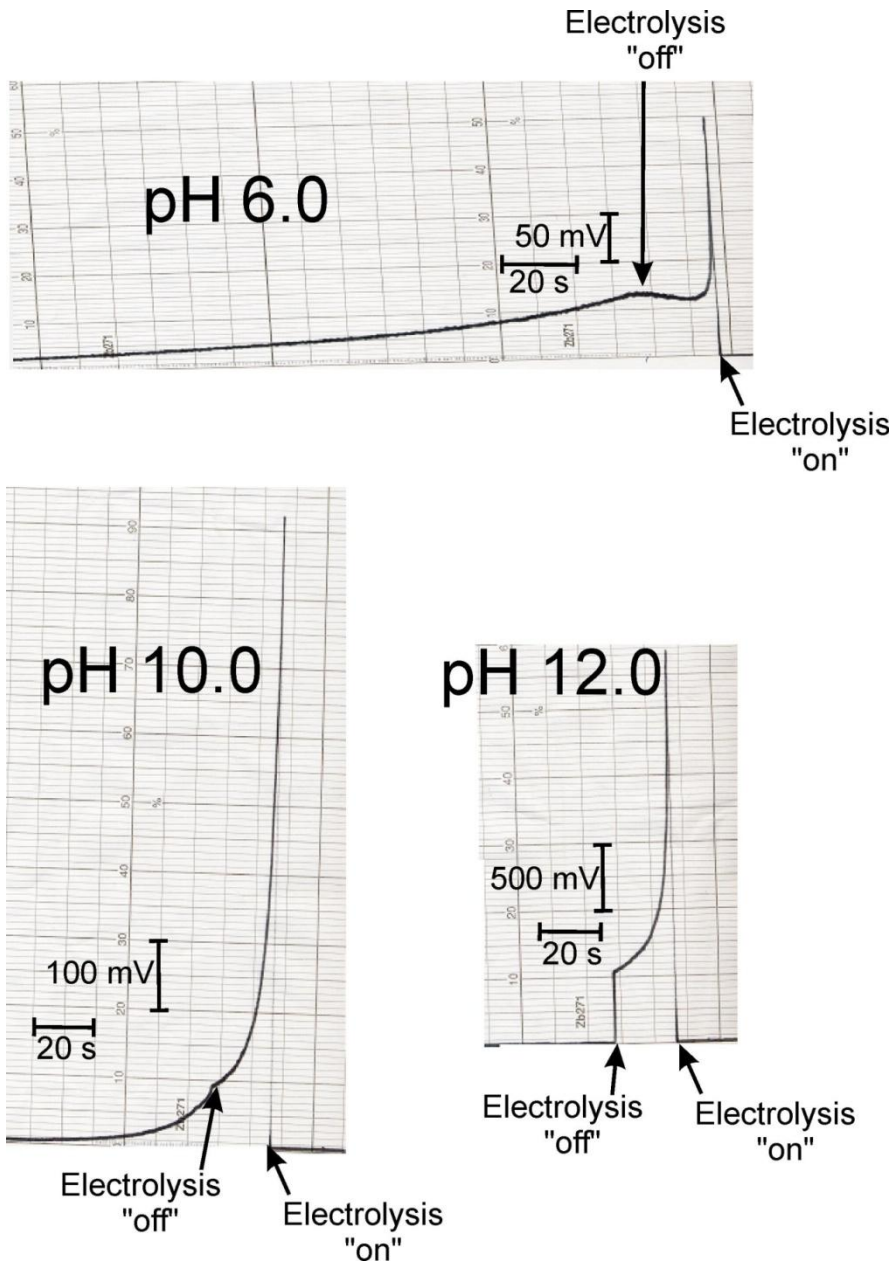

Figure 4.6: ECL transients (signal *vs.* time) obtained under a single stepped potential electrolysis (see text for parameters). The 3.0 mm diameter glassy carbon working electrode was modified with 1.0 nmol Oc_3N microdroplets and immersed into an aqueous solution containing 1.0 mM $Ru(bpy)_3^{2+}$. Panel (a) is for a solution containing only 0.1 M phosphate buffer solution; panel (b) exhibits representative data when the aqueous solution contains both 0.1 M sodium perchlorate and 0.1 M phosphate buffer solution.

It is evident that the ECL response is instantaneous with formation of $Ru(bpy)_3^{3+}$, attaining steady-state (except at higher values of solution pH) within a few seconds. Although chronoamperometric transients were recorded, these are of little value for this preliminary work since at certain solution pH values, these also contain information regarding the oxidation of the oil. It is clear from the data in Figure 4.6 that ECL occurs at every pH value in solution that was examined, with the ECL intensity being greatest for solution pH values in strongly alkaline media (pH > 10), and smallest when the aqueous phase is of low pH. Plots of the ECL signal intensity (the initial spike, or equivalently the steady-state value) against pH are illustrated in Figure 4.7.

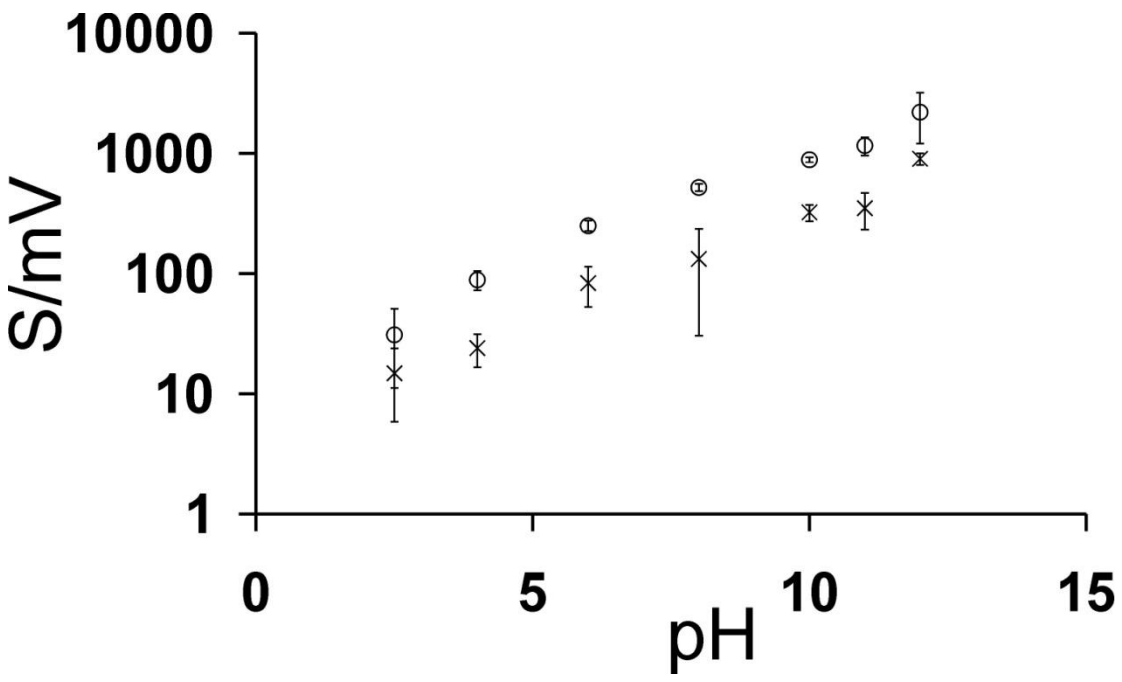

Figure 4.7: Plots of the maximal ECL signal intensity (S) as a function of the solution pH, when the aqueous solution contains 0.1 M phosphate buffer (×), or 0.1 M sodium perchlorate with 0.1 M phosphate buffer (o). Note that the ordinate axis is logarithmic. The points plotted are average data, with the standard deviation marking the error bars.

The slight discontinuity observed in these semi-logarithmic plots is a marker for the biphasic pK_a as it indicates a change in the mechanism of ECL production: above the interfacial pK_a, $Ru(bpy)_3^{3+}$ reacts with neutral trioctylamine, with electron transfer presumably occurring in concert with ion transfer (namely perchlorate ion insertion or proton expulsion) across the interface; below the heterogeneous pK_a, electron transfer across the liquid | liquid interface is apparently sluggish. Extrapolating as suggested from the data in Figure 4.7 indicates biphasic pK_a for this system is roughly between 9.7 and 10.8 (when perchlorate ions are absent or present in the aqueous phosphate buffer solution). These approximate values are reasonable estimates. We next explore the ECL transient data further.

The presence of perchlorate ions in the bathing aqueous medium exhibit a surprisingly large effect on the observed ECL magnitude; ECL signals are apparently greater when these ions exist in aqueous solution. We suggest this reflects the kinetics of the ion-coupled electron transfer process, but also, noting previous work by Bard *et.al* [27] regarding the distinct effect of halides on ECL intensity. Under strongly alkaline solution conditions, the following processes are plausible (scheme 4.2).

$$Ru(bpy)_3^{3+}(aq) + Oc_3N(l) + ClO_4^-(aq) \rightarrow Oc_3N^{+\bullet}ClO_4^-(l) + Ru(bpy)_3^{2+*}(aq) \rightarrow h\nu + Ru(bpy)_3^{2+}(aq) + Oc_3N^{+\bullet}ClO_4^-(l) \quad (a)$$

$$Ru(bpy)_3^{3+}(aq) + Oc_3N(l) \rightarrow Oc_3N^{+\bullet}(l) + Ru(bpy)_3^{2+*}(aq) \rightarrow h\nu + Ru(bpy)_3^{2+}(aq) + Oc_3N^{\bullet}(l) + H^+(aq) \quad (b)$$

Scheme 4.2

The further oxidation of the oil product can take place both at the solid electrode, or across the liquid | liquid interface. The reaction in the presence of perchlorate ions merely requires these to transfer and ion-pair from the aqueous phase as the organic oil is oxidised, to preserve the electroneutrality of the organic phases. In contrast, as hydroxide and phosphate are highly hydrophilic, we suggest charge-compensation by

ion-pair association at the interface. The alternative explanation of $Oc_3N^{+\bullet}$ "expulsion" from the oil phase cannot be ruled out.

Below the biphasic pK_a, the following mechanisms are possible.

$$Ru(bpy)_3^{3+}(aq) + Oc_3NH^+ClO_4^-(l) \rightarrow H^+(aq) + Oc_3N^{+\bullet}ClO_4^-(l) + Ru(bpy)_3^{2+*}(aq) \rightarrow h\nu + Ru(bpy)_3^{2+}(aq) + Oc_3N^{+\bullet}ClO_4^-(l) + H^+(aq) \quad (a)$$

$$Ru(bpy)_3^{3+}(aq) + Oc_3NH^+(l) \rightarrow H^+(aq) + Oc_3N^{+\bullet}(l) + Ru(bpy)_3^{2+*}(aq) \rightarrow h\nu + Ru(bpy)_3^{2+}(aq) + Oc_3N^{\bullet}(l) + 2H^+(aq) \quad (b)$$

Scheme 4.3

The first process can occur at the liquid | liquid interface (which may be perceived to be "sharp"). The last can only occur at a distance from the interface (the outer Helmholz plane equivalent), and is tantamount to suggesting that this latter reaction proceeds via a "diffuse" liquid | liquid interface. As in the case of the alkaline solution, the products of the proposed biphasic reaction may be oxidised further both at the solid electrode and at the liquid | liquid interface. The latter pathway may be the underlying cause of the increase in ECL signal intensity during the 20 s electrolysis as noticied in the low pH data reported in Figure 4.6. Alternative mechanisms such as two-electron oxidations to form Ru^I species, which may yield ECL via comproportionation with Ru^{III} species, or via excited-state quenching by Oc_3N [27], cannot be discounted.

It thus appears that ECL at liquid | liquid microinterfaces is highly sensitive to the chemical nature of the interface, and appears to be suited to the measurement of heterogeneous pK_a. It is insightful to enquire whether this droplet-modified system is able to afford any quantitative kinetics information, or even of the interfacial concentrations of protonated versus deprotonated amines as a function of aqueous pH.

The shape of the ECL transients illustrated in Figure 4.6 suggests there is a solution pH-dependent response in the cessation of ECL when the electrochemical perturbation is removed: at high pH values, ECL cessation is apparently instantaneous (within the accuracy of the recording equipment); in acidic solutions, there is a slow, first-order decay of the ECL signal. Extraction of the first-order decay constant (k) reveals a pH dependence illustrated in Figure 4.8.

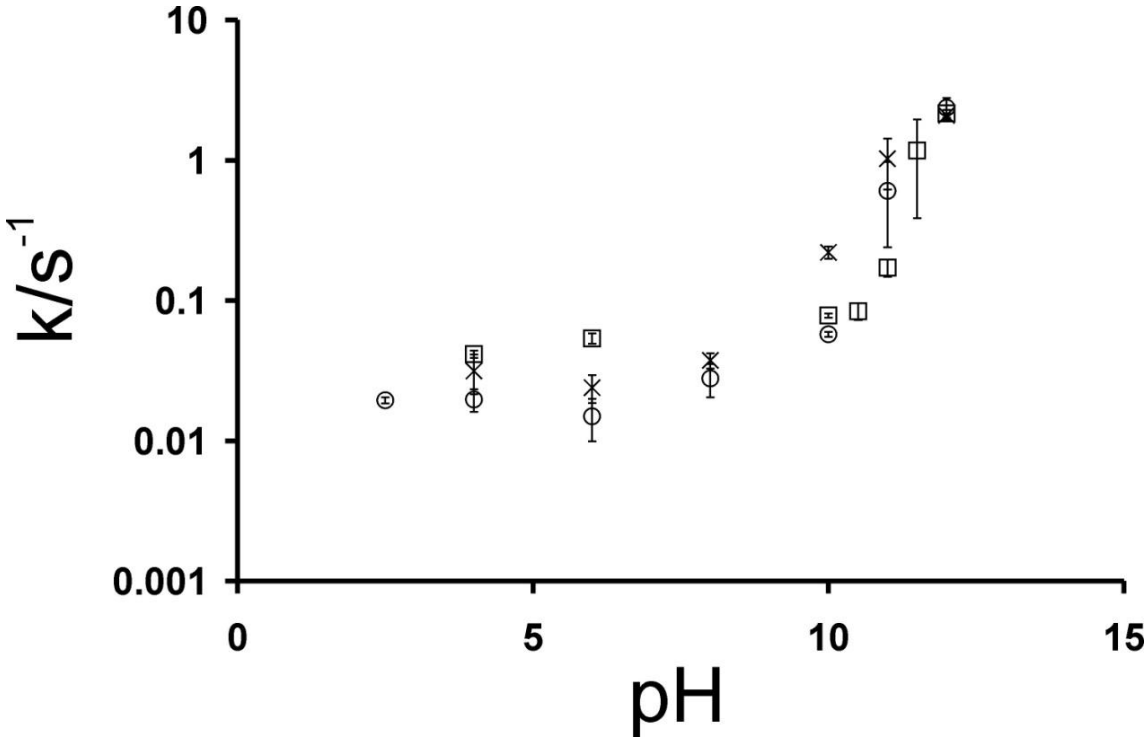

Figure 4.8: Plots of the observed first-order ECL decay constant (k) as a function of the solution pH. The solution contains 0.1 M phosphate buffer (×), or 0.01 M phosphate buffer (□), or 0.1 M sodium perchlorate and 0.1 M phosphate buffer (o) Note that the ordinate axis is logarithmic. The points plotted are average data, with the standard deviation marking the error bars.

The differences between the plots for aqueous ionic media likely stems from the enhanced interfacial conductivity discussed earlier when perchlorate ions are present in aqueous solution; the presence of electrical double layers ensure that electron transfer occurs over longer distances, so becomes slower and, correspondingly, more difficult to measure accurately. Nevertheless, such plots directly enable the extraction of the biphasic pK_a, which is found to be 10.7 when perchlorate ions are present (at 0.1 M

concentration) in the aqueous phase and 10.2 when the aqueous phase is merely phosphate buffer solution (at 0.1 M concentration). These values compare well with those reported via the measurement of the ECL signal intensity, although, these values are also merely estimates as they are extracted via reaction kinetics and have not been corrected for mass transport rates. Reducing the concentration of the phosphate buffer solution by an order of magnitude to 0.01 M effectively *increases* the apparent biphasic pK_a to 10.9 (see Figure 4.8). This is consistent with the perceived view presented in Figure 4.3b: increasing the size of the solution-phase double layer by reducing its ionic strength causes electron-transfer to occur over larger distances, demonstrating that the ECL experiment is sensitive to interfacial structure and activity effects. However, the whole picture is further complicated by anion association effects, as suggested for the case in the presence of perchlorate ions, and the possibility of diffusion-migration of the electrogenerated Ru^{III} species within the occurring in the solution phase in the droplet-centred electrical double layer, under conditions of full protonation of the liquid | liquid interface cannot be neglected.

To understand the reason for the non-instantaneous ECL decay, consider the following approximation of the reaction mechanisms, where we also include a non-radiative (NR) decay (scheme 4.4).

$$Ru^{III}(aq) + oil^{Red}(l) \underset{k_{-1}}{\overset{k_1}{\rightleftharpoons}} oil^{Ox}(l) + Ru^{II}*(aq) \quad (a)$$

$$Ru^{II*}(aq) \xrightarrow{k_2} h\nu + Ru^{II}(aq) \quad (b)$$

$$Ru^{II*}(aq) \xrightarrow{k_{NR}} Ru^{II}(aq) \quad (c)$$

Scheme 4.4

Application of the steady-state hypothesis (ignoring diffusion effects) to $Ru(bpy)_3^{2+}*$ results in the following expression for the ECL signal intensity (S):

$$S \propto k_2 \left[Ru^{II*} \right] \approx \phi k_1 \left[Ru^{III} \right] \Gamma_{oil^{Red}} \quad \textbf{Equation4.5}$$

where ϕ is the quantum yield of the ECL ($\phi = \frac{k_2}{(k_2 + k_{NR})}$), and the reverse electron transfer is assumed to be kinetically pathological, *viz.* $k_{-1}\Gamma_{oil}^{ox} \ll k_2 + k_{NR}$. Since the ECL signal measures the decay of the excited state, the associated rate constant (k_2) is, under the approximation of negligible ionic strength effects, and ignoring environmental influences, independent of the solution pH. This means that the observed decay stems from the pH-dependent bimolecular reaction kinetics at the liquid | liquid interface. With the cessation of electrolysis, Ru^{III} is no longer regenerated so as to react with the oil, causing the observed first-order signal decay. The pH-dependence thus merely reflects the slow kinetics of the liquid | liquid proton-coupled electron transfer at low solution pH, and its mechanism change when the surface is fully deprotonated. Although it is not possible to determine the activation free energy for this reaction, unless drastic approximations are made, it is possible to calculate the fraction of the interface that is protonated at each value of the solution pH, thereby determining a true, thermodynamic value of the biphasic pK_a using the values extracted from the kinetics measurements. Assuming that the most acidic conditions employed herein corresponds to a fully protonated interface (and so has a first order decay constant of k_{AH^+}), that observed at the most alkaline (solution pH 12.0) corresponds to a fully deprotonated interface (with first order decay constant of k_A), and that increases in the observed kinetics of the decay results from the linear combination of kinetics due to fast reaction between deprotonated oil and the electrogenerated oxidant, the fraction of deprotonated amine can be deduced by solving the following quadratic expression, estimating activity coefficients using the extended version of the Debye-Hückel Law:

$$\lg\left(f_{H^+}\right) = -\frac{0.5\sqrt{I}}{1+\sqrt{I}} \qquad \textbf{Equation 4.6}$$

noting that aqueous phosphoric acid has the following acid association constants at 298 K [28]: pK_{a1} = 2.15, pK_{a2} = 7.20, pK_{a3} = 12.35).

$$k = k_A\Theta_A + \left(\frac{k_{AH^+} f_{H^+}}{K_a^{biphasic} / \Gamma_{oil^{Red}}} \right) \Theta^2_{AH^+}$$ **Equation 4.7**

†Equation 4.7 also requires the assumption of the surface concentration of redox sites, $\Gamma_{oil^{Red}}$. The experimental data were undertaken using 1.0 nmol of Oc_3N. It is not unreasonable to assume the droplets are hemispherical and uniformly distributed and with a average size (r_0) of 10 μm.

Figure 4.9 shows the fractional surface concentration of protonated (AH^+) and deprotonated (A) Oc_3N.

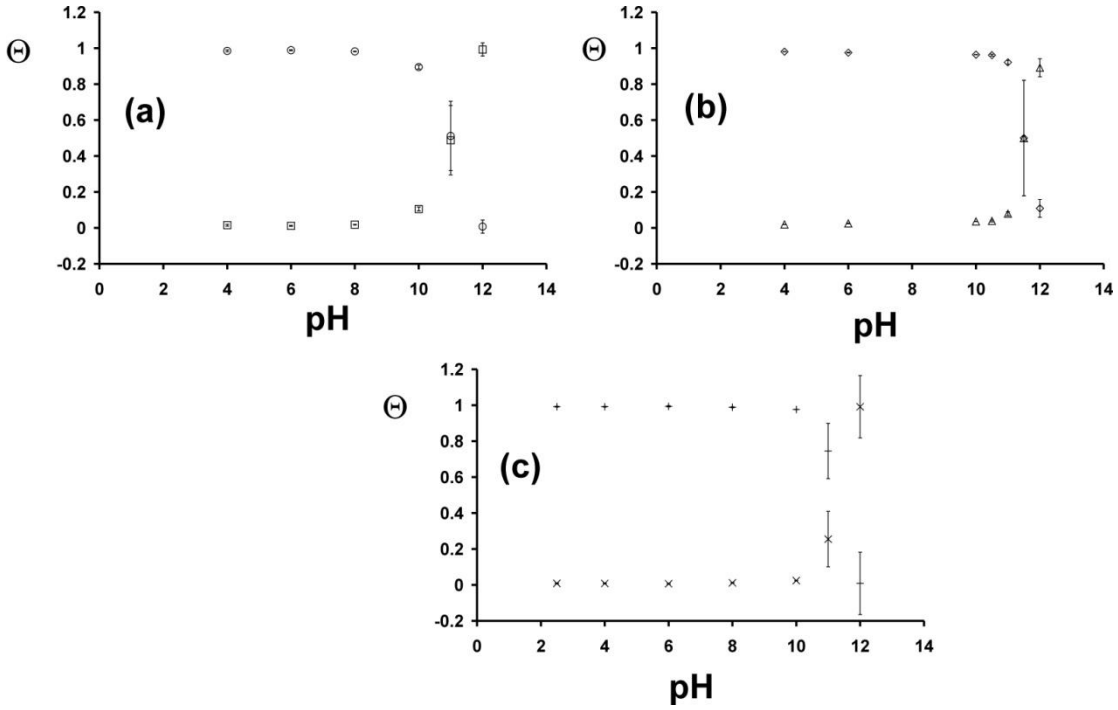

Figure 4.9: Plots illustrating the fractional surface concentration (Θ) of protonated (AH^+) and deprotonated (A) Oc_3N. (a) 0.1 M phosphate buffer solution, □ Θ_A, o Θ_{AH}^+; (b) 0.01 M phosphate buffer solution, Δ Θ_A, ◊ Θ_{AH}^+; (c) 0.1 M sodium perchlorate with 0.1 M phosphate buffer solution, × Θ_A, + Θ_{AH}^+. The points plotted are average data, with the standard deviation marking the error bars.

In this way, noting that $\Theta_{AH^+} + \Theta_A = 1$, the plots given in Figure 4.9 can be constructed, using the estimated biphasic pK_a values obtained from Figure 4.8 as an initial guess of

the true heterogeneous pK_a, and iterating through until the data become consistent. As anticipated, the plots for the individual protonated and deprotonated fractions intersect at the true biphasic pK_a, when $\Theta_{AH^+} = \Theta_A = 0.5$. It is evident that these "activity-corrected" biphasic pK_a determination plots vary little (within experimental error) on the ionic media: the estimated biphasic pK_a values are 11.2 ± 0.1 (in 0.1 M phosphate buffer solution), 11.5 ± 0.1 (in 0.01 M phosphate buffer solution), and 11.3 ± 0.1 (in 0.1 M phosphate buffer solution containing 0.1 M sodium perchlorate).

4.2.4 Amperometric and ECL Measurements in Deuterated Phosphoric and Basic Conditions.

After the study of the liquid | liquid interface using solutions with protons and the pKa calculation, the same procedure was applied for solution containing deuterium isotope (D) instead of protons. With these set of experiments the effect of the mechanism in deuterium conditions and the kinetic isotope effects were investigated.

Single step chronoamperometry at 1.2 V for 25 s was applied. When the voltage was applied (t= 0s) no ECL signal was observed. However, the signal appears after 20 s which is consisted with the results reported in Section 4.2.3. The pD of the solutions was also measured using a pH meter (Table 4.1).

Solution	$pD_{measured}$	$pD_{corrected}$
0.1 M D_3PO_4	0.94	1.34
0.06 M D_3PO_4/ 0.04 M NaOD	1.58	1.98
0.05 M D_3PO_4/ 0.05 M NaOD	1.77	2.17
0.04 M D_3PO_4/ 0.06 M NaOD	2.85	3.25
0.03 M D_3PO_4/ 0.07 M NaOD	6.83	7.23
0.02 M D_3PO_4/ 0.08 M NaOD	9.41	9.81
0.01 M D_3PO_4/ 0.09 M NaOD	13.15	13.55
0.1 M NaOD	13.78	14.18

Table 4.1: The $pD_{measured}$ and calculated $pD_{corrected}$ for the solutions in D_2O. The measured pD data could be erroneous due to the alkaline error known with pH probes.

Before the measurements were taken the pH probe was left in deuterium oxide (D_2O) solution for 3 days to condition it. According to literature the pD of a solution in D_2O can be determined by the use of Equation 4.8 [29-31]. When measuring the pH, it was noted that the measured data could be erroneous due to the alkaline error known with pH probes.

$$pD = ``pH'' + 0.40$$

Equation 4.8: The pD of the solutions is determined by adding a corrective factor of 0.40, (''pH'' is the apparent pH meter reading in D_2O solution).

The maximum signal (S_{max}) and the signal where electrolysis is stopped (S_{end}) *versus* the pD are illustrated in Figure 4.10 and Figure 4.11 respectively for 1 mM $Ru(bpy)_3^{2+}$ in $NaOD/D_3PO_4$ solution in different concentrations and 2 nmoles of the TOA droplet. Both signals increase exponentially as the pD increased, as expected and compare well with those reported in Section 4.2.3

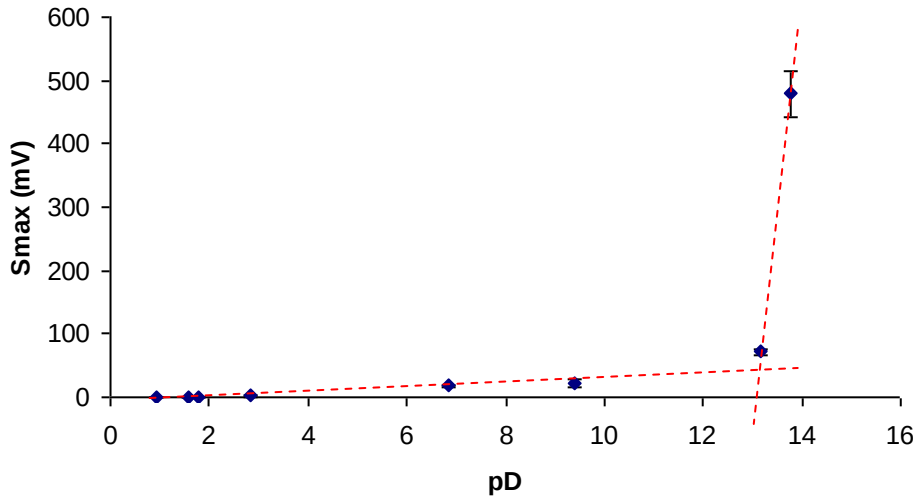

Figure 4.10: S_{max} as a function of the solution pD for 1 mM $Ru(bpy)_3^{2+}$ in $NaOD/D_3PO_4$ solution in different concentrations and 2 nmoles TOA. The points plotted are average data, with the standard deviation marking the error bars (n=3).

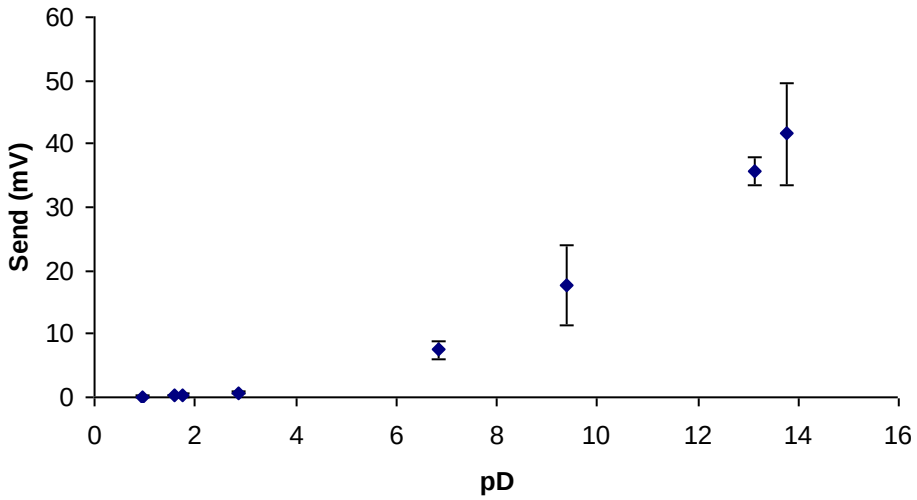

Figure 4.11: S_{end} as a function of the solution pD for 1 mM $Ru(bpy)_3^{2+}$ in $NaOD/D_3PO_4$ solution in different concentrations and 2 nmoles TOA. The points plotted are average data, with the standard deviation marking the error bars (n=3).

The resulting decay constant was plot with pD and pD corrected (Figure 4.12 and 4.13 respectively). The pKa biphasic was estimated at 13.18 without correcting the pD. When the pD is corrected an increase of the pKa biphasic is observed at 13.54.

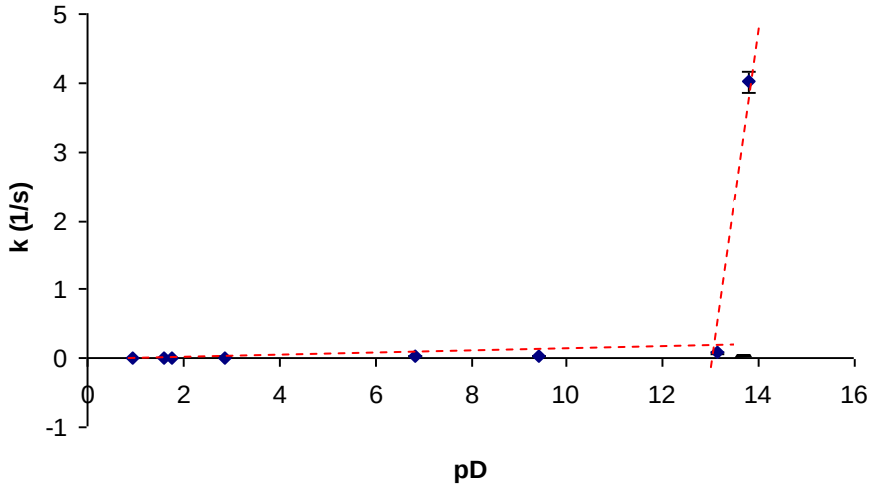

Figure 4.12: The first- order ECL decay constant (k) as a function of the solution pD for 1 mM $Ru(bpy)_3^{2+}$ in D_3PO_4 / NaOD and 2 nmoles TOA marking the error bars (n=3).

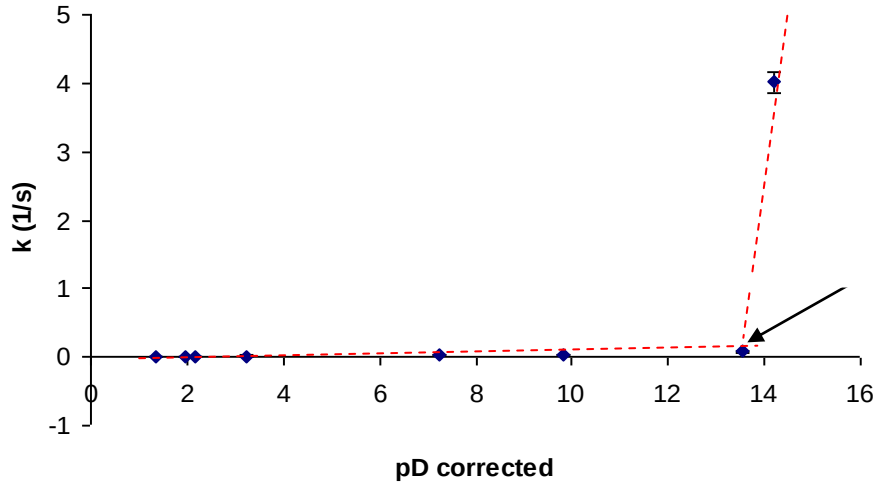

Figure 4.13: The first- order ECL decay constant (k) as a function of the solution pD corrected for 1 mM $Ru(bpy)_3^{2+}$ in D_3PO_4 / NaOD and 2 nmoles TOA.. The points plotted are average data, with the standard deviation marking the error bars (n=3).

Figure 4.14 compares the pKa between protonated and deuterated solutions. Comparing these data with the $^1H^+$ data obtained in Section 4.2.3, it is clear that there is a small kinetic isotope effect in the proton-coupled electron transfer, as anticipated, and suggests that the reaction mechanisms proposed are likely accurate.

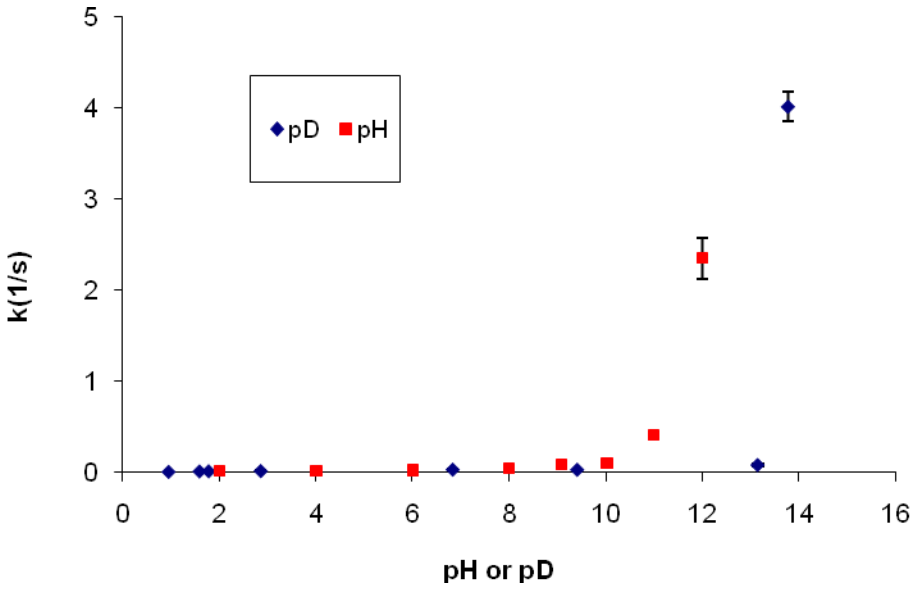

Figure 4.14: The comparison of the pKa between protonated and deuterated solutions. The first-order ECL decay constant (k) as a function of the solution pD and pH. The points plotted are average data, with the standard deviation marking the error bars (n=3).

ECL transients (Figure 4.15 and 4.16) show that the luminescence decay is first-order and is faster in strongly alkaline media, being the fastest in pD 13.78. However, the decay becomes slower when the aqueous phase goes to lower pD. This compares well to the results reported in Section 4.2.3 and in literature [2]. Moreover, the shape of the ECL transients shows that the termination of the ECL depends on the solution pD. At high alkaline solutions the ECL termination is almost instantaneous. On the other hand, in lower pD values a slow first-order decay of the signal occurs. These results are consisted with those reported for protonated solutions.

The ECL transients for the rest of the deuterated solutions are not shown due to very small ECL signals obtained.

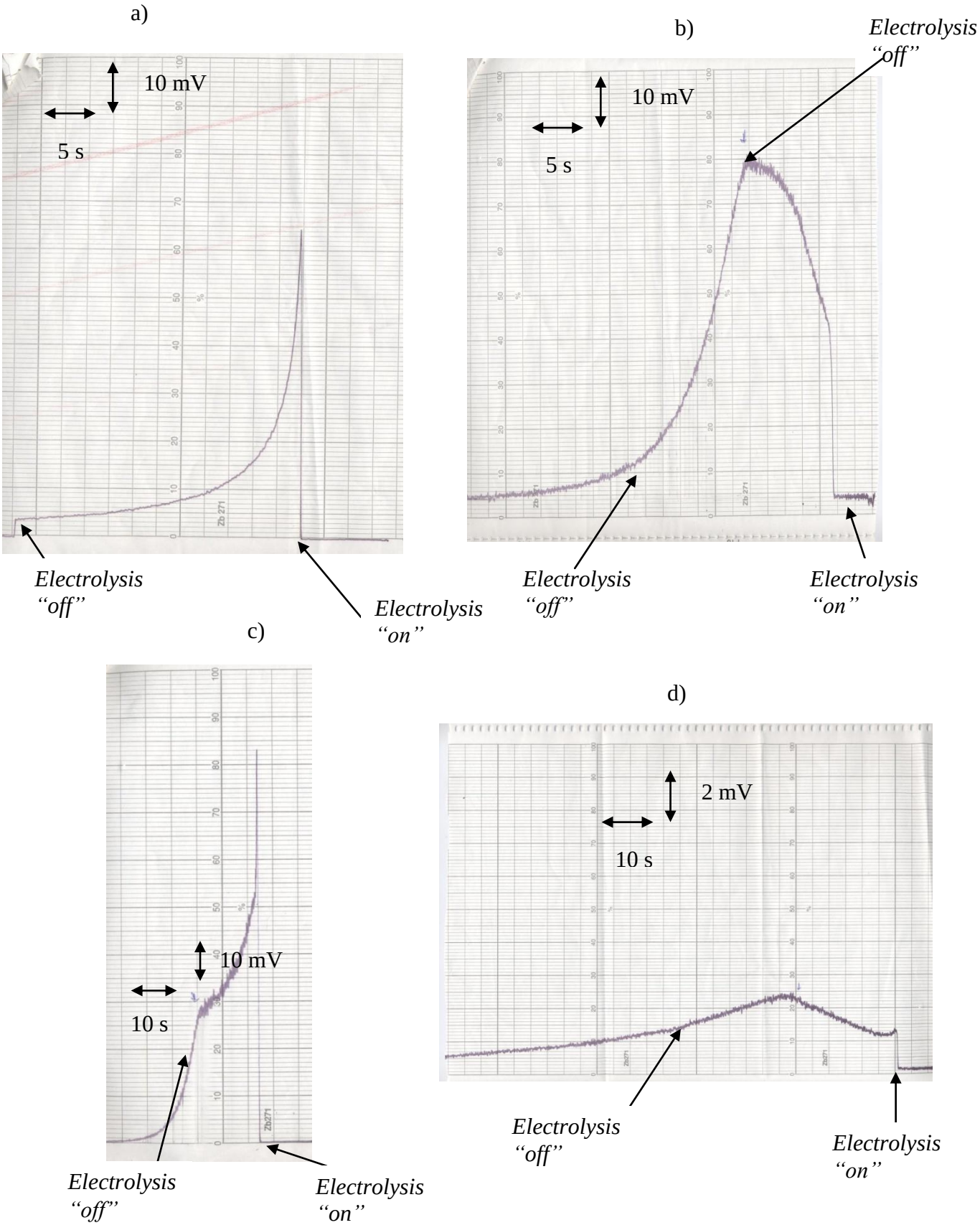

Figure 4.15: The ECL signals recorded by chart recorder (signal vs. time) for 1 mM $Ru(bpy)_3^{2+}$ with 2 nmoles TOA in D_3PO_4 / NaOD solution of a) pD 13.78 , b) pD 13.15, c) pD 9.41 and d) pD 6.83.

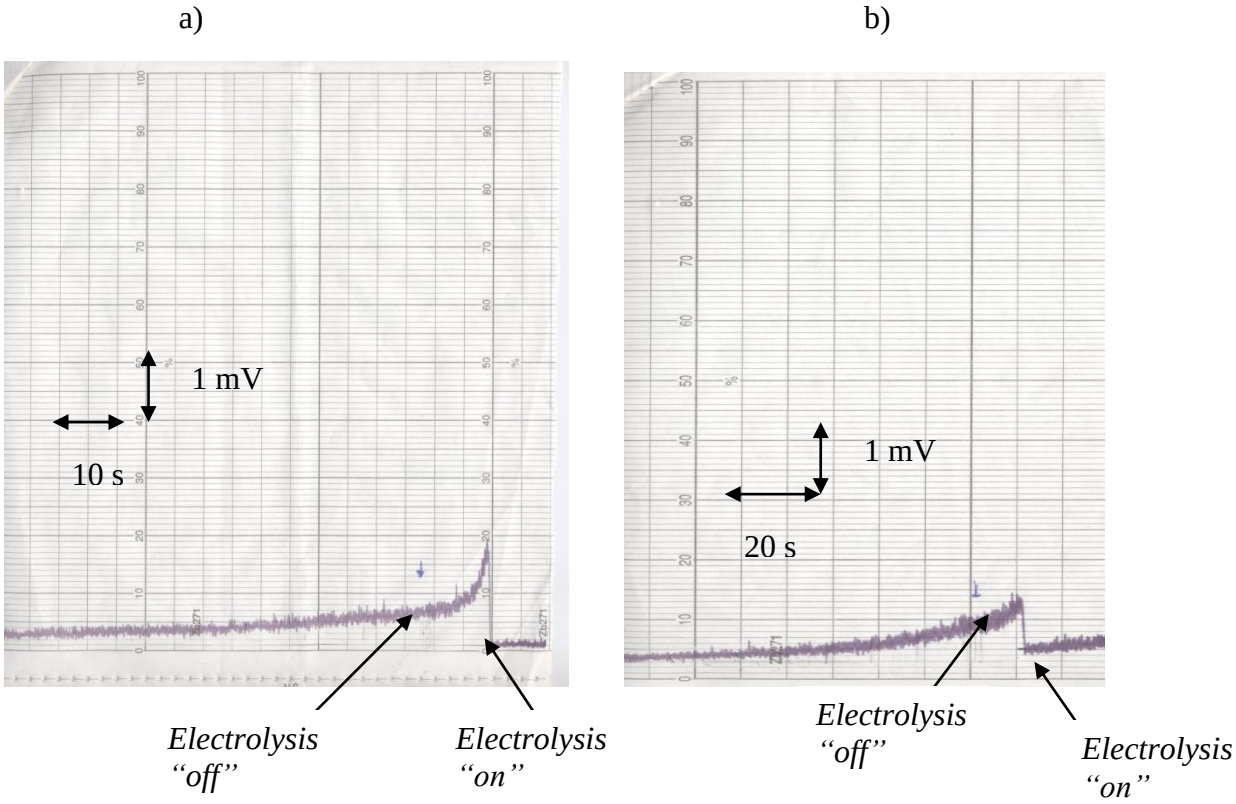

Figure 4.16: The ECL signals recorded by chart recorder (signal vs. time) for 1 mM $Ru(bpy)_3^{2+}$ with 2 nmoles TOA in D_3PO_4 /NaOD solution of a) pD 2.85 and b) pD 1.77.

4.3 Conclusions

The use of tris(2,2'-bipyridyl)ruthenium(II) as an electrochemiluminescence reagent and the modification of the electrode using microdroplets of a highly hydrophobic tertiary amine (trioctyamine) was demonstrated in this report. ECL combined with droplet-modified electrodes can give information about the molecular structure of the liquid|liquid interface and thus the heterogeneous pKa. The reaction was studied in fully protonated and deprotonated conditions in aqueous solutions. The extent of the electrochemiluminescence production is shown to be dependent on the degree of the interfacial protonation.

Analysis of the ECL transients gave an estimation of the biphasic pKa which was found to be approximately 10.8 for protonated solutions. This is satisfying close to values previously reported for trioctylamine (pKa biphasic 11) [2]. Furthermore, the mechanism was studied in deuterium conditions in order to investigate the kinetic isotope effects on the biphasic pKa. Results showed that the pKa increases to 13.18 when deuterium is used instead of protons indicating a trend.

The shape of the transients for both cases show a faster decay in highly alkaline media and a slower luminescence decay when the solutions go to lower pH. This indicates that above the pKa biphasic region an outer sphere electron transfer occurs. However, below the pKa region the amine is protonated and a proton-coupled electron transfer appears to be dominated. Moreover, the investigation of the reaction in different $Ru(bpy)_3^{2+}$ concentrations showed that the pKa is independent of the concentration of the solution, indicating that the decay is first-order as expected.

ECL at droplet-modified electrodes has been demonstrated, and has been employed to extract information regarding the molecular structure of the oil | aqueous interface, and thus its heterogeneous pK_a, under appropriate assumptions. The biphasic pK_a for trioctylamine in aqueous solution appears to be *ca.* 11. This is satisfyingly close to values previously reported for *n*-octylamine and dioctylamine (10.65 and 11.01 respectively at 298 K) and dihexylamine (11.01 at 298 K) in ethanol/water mixtures [32] and of aqueous triethylamine and tripropylamine (10.9 and 10.4 respectively at

298 K)[27].

4.4 References

1. C.E. Banks, T.J. Davies, R.G. Evans, G. Hignett, A.J. Wain, N.S. Lawrence, J.D. Wadhawan, F. Marken and R. G. Compton, *Phys. Chem. Chem. Phys.*, 2003, **5**, 4053.
2. C. Lledo-Fernandez, I. Hatay, M.J. Ball, G.M. Greenway and J. Wadhawan, *N. J. Chem.*, 2009, **33,** 749.
3. J.A. Bard and R. L. Faulkener, *Electrochemical Methods:Fundamentals and Applications, Consultants Bureau, New York,* 2nd Edition, 2001.
4. K.W. Willman and R. W. Murray, *Anal. Chem.*, 1983, **55**, 1139.
5. C.P. Andrieux and J.-M. Savéant, *Molecular Design of Electrode Surfaces*, New York, 1992.
6. C.P. Andrieux and J.-M.Savéant, *J. Electroanal. Chem.*, 1978, **93**, 163.
7. H. Matsuda, K. Aoki and K. Tokuda, *J. Electroanal. Chem.*, 1987, **217**, 1.
8. H. Matsuda, K. Aoki and K. Tokuda, *J. Electroanal .Chem.*, 1987, **217**, 15.
9. A.P. Brown and F. C. Anson, *Anal. Chem.*, 1977, **49**, 1589.
10. R.G. Compton, M.E. Laing, A. Ledwith and I. I. Abu-Abdoun, *J. Appl. Electrochem.*, 1988, **18**, 431.
11. U. Schröder, J.D. Wadhawan, R.G. Compton, F. Marken, P.A.Z. Suarez, C.S. Consorti, R.G. de Souzs and J. Dupont, *New J. Chem.*, 2000, **24**, 1009.
12. E. Laviron, *J. Electroanal. Chem.*, 1979, **100**, 263.
13. D.F. Smith, K. Willman, K. Kuo and R. W. Murray, *J. Electroanal. Chem.*, 1979, **95**, 217.
14. J.C. Lennox and R. W. Murray, *J. Am. Chem. Soc.*, 1978, **100**, 3223.
15. U. Schröder, J.D. Wadhawan, R.G. Evans, R.G. Compton, B. Wood, D.J. Walton, R.R. France, F. Marken, P.C.B. Page and C. M. Hayman, *J. Phys. Chem. B.*, 2002, **106**, 8697.
16. J.D. Wadhawan, R.G. Evans, C.E. Banks, S.J. Wilkins, R.R. France, N.J. Oldham, A.J. Fairbanks, B. Wood, D.J. Walton, U. Schröder and R. G. Compton, *J. Phys. Chem. B.*, 2002, **106**, 9619.
17. K. Aoki, P. Tasakorn and J. Chen, *J. Electroanal. Chem.*, 2003, **542**, 51.
18. A.J. Wain, A.N. Kirkham, D.J. Walton, B. Wood, R.R. France, S.D. Bull, J.D. Wadhawan and R. G. Compton, *J. Am. Chem. Soc.*, 2003, **125**, 11418.
19. J.D. Wadhawan, R.G. Evans and R. G. Compton, *J. Electroanal. Chem.*, 2002, **533**, 71.
20. O. Hammerich and H. Lund, *Organic Electrochemistry*, 4th Edition, New York, 2000.
21. F. Scholz, U. Schröder and R. Gulaboski, *Electrochemistry of Immobilised Particles and Droplets*, Berlin (Germany), 2005.
22. U. Schröder, R.G. Compton, F. Marken, S.D. Bull, S.G. Davies and S. Gilmour, *Phys. Chem. B*, 2001, **105**, 1344.
23. C. Amatore, E. Maisonhaute, B. Schollhorn and J. Wadhawan, *ChemPhysChem*, 2007, **8**, 1321.
24. M.C Buzzeo, R.G. Evans and R.G. Compton, *ChemPhysChem*, 2004, **5**, 1106.
25. G.K. Rowe and S.E. Creager, *Langmuir*, 1991, **7**, 2307.
26. L. Zhao, Y. Tao and X. Chen, *Acta Chim. Sinica.*, 2006, **64**, 320.
27. F. Kanoufi, Y. Zu and A.J. Bard, *J. Phys. Chem. B*, 2001, **105**, 210.

28. D.R. Lide, *CRC Handbook for Chemistry and Physics*, 76th Edition, Boca Raton, 1995.
29. N. C. Li, P. Tang and R. Mathur, *J. Am. Chem. Soc.*, 1981, **65**, 1074.
30. R. G. Bates, *Determination of pH*, New York, 1973.
31. J. M. El Hage Chahine and J. E. Dubois, *J. Chem. Soc. Perkin Trans. II* 1985, 25.
32. D.D. Perrin, *Dissociation Constants of Organic Bases in Aqueous Solution*, London, 1965.

Chapter 5

Electrochemical/Chemical Synthesis and Isolation of the Fully Reduced Vitamin B_{12} Species for the Catalytic Reduction of Trans-1,2-Dibromocyclohexane (DBCH)

5.0 Aims of the Chapter

Having already studied homogeneous and biphasic redox catalytic reactions involving Ru^{II} (see Chapters 3 and 4 respectively), this Chapter investigates homogeneous solutions redox catalysis involving microconfined areas afforded by microfluidic flow cells. The aim of the work in this chapter was to investigate on a micro scale a redox catalytic reaction between vitamin B_{12s} (Co(I)) (which was electrogenerated from vitamin B_{12}(Co(III)) with vicinal dibromoalkanes (*trans*-1,2-dibromocyclohexane (DBCH)) to produce an olefin (cyclohexene).

This is a complex electrochemical catalytic reaction in a single liquid phase (homogeneous phase). The work is divided in to two parts, in the first part of the work vitamin B_{12} is chemically reduced to vitamin B_{12s}. The second part of the work describes the catalytic reduction of *trans*-1,2-dibromocyclohexane (DBCH) by B_{12s} (Co (I)) and the synthesis of cyclohexene. This reaction is first carried out on a batch scale and then the advantages of using a microfluidic device for synthesis are investigated.

5.1 Introduction to the Chemistry of Vitamin B_{12}

5.1.1 History

The history of vitamin B_{12} presents different points of departure from the usual pattern of vitamin discovery and elucidation. The first real stride toward the elucidation of the vitamin B_{12} was made in 1926 by Minot and Murphy when they demonstrated control pernicious anemia by ingestion of liver.

In 1948 a red crystalline compound designated vitamin B_{12} was described by Rickes *et.al.*[1]. West [2] found that this new crystalline compound was clinically active giving haematological response in patients with pernicious anemia.

The elucidation of the chemical structure of the vitamin B_{12} was first published in 1955 by Hodgkin and Smith[3]. The vitamin B_{12} coenzymes were first discovered by Barker and his colleagues [4, 5].

5.1.2 Isolation and Purification

There are basically two main methods to isolate vitamin B_{12}. The method used by Lester, Smith and Parker [6] in which vitamin B_{12} was extracted from liver extracts as follows. Proteolysed liver extract was treated with charcoal, and the adsorbate was eluted with hot 65% ethanol. Partition chromatography on damp silica or starch using aqueous butanol or isopropanol as the moving phase, was used to purify the extract.

5.1.3 Structure

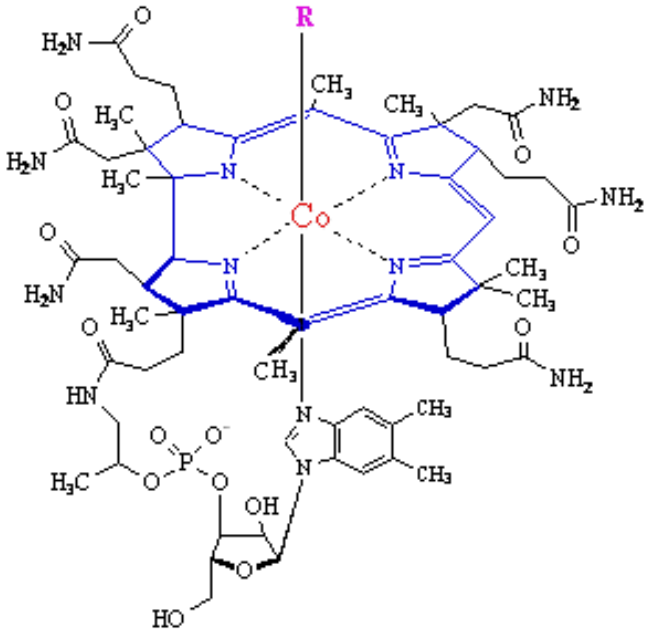

Figure 5.1: Structure of vitamin B_{12} (adapted from reference [7]).

The molecular structure of vitamin B_{12} is extremely complex. Vitamin B_{12} is a member of the vitamin B complex, the so-called cobalamins which are octahedral Co (III) complexes. Vitamin B_{12} is a cobalt coordination complex containing one replaceable cyano group which is tightly and co-ordinately bound to the cobalt atom [7]. The trivalent state to the cobalt form is assigned by magnetic susceptibility measurements [8-10], which indicated the diamagnetic character of the vitamin.

As can be seen from Figure 5.1 the structure of the vitamin B_{12} is a corrin ring (Figure 5.2) with various attached sidegroups co-ordinated in the equatorial positions by the polycyclic corrin nucleous and in the axial positions by a 5,6-dimethylbenzimidazole residue and an R group. Vitamin B_{12} has the similar structure of porphyrin, but with one of the bridging methylene groups removed. All the nitrogen from the pyrroles are linked to the central cobalt.

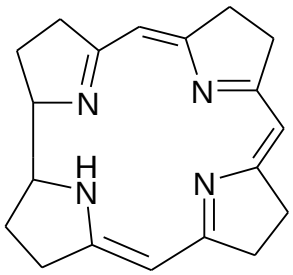

Figure 5.2: Structure of corrin ring.

The cobalt can link to R which can be:

a) CH_3 – as in methylcobalamin.
b) CN –as in cyanocobalamin.
c) 5'-deoxyadenosine at the 5' position- as in adenosylcobalmin (coenzyme B_{12}).

By treatment with hydrogen and a catalyst, photolysis or with sulphurous acid the cyano group attached to the central cobalt atom can be removed. This group therefore, can be substituted by other radicals or by hydroxyl, giving a series of cobalamins *e.g.*, when R = CN and HCl is bound to OH the molecule is called hydroxycobalamin (B_{12a}), and nitrito-cobalamin (vitamin B_{12c}) occurs when in an acid solution changes to the basic aquo-cobalamin with co-ordinated water molecules.

The reduced forms of vitamin B_{12} are Co (II) (B_{12r}) and Co (I) (B_{12s}).

5.1.4 Metabolic Role, Functions and Importance

Vitamin B_{12} is not synthesised by plants or animals, a bacteria named archae is the only type of organism able to synthesise the vitamin [11]. It is found primarily in meat, eggs and dairy products. It is the only nutrient known that contains cobalt. The commercial production of cyanocobalamin and its related analogous are achieved either by fermentation of *Streptomyces griseus* or *Streptomyces aureofaciens* or as a product of antibiotic production.

The importance of vitamin B_{12} is enormous for the synthesis of red blood cells, the maintenance of a healthy nervous system, growth and development in children and the normal functioning of the brain. It is generally involved in other functions in the body such as synthesis of fatty acid, production of energy, synthesis and regulation of DNA during cell division.

Deficiency of vitamin B_{12} can cause irreversible and severe damage especially to the nervous system and the brain. When the levels of vitamin B_{12} are slightly lower than the normal levels a range of symptoms may be experimented in humans, such as depression, fatigue, poor memory and poor growth, degenerative changes in spinal cord, nervous symptoms, decreased blood and tissue lipids, disturbed carbohydrate metabolism-excretion of methylmalonic acid, gastrointestinal tract changes [12]. Addison's and Biermer's (pernicious anemia) disease are the main syndrome of vitamin B_{12} deficiency [13].

5.1.5 The Reduction of the Vitamin B_{12}

The cobalt atom in cobalamins and cobinamides can exist under three main formal oxidation states, Co(III), Co(II), Co(I), which display quite different chemical properties. By studying the voltammograms Co(III) can appear as an electrophile, Co(II) as a radical, and Co(I) as a nucleophile. The oxidoreductive conversions between the three oxidation states are very important in the chemistry of vitamin B_{12}. Electrochemistry is an important valuable source of information for investigating the redox chemistry of vitamin B_{12}. It can be used to study the reduced forms. Over the last

three decades cyclic voltammetry (CV) has been used to describe the electrochemistry behaviour of B_{12} [14-16], B_{12a} [14], B_{12r} [14, 15, 17] and B_{12s} [14, 15].

One of the most unusual features of vitamin B_{12} is its reducibility to vitamin B_{12s} the highly reactive species which is now well-recognised to be a Co (I) complex [18-24].

The spin-paired species Co(I) is in vitamin B_{12s} the predominant form in alkaline solutions, in which the cobalt atom has the properties of a strong nucleophile [18]. To date vitamin B_{12s} is the most powerful nucleophile known, therefore reacts very well with species such as trans 1,2-dibromocyclohexene (DBCH) producing cyclohexene. The mechanism is illustrated in Section 5.2

Two main methods have been described in the literature for the reduction of vitamin B_{12}. Diehl and Murie [25, 26] used catalytic hydrogenation, lithium boron hydride in aqueous solution or sodium boron hydride and chromous acetate in aqueous solution[18]. Alternatively, Boos, Carr and Conn [27, 28] used ethylenediaminetetraacetate buffer at pH 9.5 with chromous acetate. Other reducing agents [19, 29] that have been employed include: DL-cysteine in alkali solution [30, 31], zinc dust in aqueous solution or as reported by Scheffold *et. al.*,[32] where the zinc is activated by using 0.1 M hydrochloric acid and washed with water, ammonium chloride[18, 28], or hypophosphorous acid [27].

5.2 Mechanism

Over the last decades the importance of the electrochemistry of vitamin B_{12} has been reported by different authors [33-40]. The redox catalytic reactions can be seen in Figure 5.3.

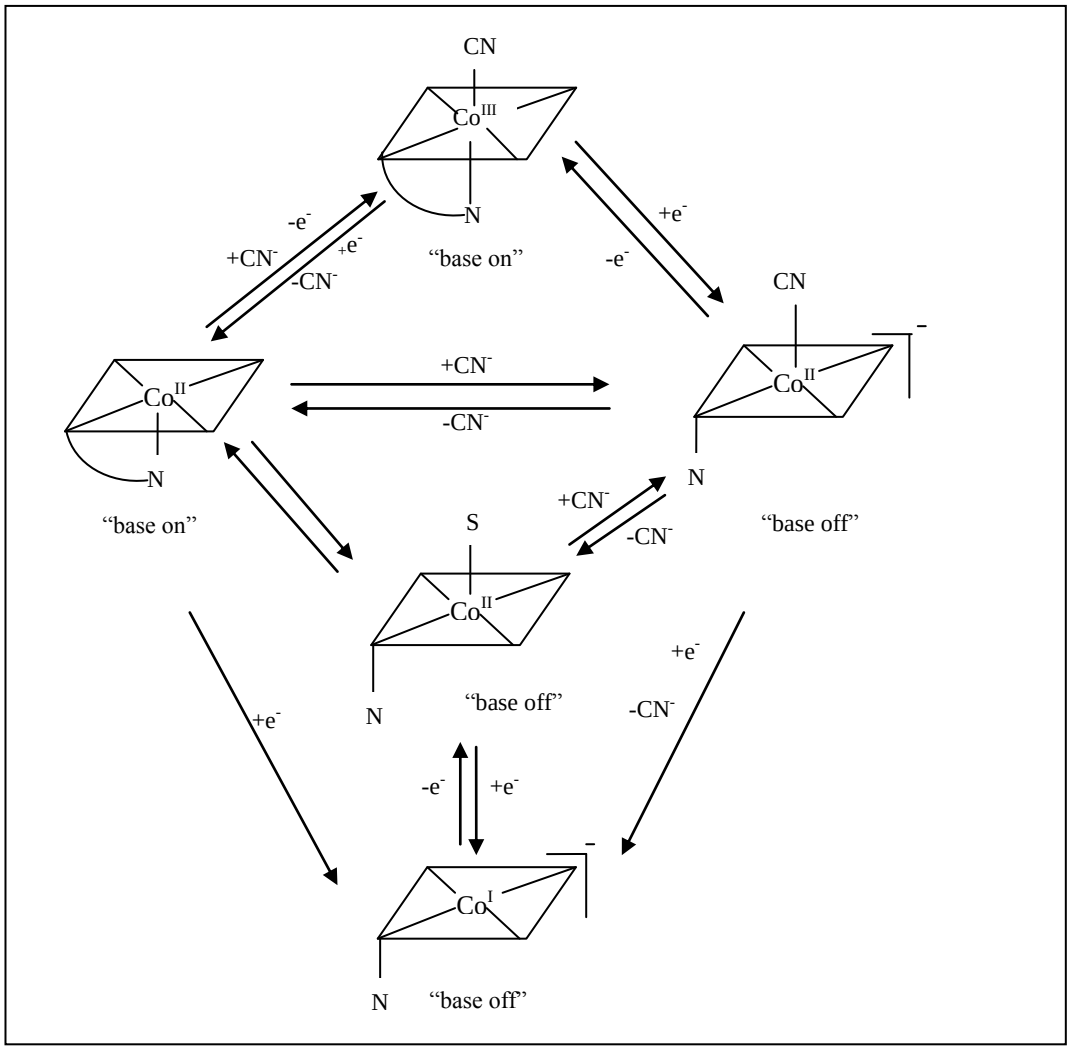

Figure 5.3: Oxidation-reduction chart for cyanocobalamin B_{12} adapted from reference [37, 41, 42].

The reduction process can take place at an electrode and the electrocatalytic reaction between vitamin B_{12} and DBCH is shown in Equation 5.1:

Electrode: $Co(III)L + e^{-} \rightarrow Co(II)L$

Electrode: $Co(II)L + e^{-} \leftrightarrow Co(I)L$

Solution: $Co(I)L + DBCH \rightarrow BrCo(III)L + R^{'} + Br^{-}$

Solution: $BrCo(III)L + Co(I)L \rightarrow 2Co(II)L + Br^{-}$

Equation 5.1: Equation adapted from reference [43].

In the reaction Co(II)L (or vitamin B_{12r}) is reduced to Co(I)L at the electrode surface. The coupled electrochemical homogeneous reactions follow an electrocatalytic pathway, in which a fast electron transfer occurs between the Co(I) macrocycle and the DBCH. This leads to the formation of the cyclohexene and the regeneration of the Co(II)L [44]. This can be seen more clearly in Scheme 5.1.

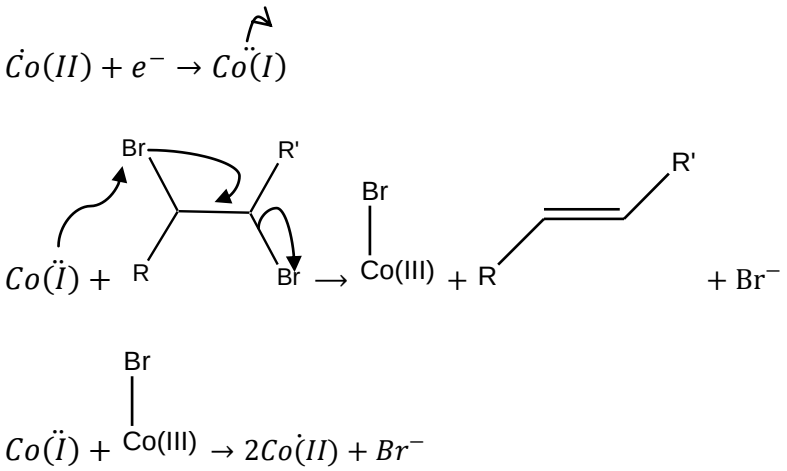

Scheme 5.1: Homogeneous reaction pathway for the vitamin B_{12} mediated reduction of DBCH (adopted from ref [43]).

5.3 Microfluidic Devices

A microfluidic device is shown in Figure 5.4. These devices, or micrometre-scale total analysis systems (μTAS) or so called 'lab-on-chip' can be defined as the science and technology of systems that manipulate or process small (10^{-7} to 10^{-18} litres) amounts of fluids using channels with dimensions of tens to hundreds of micrometers with high precision and efficiency [45-47].

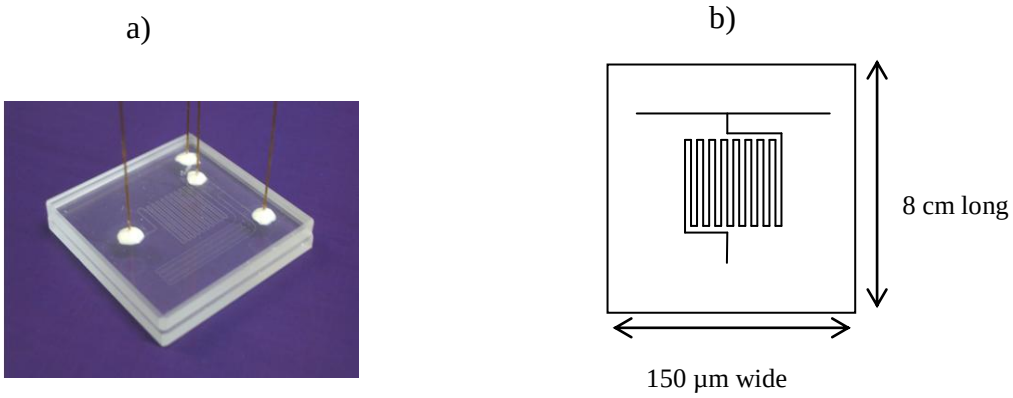

Figure 5.4:a) Illustrates a glass microfluidic device (adapted from reference [48]) and b) a serpentine device which dimensions were 150 µm wide x 50 µm deep x 8 cm long.

It is only within the last decade that the concepts of miniaturization have been applied to chemical and biological problems. The development and application of lab-on-a-chip technology has been very interesting over the last decade. These microscale analytical instruments use micromachined features such as: electrodes, channels, reactors and filters.

The first applications of microfluidic technologies were in analysis, where they offer a number of useful capabilities compared to their conventional (larger) analogues, such as: performing separations and detection with high resolution and sensitivity, the use of very small quantities of samples and reagents, low cost, short times for analyses and small footprints, they can be less hazardous to use and more environmentally appealing [49].

Microfluidics can also be portable; the battery power becomes sufficient, therefore measurements on site can be possible.

Microfluidic devices have been used in a wide variety of applications such as: nucleic acid separations, protein analysis, process control, small-molecule organic synthesis, DNA amplification, immunoassays, DNA sequencing and cell manipulations [50, 51].

The combination of efficiencies of mixing and separation with high rates of thermal mass transfers makes microfluidic ideal in order to rapidly process valuable or hazardous reactions components and to improve reaction selectivities (therefore yielding “higher quality” products) [52].

5.3.1 Properties of Mixing

Mixing is carried out on macroscale using mechanical or magnetic stirrer whereby large eddies (circular motion) are produced, allowing bulk diffusion to dominate [53]. On the other hand when microscale is employed turbulence cannot be induced and mixing is limited to molecular diffusion due to high viscous forces (laminar flow).

Usually, the pattern of flow of fluids can be described either as laminar or turbulent. The evaluation and comparison of the Reynold number with the transitional number 2000 is usually employed in order to determine the flow. Reynold number (Re) can be calculated using the Equation 5.2 [54, 55]:

$$Re = \frac{\rho UL}{\mu} = \frac{UL}{v}$$

Equation 5.2: Determination of the Reynolds number (Re) in terms of kinematic viscosity.

where,

$$v = \frac{\mu}{\rho}$$

Equation 5.3: Kinematic viscosity.

Re = Reynolds Number (dimensionless)

ρ = density (kg m $^{-3}$)

U= characteristic velocity (m s^{-1})

μ = dynamic viscosity (Ns m^{-2})

L = characteristic length (m)

ν = kinematic viscosity (N s m kg^{-1})

From Equation 5.2 it can be seen that the size of the reactor vessel and the fluid viscosity are the dominant parameters when considering fluidic mixing. Therefore, in a large vessel (Re > 3000) turbulent flow is observed for a non-viscous fluid but laminar flow dominates for the same fluid in a small vessel (Re < 1000). Consequently, mixing is diffusion limited (Re < 10) for micro channels (5 to 400 μm diameter) and as a result only occurs at the interface between reagents stream. In this work micro channels have been employed. The rate with which diffusion occurs is conversely dependent upon the width of the channel *i.e.*, mixing can occur in a matter of tens seconds when channels width on the order of 100 μm are used. On the other hand, if the channel widths are tens of microns the time of mixing decrease till matter of seconds.

5.3.2 Enhanced Mixing in Micro Reactor

More efficient methods of mixing on the microscale are required in order to increase the throughput of micro reactors. To date, the types of micro mixers developed can be classified in two main categories: passive and active. In passive mixing the geometric properties of the channel or fluidic stream are used to maximize the area over which diffusion can occur. In active mixing the control of the reagent flow or the use of varying pressure gradients is utilised [56-58].

Both approaches, allow the mixing to occur in a very rapid and controlled manner which has great advantages over macroscale systems and provide solutions to a number of key problems found in contemporary systems, including the ability to probe ultra-fast chemical reactions using a low sample consumption [59].

Due to their simplicity and operational flexibility passive mixers have found the widest use in synthetic applications. Rapid mixing can occur if dimensions are kept small, and chaotic advection can be used to enhance mixing. Chaotic advection can be achieved by introducing obstacles within the channels or by using serpentine channels. This helps mixing by enhancing the stretching folding and breaking of the flow [60, 61].

In this work two microfludic channel designs were used, a simple 'T' shape and a serpentine design to evaluate the mixing efficiencies and therefore the enhancement of the yield as described in detail in Section 5.5.

5.4 Experimental

5.4.1 Chemical Reagents

Chemicals. *Trans* 1,2-dibromocyclohexane (DBCH 99%) was obtained from Sigma Aldrich. Vitamin B_{12a} was also obtained from Sigma Aldrich as hydroxocob(III)alamin hydrochloride (crystalline, ca. 98%), which was a complex of Co(III). This species can perform two separate one-electron reductions to produce Co (I) to react with DBCH. The reducing agents, tetrabutylammonium perchlorate (TBAP) and dimethyl formamide (DMF) were also obtained from Sigma Aldrich.

5.4.2 Instrumentation

5.4.2.1 Cyclic Voltammetry

The cyclic voltammetry as described in Chapter 2 was employed to investigate the reduction of vitamin B_{12} and its reaction with DBCH. It was carried out with a 3 mm glassy carbon working electrode, platinum counter electrode and a calomel reference electrode at a scan rate of 0.1 Vs^{-1}. The electrolyte was TBAP and DMF was used as the solvent.

5.4.2.2 Bulk Electrolysis Experiments

Bulk electrolysis experiments were also carried out. One set of experiments were carried out in a "one pot" system using the same conditions as for the cyclic voltammetry but the working electrode was changed to a graphite rod to increase the surface of the electrode, thus increasing the current.

A "two pot" system was also utilised again using TBAP as the electrolyte and DMF as the solvent. The vitamin B_{12a} was placed in one pot with the graphite and reference electrode. A salt bridge with TBAP and DMF was used to connect with the other pot containing DMF and TBAP in which the platinum counter electrode was placed.

5.4.2.3 Spectroscopic Characterisation

The reaction process was evaluated using spectroscopic methods. Unless otherwise stated, nuclear magnetic resonance (^{1}H-NMR and ^{13}C-NMR) spectra were recorded at room temperature as solutions in deuteriochloroform ($CDCl_3$), using tetramethylsilane (TMS) as an internal standard. The spectra were recorded on a Jeol GX400 spectrometer and the chemical shifts are given in parts per million (ppm) with coupling constants in Hertz (Hz).

5.4.2.4 Experimental Set-Up Employed in Microfluidic Devices

Two different designs of microfluidic device were utilised for this work. One had a simple T shape and the other has a longer reaction path length incorporated in a serpentine design.

Both devices had three-reservoirs and the dimensions of the channels of the T device were 151 µm wide x 55 µm deep x 3.2 cm long and the serpentine were illustrated in Figure 5.4b. The flow was controlled by a syringe pump (MD-1001, Bionalytical Systems Inc.) which was connected to the microfludic devices using a series of 1/16" HPLC connectors and Peek tubing (Supelco). This was positioned above the channel through a 1mm hole in the top plate and secured using epoxy resin (Araldite 2014, Ciba Speciality Chemicals) (Figure 5.5).

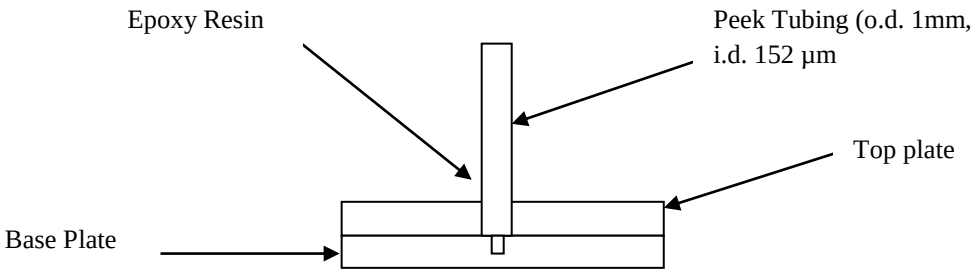

Figure 5.5: Schematic of the interface between the glass device and PEEK tubing.

The experimental set up of a microfludic devices are shown in Figure 5.6.

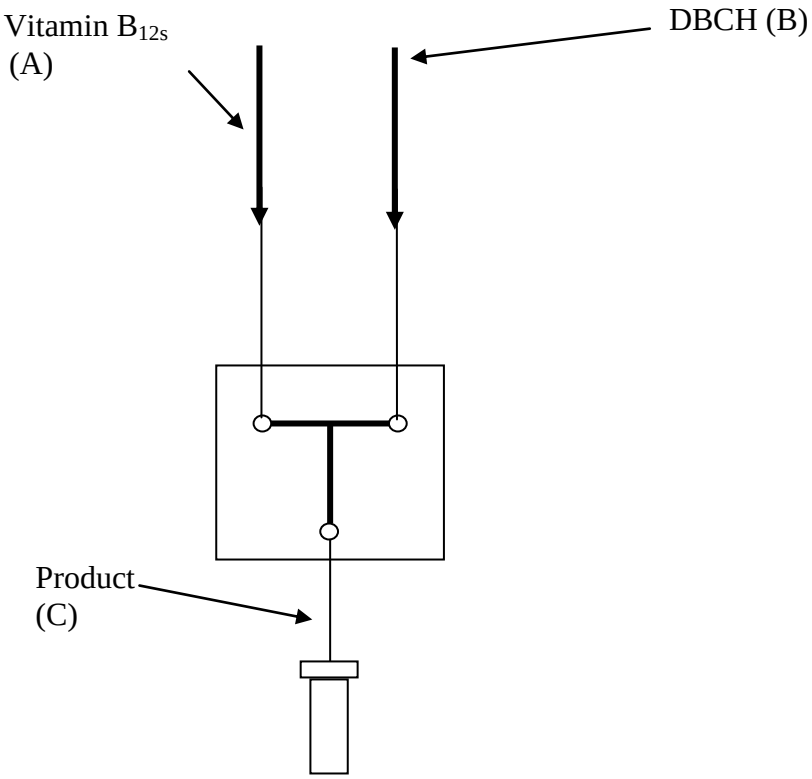

Figure 5.6: Schematic of the device used to investigate the reaction between B_{12s} and DBCH (T-shape).

5.4.2.5 Procedures for Batch Reactions

Batch reactions were carried out for comparison with the microfludic system using vitamin B_{12} and DBCH and four different reducing agents, Na(Hg)/amalgam, $NaBH_4$/20% NaOH, DL-cysteine in alkali solution, Zn-dust/NH_4Cl.

5.4.2.5.1 Batch Catalytic Reduction of the Vitamin B_{12} with Na(Hg)/Amalgam

Na(Hg)/amalgam was one of the reducing agent employed, the method used was described as follows.

Vitamin B_{12}(CoIII) (0.20 g, 0.15mmole) and 1% Na(Hg)/amalgam (0.006708 g, 3mmole) were dissolved in anhydrous DMF (20ml) and stirred over a period of 30 minutes under N_2. The Na(Hg)/amalgam was withdrawn from the solution, the latter was then treated with a stoichiometric amount of trans-1,2-dibromocyclohexane (20.4 µL) with stirring for 30 minutes.

A syringe was used to remove any remaining DMF from the amalgam. Addition of hexane (2 x 25 ml) enabled the liquid/liquid extraction of the product (cyclohexene). After extracting, the product was washed with water to remove any vitamin B_{12} residue. The hexane was subsequently removed using a rotary evaporator (Bpt cyclohexene = ~ 80 °C and Bpt hexane = 75 °C), so as to isolate the product. The latter were then subjected to ^{1}H-NMR analysis. Spectra of pure cyclohexene and DBCH (see Appendix II) were run in order to be compared with the extracted product.

5.4.2.5.2 Batch Catalytic Reduction of Vitamin B_{12} Using $NaBH_4$/20% NaOH

Vitamin B_{12}(CoIII) (0.0097 g, 0.0071 mmole) and $NaBH_4$ (0.154 g, 4.07 mmole) were dissolved in (1 ml NaOH 0.2 M) and stirred over a period of 30 minutes under N_2. The colour changed from red to grey which indicates the reduction of the vitamin B_{12} to B_{12s} was completed.

When the formation of Co (I) is completed a stoichiometric aliquot of DBCH was added into the solution. The vial sample was vigorously shaken, after addition of an aliquot of

$CDCl_3$ the formation of two phases (transparent bottom) and (pink top) were observed. The transparent phase was extracted and characterised by using ^{1}H-NMR and ^{13}C-NMR.

5.4.2.5.3 Batch Catalytic Reduction of the Vitamin B_{12} with DL-Cysteine in Alkali Solution

The procedure for reducing vitamin B_{12} to vitamin B_{12s} was as described in literature [30]. The reaction method employed was the same as used in Section 5.4.2.5.2. Once the complete reduction of vitamin B_{12} was observed a stochiometric aliquot of DBCH was added and the vial was vigorously shaken. $CDCl_3$ was added and two phases were formed. ^{1}H-NMR and ^{13}C-NMR were employed to characterise the formation of the product.

5.4.2.5.4 Batch Catalytic Reduction of the Vitamin B_{12} with Zn-Dust/ NH_4Cl

The procedure for reducing vitamin B_{12} to vitamin B_{12s} was as described in literature [31]. A 100 cm^3 flask, equipped with a magnetic stirrer bar, under N_2, was charged with Zn-dust (2.1g, 30 mmol) and ammonium chloride (NH_4Cl) (1.16 g, 20 mmol). Then 2 mol of vitamin B_{12} (with respect to the substrate 100%, 0.19g, 0.14 mmol) was dissolved in 20 cm^3 of ethanol. The mixture was stirred for 30 min until the reduction of Co (III) from vitamin B_{12} to Co (I) was completed. The reaction method was then the same as in Section 5.4.2.5.2.

5.5 Results and Discussion

5.5.1 Cyclic Voltammetry Investigation of the Electrocatalytic Reaction with Vitamin B_{12} and DBCH

For this work vitamin B_{12a} (hydroxocob(III)alamin hydrochloride) was selected due to its higher solubility that vitamin B_{12}. This means that the experiments take place in a

homogeneous system. Figure 5.7 shows a series of cyclic voltammograms with 1 mM vitamin B_{12a} in 1mM TBAP with DMF solvent and 14 successive 15 µl aliquots of DBCH. The blank (black dots) in Figure 5.7 had 1 mM vitamin B_{12a} in 1mM TBAP in DMF.

Four peaks are seen in Figure 5.7. These are due to the two chemically reversible redox (two electron process) couples for vitamin B_{12a}/B_{12r} (Co(III)/CO(II)L) and B_{12r}/B_{12s} (Co(II)L/Co(I)).

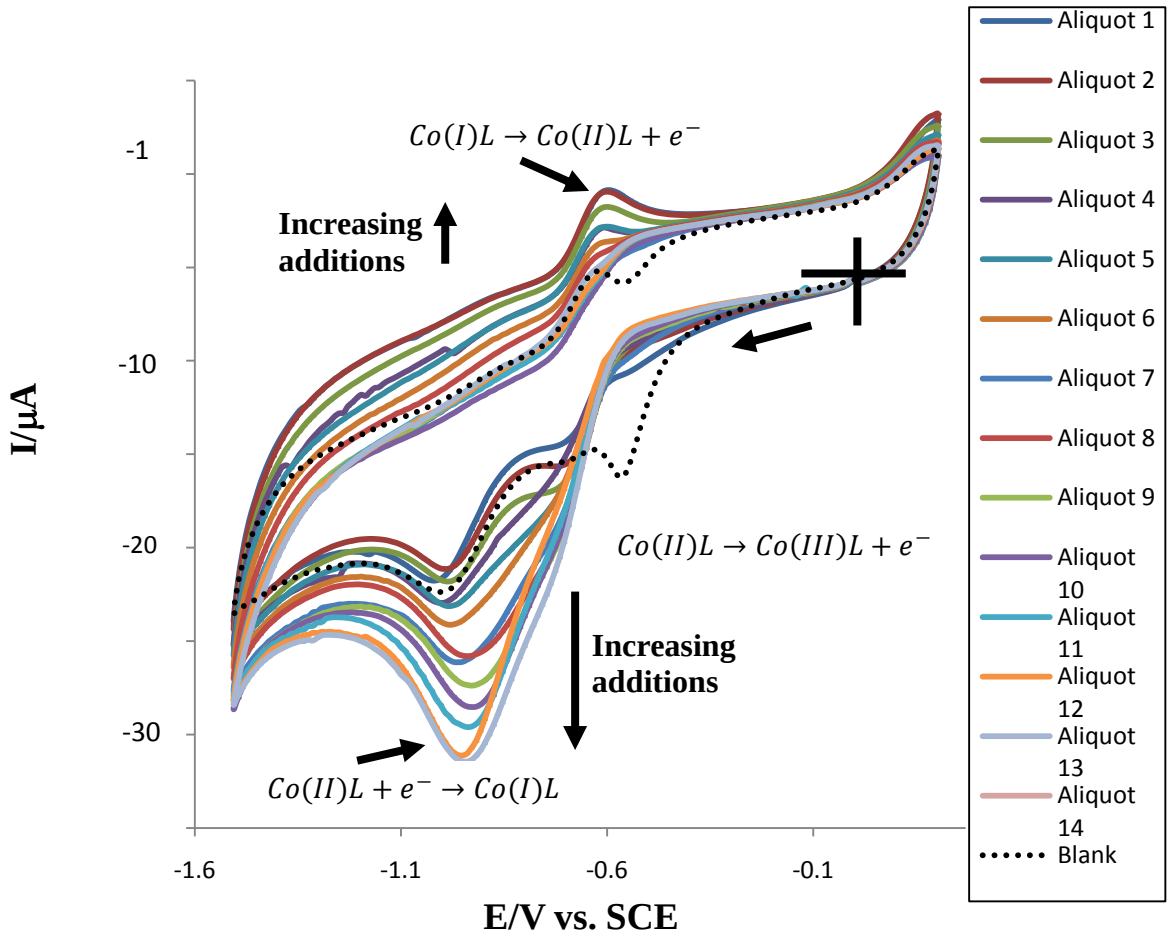

Figure 5.7: Cyclic voltammograms recorded at 0.1 Vs^{-1} at a glassy carbon electrode 1mM Vitamin B_{12a}-DMF-1 mM TBAP. Apart from the black dotted curve, the solutions also contain aliquots of DBCH. The cross-lines indicate the point of origin, and the arrow shows the direction of the initial potential sweep.

For the blank (black dotted curve in Figure 5.7), on scanning to negative potentials, cathodic waves are observed at -0.55 V *vs.* SCE due to the B_{12a}/B_{12r} couple and at -1.00 V *vs.* SCE due to the B_{12r}/B_{12s} couple. Upon scan reversal, the former couple gives rise an oxidative wave at -0.60 V *vs.* SCE due to the B_{12a}/B_{12r} couple and much less obvious, another oxidation peak appears at approximately -0.40 V *vs.* SCE (B_{12r}/B_{12s} couple).

As can be observed from Figure 5.7 in the presence of aliquots of DBCH the B_{12a}/B_{12r}(Co(III)/Co(II)) couple is significantly affected and gives the same response as the blank. Therefore, neither Co(II)L or Co(III)L react with DBCH at a significant rate. In comparison the reduction of B_{12r}(Co(II)) to B_{12s}(Co(I)) can be observed in the presence of DBCH. The electrocatalytic reaction allows the B_{12r} to be regenerated (Equation 5.1) and the amount of DBCH increases the current increase.

As the DBCH concentration increase there is a slight shift to more positive potentials showing a fast homogeneous reaction. Furthermore to the increased peak current, there is the loss of the peak at -0.55 V which was due to the B_{12a}/B_{12r} couple. Instead the Co(III) is going directly to Co(I) this occurs due to the fast homogeneous kinetics and the 2 electrons are used to reduce DBCH and form via an E2 elimination cyclohexene. Before the electrogenerated Co(I)L can be oxidised back to Co(II)L at the electrode surface, it reacts with DBCH as shown in Scheme 5.1. The results obtained agree with those results obtained by Davies *et al.*[43].

To investigate the relationship between the current intensity and concentration of DBCH a plot of Ip^{red} versus concentration of DBCH was obtained as shown in Figure 5.8.

As stated previously the Ip^{red} increases with the concentration of DBCH. The graph is not however linear over the full range as anticipated for redox catalytic systems, the steepest increase occurs at the lower concentrations.

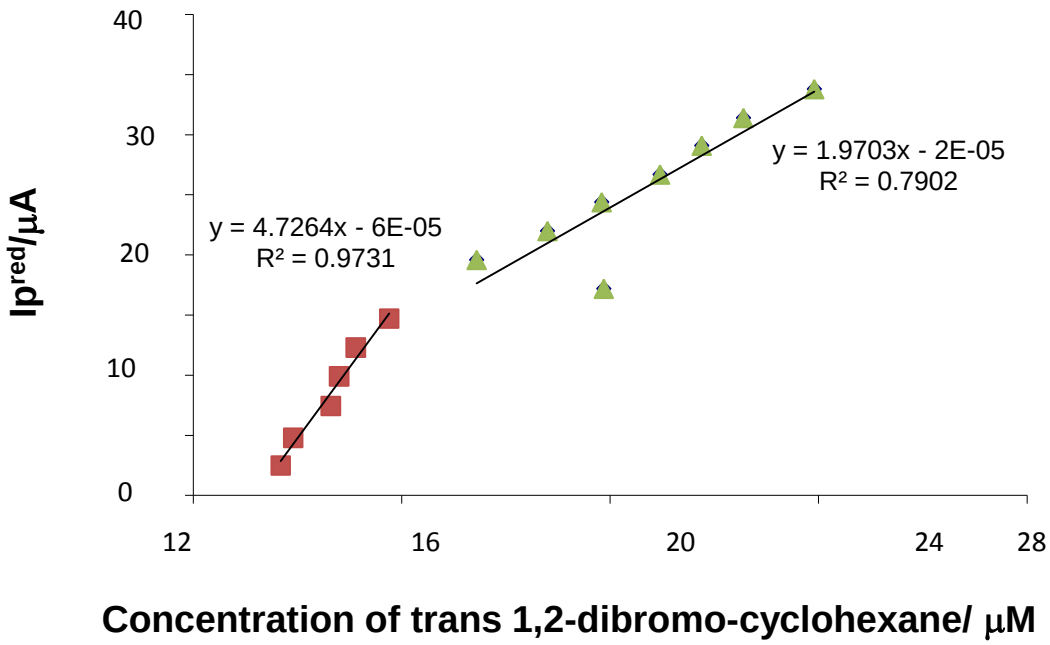

Figure 5.8: Ip^{red} *vs* Concentration of trans-1,2-dibromo-cyclohexane.

This work has successfully demonstrated the electrocatalytic reaction of vitamin B_{12} with DBCH. The next step was to look at batch reactions, and in order to reduce vitamin B_{12} to vitamin B_{12s} bulk electrolysis using a "one pot" system was employed. Unfortunately this method did not succeed. This is likely to be due to the fact that cathodically synthesised Co(I)L was reoxidised at the anode, so that current would continually pass through the electrolysis cell but the overall Faradaic efficiency was small. A "two pot" system was briefly investigated however the employed arrangement had poor potential control, likely due to the stability of salt bridge. Rather than investigate this further, as the ultimate goal was to undertake the reaction of Co(I) with DBCH, alternative chemical methods of synthesis of Co(I) were employed for reactions follow the generic type recently expanded by J. Yoshida [62].

5.5.2 Chemical Reduction of the Vitamin B_{12}

Alternative chemical methods were then investigated to reduce the vitamin B_{12}. These are shown in Table 5.1.

Reagent	Strength of the reducing agent	Reference
Na(Hg)/Amalgam	Mild	Patel [63]
$NaBH_4$/20% NaOH	Strong	Schrauzer [18]
DL-cysteine in alkali solution	Strong	Beaven [19]
Zn-dust/ NH_4Cl	Strong	Petrovic [31]

Table 5.1: Reducing Agents.

The Na(Hg)/amalgam was only a mild reducing agent and following the procedure described in 5.3.2.5 a full reduction was not seen and when the reaction with DBCH (see structure in Figure 5.9) was carried out no product was seen therefore the other stronger reducing agents were investigated in more detail.

5.5.2.1 NMR of Reactants and Products

DBCH

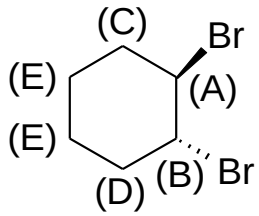

Figure 5.9: Trans-1,2 dibromocyclohexane with assignment of H.

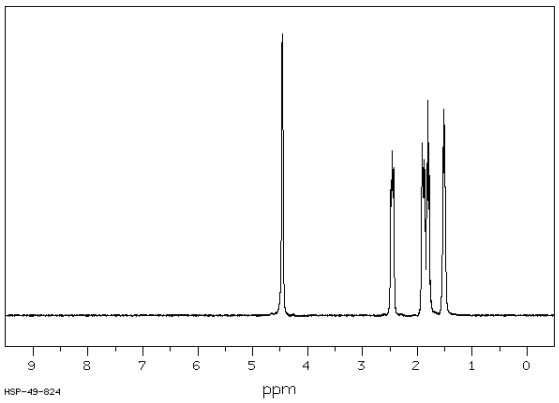

Figure 5.10: Standard spectra of DBCH (see cllf52 in appendix II for more details).

Assign	Shift ppm
A	4.46
B	2.46
C	1.90
D	1.81
E	1.52

Table 5.2 Assignment of ^{1}H-NMR spectrum for DBCH.

Cyclohexene

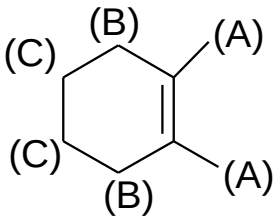

Figure 5.11: Assignations of protons in ^{1}H-NMR for cyclohexene.

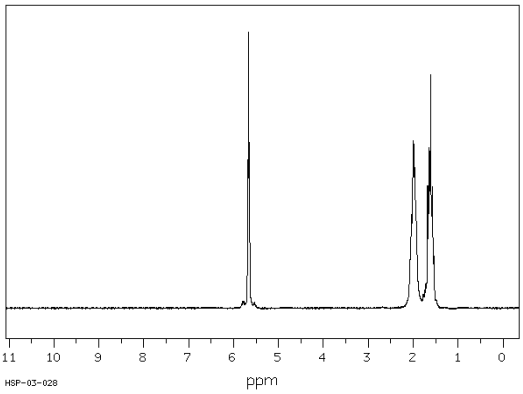

Figure 5.12: ^{1}H-NMR original spectro of cyclochexene (see cllf57 in appendix II for more details).

Assign	Shift ppm
A	5.66
B	1.99
C	1.61

Table 5.3: Assignment of ^{1}H-NMR spectrum for cyclohexene.

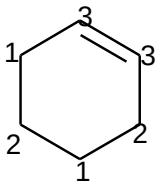

Figure 5.13: Assignations of protons in ^{13}C-NMR.

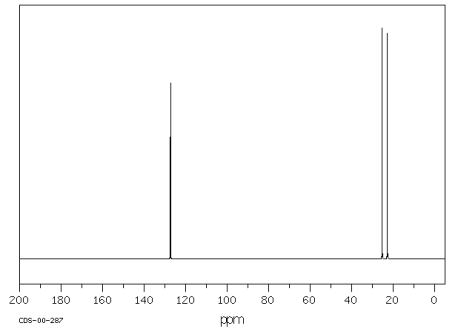

Figure 5.14: ^{13}C-NMR original spectro of cyclohexene.

Assign	Shift ppm
1	22.81
2	25.31
3	127.31

Table 5.4: Assignment of ^{13}C-NMR spectrum for cyclohexene.

5.5.2.2 Batch Catalytic Reduction of B_{12} Using $NaBH_4$/20% NaOH

Following the procedures described in Section 5.4.2.5 the reaction was carried out using then $NaBH_4$/20% NaOH as the reducing agent. The ^{1}H-NMR spectrum for the resultant product is shown in Figure 5.15.

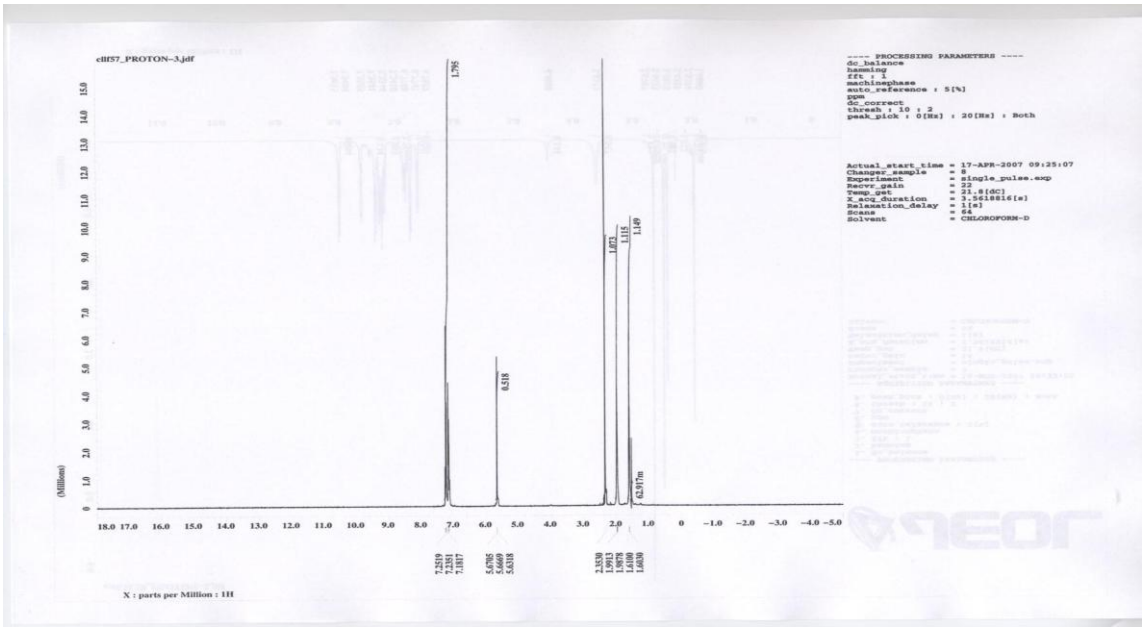

Figure 5.15: ^{1}H-NMR spectra of cyclohexene (see cllf57 in appendix II for more details).

The spectrum obtained perfectly matched the standard spectrum for cyclohexene indicating the formation of cyclohexene. This was further confirmed by a ^{13}C-NMR spectrum as shown in Figure 5.16. No DBCH was found and the percentage conversion was then calculated using the data from the spectra and this was found to be 100% as given in Table 5.5. This method was therefore suitable to investigate further for the microfluidic device. This simple, surfactant-free batch method has not been previously reported although Rusling [64] and Cambell [65] did report the synthesis using microemulsions. They used microemulsions to overcome the lack of solubility of vitamin B_{12} in DBCH, however by simply using rigorous shaking the batch method has been shown to be feasible. Wadhawan also reported a similar method but this required ultrasonic irradiation [66].

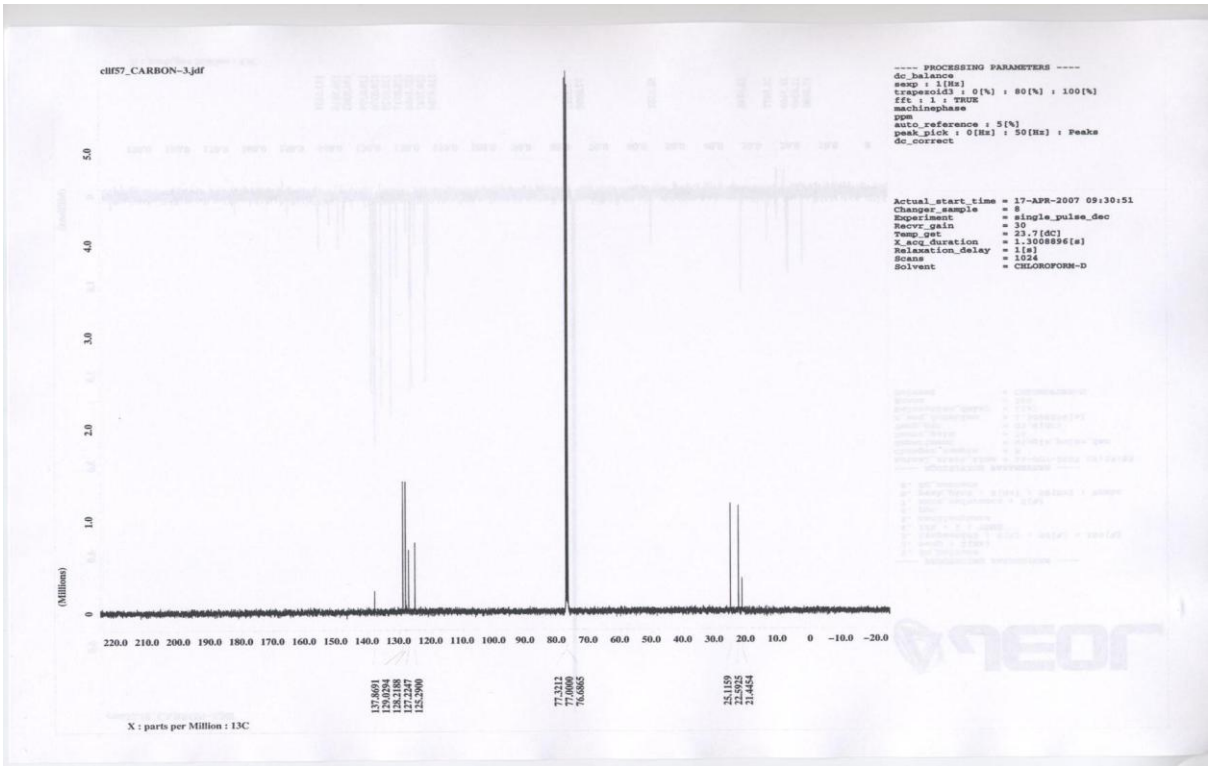

Figure 5.16: ^{13}C-NMR spectrum showing the formation of cyclohexene (see Figure 5.13 and 5.14 for more details).

5.5.2.3 Batch Catalytic Reduction of the Vitamin B_{12} with DL-Cysteine in Alkali Solution

Following the procedures described in Section 5.4.2.5 the reaction was carried out using DL-cysteine in alkali solution. This novel method also gave 100 % conversion to cyclohexene as confirmed by ^{1}H-NMR and^{13}C-NMR spectra and was therefore investigated further in the microfluidic system.

5.5.2.4 Batch Catalytic Reduction of the Vitamin B_{12} with Zn-Dust/NH_4Cl

Following the procedures described in Section 5.4.2.5 the reaction was carried out using Zn-dust/NH_4Cl. This novel method also gave 100 % conversion to cyclohexene as confirmed by ^{1}H-NMR and^{13}C-NMR spectra.

5.5.3 Application of the Microfludic Device for the Reaction of DBCH with B_{12s}

Although eventually the aim would be to carry out the reduction in the microfluidic device for this work the vitamin B_{12} was reduced before using it on the device. Two methods which gave 100% conversion (Table 5.5) were selected for the reduction, these were $NaBH_4$/20% NaOH and DL-cysteine in alkali solution. The method with Zn-dust/ NH_4Cl was not used as it was thought it would block the microfluidic channels. As previously, the conversion of the cyclohexene was characterised using ^{1}H-NMR and ^{13}C-NMR.

Reagent	%Conversion of cyclohexene (Batch)	% Conversion of cyclohexene in Microfluidic Device
Na(Hg)/Amalgam	0	0
$NaBH_4$/20% NaOH	100	1-12
DL-cysteine in alkali solution	100	1-12
Zn-dust/ NH_4Cl	100	N/A

Table 5.5: A comparison of percentage conversions for different reducing agents in a microfluidic device and in batch.

5.5.3.1 Microfluidic Catalytic Reaction with Previous Reduction of B_{12} Using $NaBH_4$/20% NaOH

The reaction between DBCH and B_{12s} was then moved to the microfluidic device using the set up shown in Figure 5.5. A standard solution of B_{12s} in aqueous NaOH was placed in reservoir A and a solution of pure DBCH was placed in reservoir B. The reaction products were collected in reservoir C. The main variable that can be used to optimise the reaction is the flow rate. The flow rate was therefore varied between 0.1 and 20 µL min^{-1}.

The results obtained when a T-shape microfluidic device was employed, are shown in Table 5.6 as follows.

Flow rate *(µL/min)*	**Average conversion cyclohexene %**	**Replicate 1**	**Replicate 2**	**Replicate 3**	**Standard deviation**	**%Relative standard deviation**
0.1	**9.39**	**8.65**	**9.32**	**10.20**	**0.77**	**8.25**
0.5	**8.03**	**8.14**	**8.29**	**7.65**	**0.33**	**4.15**
0.8	**7.41**	**7.49**	**7.02**	**7.72**	**0.36**	**4.8**
1	**5.54**	**5.14**	**5.97**	**5.52**	**0.42**	**7.51**
1.5	**6.69**	**5.25**	**6.77**	**7.99**	**1.37**	**20.54**
5	**3.15**	**3.15**	**2.96**	**3.34**	**0.19**	**5.98**
10	**1.60**	**1.54**	**1.58**	**1.68**	**0.07**	**4.28**
20	**1.54**	**1.74**	**1.45**	**1.44**	**0.17**	**11.14**

Table 5.6: The conversion of cyclohexene at different flow rates when a T-shape microfluidic reactor is employed.

As Table 5.6 illustrates, the conversion to cyclohexene was seen to increase by 16% as the flow rate was reduced from 20 to 0.1 µL min^{-1}. This would be expected because at the lower flow rate there is an increase in residence time within the device. One might have expected a great increase in the conversion with a ten-fold reduction in flow rate. The low conversion rate suggests better mixing is required and one way to achieve this is to include a longer serpentine channel as shown in Figure 5.5 [67, 68]. The results obtained with the serpentine channel are shown in Table 5.7.

Flow rate *(µL/min)*	**Average conversion cyclohexene %**	**Replicate 1**	**Replicate 2**	**Replicate 3**	**Standard deviation**	**%Relative standard deviation**
0.1	**10.36**	**10.79**	**10.24**	**10.04**	**0.39**	**3.74**
0.5	**9.80**	**9.89**	**10.42**	**9.08**	**0.67**	**6.87**
0.8	**7.48**	**7.99**	**7.29**	**7.16**	**0.44**	**5.95**
1	**6.94**	**6.96**	**6.32**	**7.53**	**0.60**	**8.66**
1.5	**5.98**	**5.84**	**6.44**	**5.65**	**0.41**	**6.89**
5	**5.43**	**5.77**	**5.57**	**4.95**	**0.43**	**7.94**
10	**1.26**	**1.21**	**1.32**	**1.24**	**0.06**	**4.72**
20	**1.11**	**1.01**	**1.27**	**1.05**	**0.14**	**12.67**

Table 5.7: Shows the conversion of cyclohexene at different flow rates when a serpentine-shape microfluidic reactor is employed.

As Table 5.7 illustrates the conversion rate was not greatly enhanced by using the serpentine channel, in fact the results are the same within experimental error 10.4 ± 0.4 % and 9.4 ± 0.8 %. The conversion to cyclohexene was seen to increase by 10% as the flow rate was reduced from 20 to 0.10 µL min^{-1}.

From a practical point of view there were some problems carrying out the experiments. At lower flow rates although the mixing was better giving higher yields the risk of blockages increased. At higher flow rates the risk of blockage was lower. The blockage formation was initially attributed to the generation and formation of bubbles due to the use of excess $NaBH_4$ to reduce the vitamin B_{12} before the reaction. In attempt to overcome this problem, lower concentrations of $NaBH_4$ were employed. Although the frequency with which the blockages occurred was slightly reduced, as a result of employing reduced reagent concentrations the conversion was still low. Therefore other DL-cysteine in alkali solution was investigated.

5.5.3.2 Microfluidic Catalytic Reaction with Previous Reduction of B_{12} Using DL-Cysteine in Alkali Solution

As described in previous section vitamin B_{12} was reduced before was moved onto chip. The conversion of the cyclohexene was characterised using ^{1}H-NMR and ^{13}C-NMR.

The results obtained when a T-shape microfluidic device was employed, are shown in Table 5.8 as follow:

Flow rate *(µL/min)*	Average conversion cyclohexene %	Replicate 1	Replicate 2	Replicate 3	Standard deviation	%Relative standard deviation
0.1	**9.58**	**10.53**	**8.45**	**9.76**	**1.05**	**10.98**
0.5	**8.56**	**8.35**	**9.53**	**7.81**	**0.88**	**10.28**
0.8	**8.98**	**8.12**	**8.68**	**10.13**	**1.03**	**11.55**
1	**7.60**	**8.90**	**7.12**	**6.78**	**1.14**	**14.98**
1.5	**7.53**	**7.65**	**8.09**	**6.86**	**0.62**	**8.28**
5	**6.58**	**7.11**	**6.23**	**6.42**	**0.46**	**7.04**
10	**3.77**	**4.36**	**3.78**	**3.19**	**0.58**	**15.49**
20	**1.53**	**2.26**	**0.95**	**1.39**	**0.67**	**43.47**

Table 5.8: Shows the conversion of cyclohexene at different flow rates when a T-shape microfluidic reactor is employed.

As Table 5.8 illustrates, the conversion to cyclohexene was similar to that obtained with the previous reducing agent with an increase of 16% as the flow rate was reduced from 20 to 0.10 µL min^{-1}. This is would be expected for the same flow rates and microfluidic device design.

The results obtained with the serpentine channel are shown in Table 5.9.

Flow rate *(µL/min)*	**Average conversion cyclohexene %**	**Replicate 1**	**Replicate 2**	**Replicate 3**	**Standard deviation**	**%Relative standard deviation**
0.1	**9.89**	**11.24**	**8.32**	**10.13**	**1.47**	**14.90**
0.5	**9.41**	**10.31**	**9.27**	**8.64**	**0.84**	**8.96**
0.8	**8.51**	**8.30**	**9.15**	**8.07**	**0.57**	**6.69**
1	**8.37**	**7.68**	**8.33**	**9.11**	**0.72**	**8.55**
1.5	**6.66**	**7.25**	**6.78**	**5.94**	**0.66**	**9.96**
5	**4.59**	**5.89**	**4.12**	**3.78**	**1.13**	**24.65**
10	**2.17**	**3.18**	**1.38**	**1.96**	**0.92**	**42.27**
20	**1.08**	**1.13**	**0.56**	**1.55**	**0.49**	**46.01**

Table 5.9: Shows the conversion of cyclohexene at different flow rates when a serpentine-shape microfluidic reactor is employed.

Similarly as Table 5.9 illustrates the use of the serpentine channel had little effect. Again blockages occurred. The blockage formation was initially attributed to the precipitation of DL-cysteine and air bubbles within the channel network, therefore in attempt to overcome this problem, lower concentrations of DL-cysteine were employed. Although the frequency with which the blockages occurred was reduced, as a result of employing reduced reagent concentrations there was no increase in yield.

5.6 Conclusions

In this work the electrocatalytic reaction of B_{12a} with DBCH in a homogeneous DMF media was studied by cyclic voltammetry. Four peaks were seen due to the two chemically reversible redox (two electron process) couples for vitamin B_{12a}/B_{12s} (Co(III)/CO(II)L) and B_{12r}/B_{12s} (Co(II)L/Co(I)). These results agreed with those found by Davies *et al.*[43]. The aim was to then carry out a full synthetic reaction B_{12} with DBCH. When however the bulk electrocatalytic reaction was tried in a "one pot" system the reduction could not be achieved. The cathodically synthesised Co(I)L was thought to be reoxidised at the anode. A "two pot" system did not have sufficient potential control and therefore chemical reduction was investigated.

Four reducing agents (Na(Hg)/amalgam, $NaBH_4$/20% NaOH, DL-cysteine in alkali solution and Zn-dust/NH_4Cl) were studied to reduce B_{12} to B_{12s} for a simple biphasic batch reaction of vitamin B_{12s} with DBCH. The mild reducing agent Na(Hg)/amalgam was not successful but the other three methods were shown to give gave 100% yield if the reaction vials were rigorously shaken. This simple type of green, surfactant free reaction has not been previously reported.

The reaction was then investigated in a microfluidic systems. For this work the vitamin B_{12} was reduce before being introduced into the microfludic device. $NaBH_4$/20% NaOH and DL-cysteine in alkali solution were selected as the most compatible reducing agents for the microfluidic device. Two types of microfluidic device were employed one with a T-shape channel and one with a serpentine channel. The conversions (approximately 10%) obtained with the microfludic device were much lower than for the simple batch reactions (100%). The yield increased as the flow rate decreased and the residence time increased. Using the serpentine channel made no noticeable difference to the conversion rate. Problems were also seen due to the use of excess reducing agent prior to introduction of the reduced vitamin B_{12} into the microfluidic device as this could cause blockages and bubbles. However, the main problem was the lack of mixing in the device. One way to overcome this would be to use an ultrasonic transducer with the microfluidic device, but although preliminary experiments were carried out, there was not time to fully investigate this approach.

5.7 References

1. E.L. Rickes, N.G. Brink, F.R. Koniusky, T.R. Wood and K. Folkers, *Science*, 1948, **107**, 396.
2. R. West, *Science*, 1948, **107**, 398.
3. Chase Chemical Co., *B.P. 834384*, 1955.
4. H.A. Barker, L.L. Merritt Jr, J.A. Dean and F. A. Settle, *Proc. Nat. Acad. Sci.*, 1958, **44**, 1093.
5. H.A. Barker, L.L. Merritt Jr, J.A. Dean and F. A. Settle, *Proc. Nat. Acad. Sci*, 1959, **45**, 521.
6. E.L. Smith and L.F.J. Parker, *J. Biochem.*, 1948, **8**, 43.
7. N.G. Brink, F.A. Kuehl and K. Folkers, *Science*, 1950, **112**, 354.
8. H. Diehl, R.W. Vandeer Haar and R.R. Sealock, *J. Am. Chem. Soc.*, 1950, **72**, 5312.
9. F. Grun and R. Menasse, *Experentia*, 1950, **6**, 263.
10. J.C. Wallmann, B.B. Cunningham and M. Calvin, *Science*, 1951, **113**, 55.
11. G. Loeffler, *Basiswissen Biochemie*, 2005, 606.
12. *Dietary Supplement Fact Sheet: Vitamin B12*.
13. A. Dowzenko, *Clinical Neurology*, 2000, 451.
14. P.G Swetic and D. G. Brown, *J. Electroanal .Chem.*, 1974, **51**, 433.
15. P.G. Swetic and D. G. Brown, *Biochem. Biophys. Acta.*, 1974, **343**, 641.
16. J. Halpern, *"Chemistry"*, New York, 1982.
17. R.L. Birke, G.A. Brydon and M. F. Boyle, *J. Electroanal. Chem.*, 1974, **52**, 237.
18. G.N. Schrauzer, E. Deutsch and R. J. Windgassen, *J. Am. Chem. Soc.*, 1968, **90**, 2441.
19. G.H. Beaven and E. A. Johnson, *Nature*, 1955, **176**, 1264.
20. O. Muller and G. Muller, *Biochem. Z.*, 1962, **336**, 299.
21. E.L. Smith and L. Mervyn, *J. Biochem.*, 1963, **86**, 2.
22. S.L. Tackett, J.W. Collatt and J. C. Abott, *Biochem.*, 1963, **2**, 919.
23. G.N. Schrauzer, R.J. Windgassen and J. Kohnle, *Chem. Ber.*, 1965, **98**, 3324.
24. P.K. Das, H.A.O. Hill, J.M. Pratt and R. J. P. Williams, *Biochim. Biophys. Acta*, 1967, **141**, 644.
25. H. Diehl and R. Murie, *Iowa State Coll. J. Sci.*, 1952, **23**, 555.
26. B. Jaselskis and H. Diehl, *J. Am. Chem. Soc.*, 1954, **76**, 4345.
27. R.N. Boos, J.E. Carr and J. B. Conn, *Science*, 1953, **117**, 603.
28. O. Schindler, *Helv. Chim. Acta*, 1951, **34**, 1356.
29. R. Bonnet, *Chem. Rev.,*, 1963, 573.
30. H. Li, T. Li and E. Wang, *Talanta*, 1995, **42**, 885.
31. Z. Petrovic, B. Mojsilovic and Z. M. Burgarcic, *J. Mol. Catal. A: Chem.*, 2001, **170**, 267.
32. R. Scheffold and E. Amble, *Angew. Chem.*, 1980, **8**, 629.
33. N.R. de Tacconi, D. Lexa and J. M. Saveant, *J. Am. Chem. Soc.*, 1979, **101**, 467.
34. P. Tomcik, C.E. Banks, T.J. Davies and R. G. Compton, *Anal. Chem.*, 2004, **76**, 161.
35. D. Lexa, J.M. Saveant and J. Zickler, *J. Am. Chem. Soc.*, 1977, **99**, 2786.
36. D. Lexa and J. M. Saveant, *J. Am. Chem. Soc.*, 1978, **100**, 3220.
37. D. Lexa, J.M. Saveant and J. Zickler, *J. Am. Chem. Soc.*, 1980, **102**, 2654.
38. D. Lexa and J. M. Saveant, *J. Am. Chem. Soc.*, 1976, **98**, 2652.

39. C.L. Schmidt, C.F. Kolpin and H. S. S. Jr., *Anal. Chem.*, 1981, **53**, 41.
40. A. Owlia, Z. Wang and J. F. Rusling, *J. Am. Chem. Soc.*, 1989, **111**, 5091.
41. D. Lexa and J. M. Saveant, *Acc. Chem. Res.*, 1983, **16**, 235.
42. M.C. Lagunas, D.S. Silvester, L. Aldous and R. G. Compton, *Electroanal.*, 2006, **22**, 2263.
43. T.J. Davies, A.C. Garner, S.G. Davies and R. G. Compton, *Chem. Phys. Chem.*, 2005, **6**, 2633.
44. T.F. Connors, J.V. Arena and J. F. Rusling, *J. Phys. Chem.*, 1988, **92**, 2810.
45. G.M. Whitesides, *Nature (Insight Overview)*, 2006, **442**, 268.
46. C. Erbacher, F.G. Bessoth, M. Busch, E. Verpoorte and A. Manz, *Mikrochim. Acta*, 1999, **131**, 19.
47. A. Manz, *J. Chromatogr.*, 1992, **593**, 253.
48. G.M. Greenway, *Private Communication. University of Hull*.
49. D. Janasek, J. Franzke and A. Manz, *Nature (Insight Review)*, 2006, **442**, 374.
50. M. Krishman, V. Namasivayam, R. Li, R. Pal and M. A. Burns, *Curr. Opin. Biotech.*, 2001, **12**, 92.
51. S.C. Jakeway, A.J. de Mello and E. L. Rusell, *J. Anal. Chem.*, 2000, **366**, 525.
52. A.J. de Mello, *Anal. Bional. Chem.*, 2002, **372**, 12.
53. N. Harnby, M.F. Edwards and A. W. Nienow, *Mixing in the Process Industry*, Butterworths, 1985.
54. O. Reynolds, *Philos. Trans.*, 1883, **174**, 935.
55. O. Reynolds, *Philos. Trans.*, 1895, **186**, 123.
56. A.J. de Mello, *Nature (Insight Review)*, 2006, **442**, 394.
57. D. Bokenkamp, D. Desai, X. Yang, Y.C. Tai, E.M. Marzluff and S. L. Mayo, *Anal. Chem.*, 1998, **70**, 232.
58. W. Ehrfeld, V. Hessel and H. Lehr, *Microsystem Technology in Chemistry and Life Sciences (eds). A. Manz and H. Becker*, Berlin-Heidelberg, 1998.
59. M.C.R. Shastry, S.D. Luck and H. A. Roder, *J. Biophys.*, 1998, **74**, 2714.
60. J.M. Ottino, *Sci. Am.*, 1989, **260**, 56.
61. J.M. Ottino, *Ann. Rev. Fluid Mech.*, 1990, **22**.
62. J. Yoshida, K. Kataoka, R. Horcajada and A. Nagaki, *Chem. Rev.*, 2008, **108**, 2265.
63. V.F. Patel, G. Pattendem and J. J. Russell, *Tetrahedron Lett.*, 1986, **27**, 2303.
64. J.F. Rusling, *Pure Appl. Chem.*, 2001, **1**, 1895.
65. C.J. Campbell, D.M. Haddleton and J. F. Rusling, *Electrochem. Commun.*, 1999, **1**, 618.
66. T.J. Davies, C.E. Banks, B. Nuthakki, J.F. Rusling, R.R. France, J.D. Wadhawan and R.G. Compton, *Green Chem.*, 2002, **4**, 570.
67. I. Schneegass, R. Brautiam and J. M. Kohler, *Lab Chip*, 2001, **1**, 42.
68. M.T. Bloom, E.F. Hasselbrink, H. Wensink and A. v. d. Berg, *'Micro Total Analysis Systems 2001'*, Kluwer Academic Publishers, Enschede 2001.

Chapter 6

Conclusions and Future Work

Conclusions

This thesis discusses and demonstrates the utility and advantages of redox catalytic reactions for analytical and small scale synthetic applications. In particular electro-electrogenerated chemiluminescence (ECL) reactions are investigated. The main conclusions resulting from each piece of work have already been discussed at the end of each chapter, however they are emphasised again within this Chapter, along with further suggestions for future work.

The Analytical Scope of ECL

The occurrence, mechanisms and current analytical applications of ECL were reviewed and it was concluded that a large potential existed for the application of this phenomena to analytical chemistry, warranting further investigations. Specifically several potential advantages of the use of ECL were identified in addition to advantages of sensitivity and selectivity inherent to convectional CL methodology. This is primarily because there is the greater control over the initiation, rate and pathways of the reactions by altering the potential applied to the electrode, since reagents needed for the CL reaction are generated *in situ* at the electrode surface. This control can be to the extent that the CL reaction can effectively switched 'on and off', enabling the use of signal modulation and background correction techniques. Also it was thought that ECL should allow existing CL methods to be simplified by using reduced numbers of reagents since active reagents could be electrochemically produced from passive precursors in the sample or carrier system.

Since the ECL is an electrochemical technique, additional analytical information could be obtained by monitoring the electrochemical activity of reaction using cyclic voltammetry techniques, as well as recording the light output.

By the use of ECL, particularly unstable reagents and intermediates can be generated and allowed to react *in situ* as soon as they are formed.

Some reagents such as $Ru(bpy)_3^{2+}$, and occasionally some analytes, can be regenerated at the electrode, allowing the ECL to be sustained.

Sol gel modified electrodes

The electrode coated with a sol-gel physically entrapping $Ru(bpy)_3^{2+}$ gave an ECL signal and a calibration was obtained. The ECL signal was found however to decrease when the experiments were repeated, as the water soluble $Ru(bpy)_3^{2+}$ leached into the aqueous analyte solution. This system therefore needed to be further developed in order to prevent reagent leaching and therefore loss of the ECL signal. The development of a $Ru(bpy)_3^{2+}$ derivative capable of covalently bonding to the sol-gel matrix was examined. This involved a study of the covalent immobilization of a $Ru(bpy)_3^{2+}$ derivative, 4,4'-bis[(3-triethoxysilylpropyl)amide]-2,2'bipyridine] bis-(2,2'-bipyridine)ruthenium(II) dichloride to the silica sol-gel. This approach was found to be successful and a log linear calibration was obtained and a limit of detection of 2.65×10^{-6} M was obtained for codeine. The $Ru(bpy)_3^{2+}$ did not now leach from the system and stable results were obtained in aqueous conditions. The $Ru(bpy)_3^{2+}$ was recycled at the electrode and the drug could be determined by dipping the sensor into a pH adjusted solution of the analyte. This approach would be very promising for a portable drug detection system.

The sensor was not so successful for drugs such as rohypnol which was insoluble in aqueous solution. The ECL signal was degraded in organic solvent such as methanol and therefore an alternative approach was needed.

Oil Droplet Modified Electrodes

ECL at droplet-modified electrodes was demonstrated for the first time. As well as investigating this approach for the analysis insoluble compounds this approach was also used to extract information regarding the molecular structure of the oil | aqueous interface, and thus its heterogeneous pK_a, under appropriate assumptions. Using ECL transient measurements the biphasic pK_a for interfacial trioctylamine was found to be approximately 10.8 for protonated solutions. This is close to values previously reported

for *n*-octylamine and dioctylamine (10.65 and 11.01 respectively at 298 K) and dihexylamine (11.01 at 298 K) in ethanol/water mixtures, and of aqueous triethylamine and tripropylamine (10.9 and 10.4 respectively at 298 K).

Furthermore, the mechanism was studied in deuterium conditions in order to investigate the kinetic isotope effects on the biphasic pKa. Results suggest that the pKa increases to 13.2 when deuterium is used instead of protons indicating a trend. The shape of the transients for both cases show a faster decay in highly alkaline media and a slower luminescence decay when the solutions go to lower pH. This indicates that above the pKa biphasic region an outer sphere electron transfer occurs. However, below the pKa region the amine is protonated and a proton-coupled electron transfer appears to be dominated. Moreover, the investigation of the reaction in different $Ru(bpy)_3^{2+}$ concentrations showed that the pKa is independent of the concentration of the solution, indicating that the decay is first-order as expected.

Catalytic Reactions of Vitamin B_{12}

Finally, the electrocatalytic reduction and oxidation of Vitamin B_{12} with DBCH has been studied. The cyclic voltammetry results show that B_{12s} [Co(I)], the reduced form of Vitamin B_{12}, acted as an electrocatalyst toward DBCH reduction. The reduction current started at −0.4 V and became higher at more negative potentials. The current maximum of the DBCH/B_{12} reduction occurs at -1.68V, coinciding with the second reduction peak of Vitamin B_{12} itself, but its onset its actually situated at less negative potentials than the first Co(III)/Co(I) reduction of Vitamin B_{12}. On the reverse scan, the Co(I)/Co(II) oxidation peak is absent, while the two Co(II)/Co(III) oxidation remain largely unchanged. These are typical of the rapid Co(I)-electrocatalyzed reduction of DBCH. When the reaction was transferred to a bulk electrolysis the reaction did not proceed as the cathodically synthesised Co(I)L was thought to be being reoxidised at the anode.

This reaction was thus investigated using chemical reducing agents. The reaction was biphasic and the initial experiments were in batch in which rigorous mixing was used to ensure the reaction proceeded. The strong reducing agents $NaBH_4$/NaOH, Zn

dust/NH_4Cl and DL-Cysteine all gave 100% conversion. This is a type of green, surfactant-free synthetic reaction.

Two different design of microfluidic devices were then employed, a T-shape and a Serpentine shape to see if the advantages seen with microfluidic systems could be applied in this case. The flow rate studied was in the range between 0.1 to 20 μL min^{-1} and the conversion of cyclohexene obtained varied from 1-10%.

The low conversions are probably related to poor mixing; new designs of microfluidic devices will have to be investigated.

Future Work

Covalent attachment compared to the physical entrapment of the CL reagent was advantageous as it ensured homogeneous distribution of the reagent within the matrix and prevented leaching. This reduced analysis costs, extended sensor lifetime and gave reproducible analyte responses. The method however could not be extended to insoluble drugs such as rohypnol and an alternative approach is required. One such approach would be to use a biphasic system. ECL at droplet modified electrodes looks like a promising approach for analysis of this type of compounds.

In the short term to improve the conversion of the DBCH better mixing of the biphasic mixture is required. This would probably be best achieved using ultrasound. An ultrasonic transducer could be attached to the outside of the microfluidic device and by tuning the device such that the system was suitable matched mixing should be achieved. Initial experiments were carried out to investigate this approach but there was not sufficient time to optimise the system.

In the longer term the work in this thesis has shown the feasibility of developing a portable detection device for tertiary amine compounds. Future work would involve developing a robust prototype system.

Chapter 7

Publications and Presentations

The following is a list of publications and presentations resulting from the work described contained within this thesis.

7.1 Publications

1. Electrogenerated Chemiluminescence at Droplet Modified Electrode: Towards Biphasic pKa Measurements via Proton-Coupled Electron Transfer at Liquid | Liquid interfaces.
   Carlos Lledo-Fernandez, Imren Hatay, Michael J. Ball, Gillian M. Greenway and Jay Wadhawan. *New J. Chem.*, 2009, **33**, 749.
2. Electrogenerated Chemiluminescence at Droplet Modified Electrode: The isotopic effect- Biphasic pDa measurements via Proton-Coupled Electron Transfer at Liquid | Liquid interfaces.
   Carlos Lledo-Fernandez, Evangelia Christoforou, Gillian M. Greenway and Jay Wadhawan. In preparation.

7.2 Presentations

1. The Application of Chemiluminescence and Electrochemiluminescence Detection Metal/Metalloid. Poster presentation at the University Of Plymouth (Analytical Research Forum, July 2005).
2. Mapping of Hydrofobic Electrode Surfaces. Poster presentation at University of Cork (Analytical Research Forum, July 2006)
3. Electrochemical Luminescence at the Liquid | Liquid Interface. Oral presentation at University of Hull (Robin Hood Interdisciplinary Network in Electrochemistry December 2006).
4. Electrogenerated Chemiluminescence at Liquid | Liquid interface: evidence inverted & proton-coupled electron transfer. Poster presentation at University of Hull (Analytical Research Forum, July 2008).

Appendix I

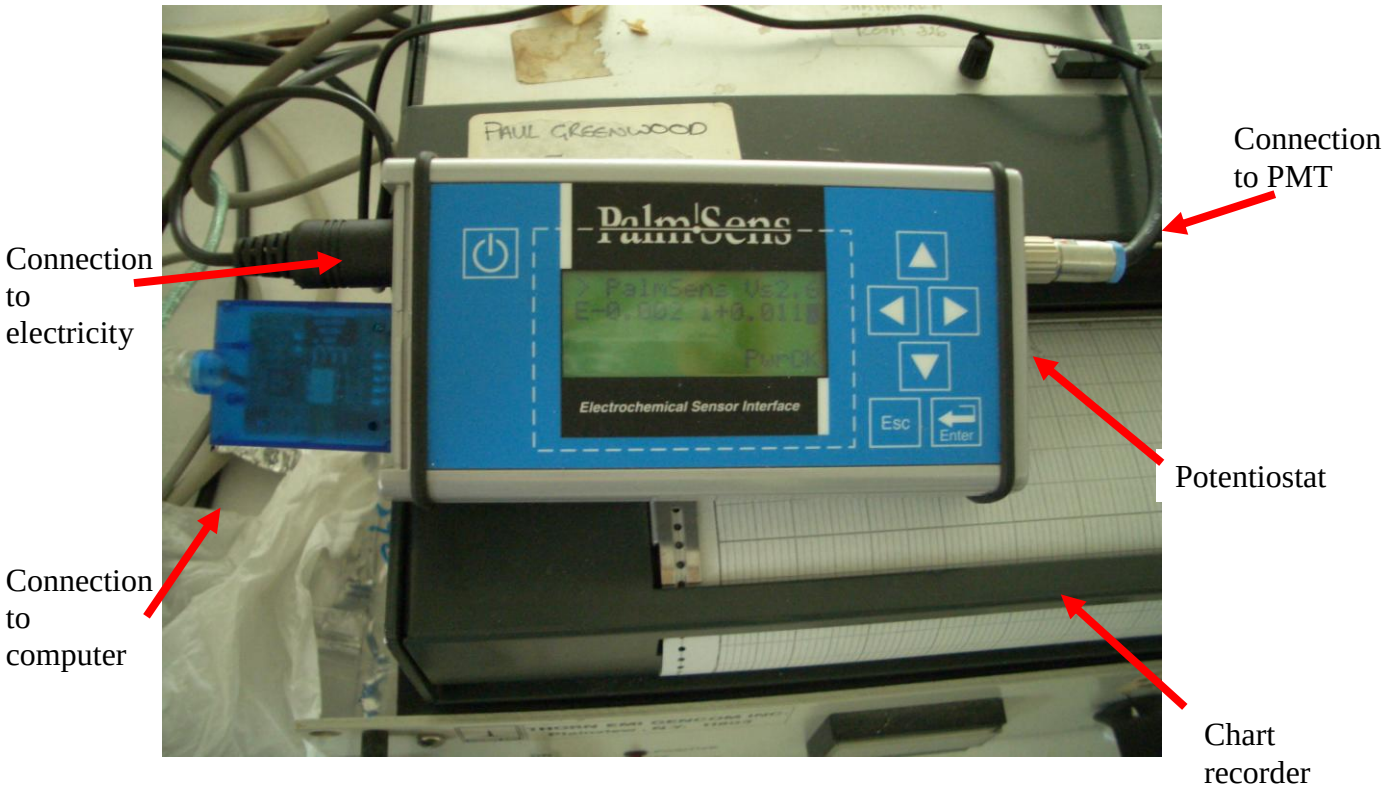

Figure 1.1: Electrodes in electrochemiluminescence detector system.

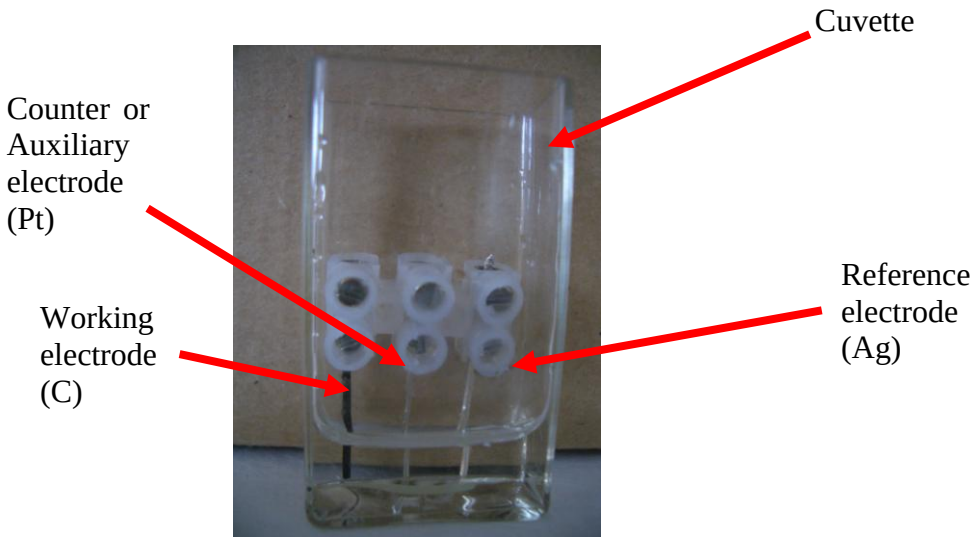

Figure 1.2: Electrodes into the cuvette.

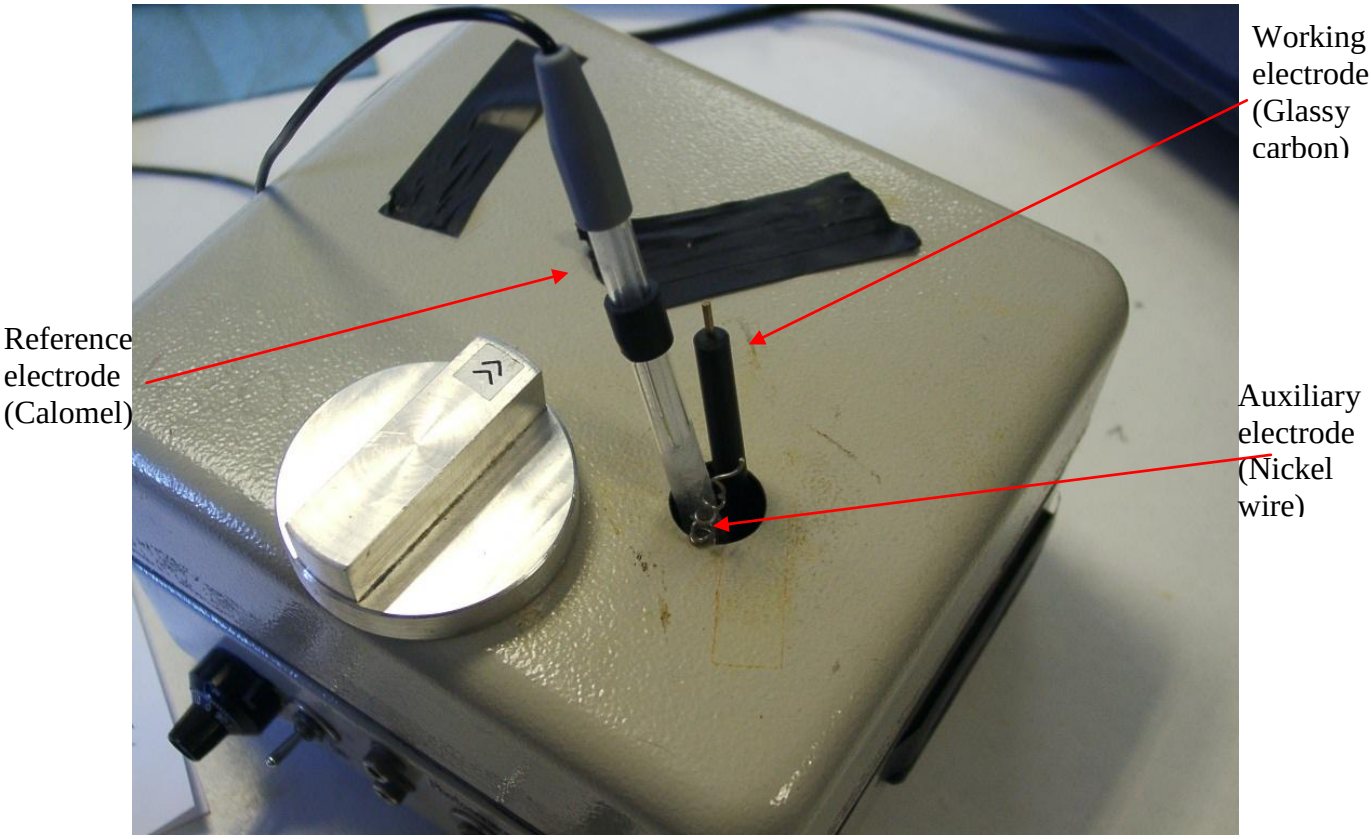

Figure 1.3: Electrodes in electrochemiluminescence detector system.

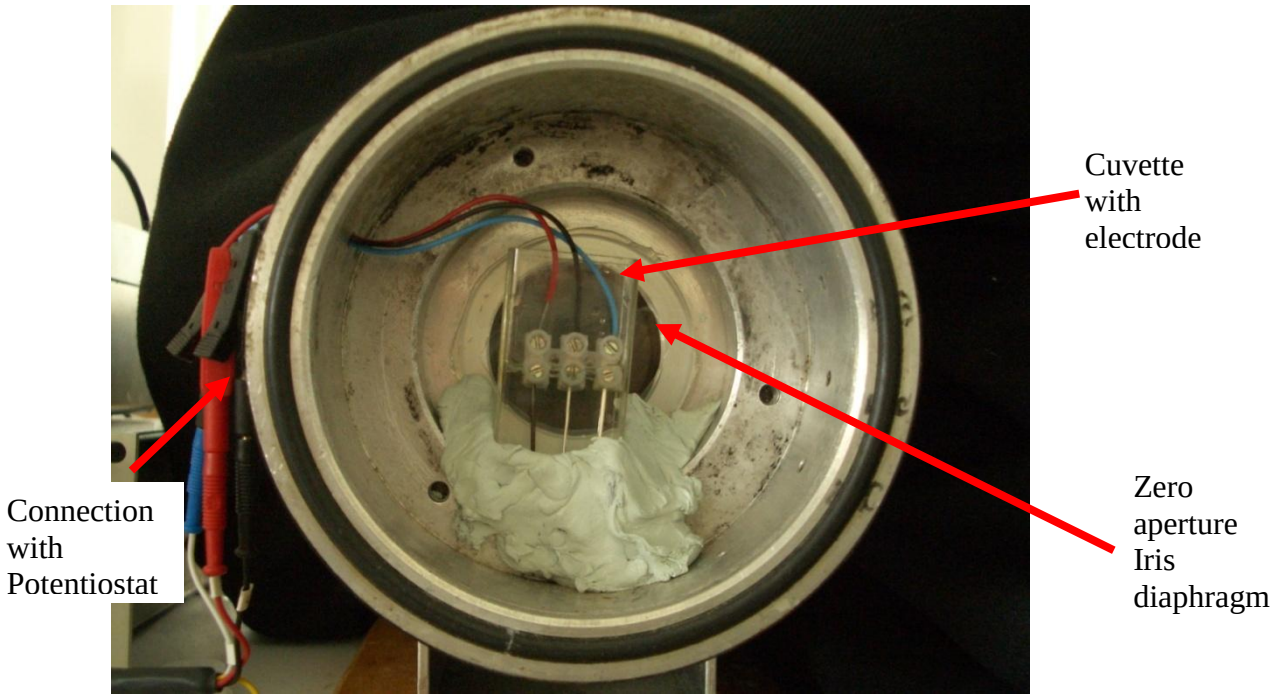

Figure 1.4: PMT casing and ECL cell (front view).

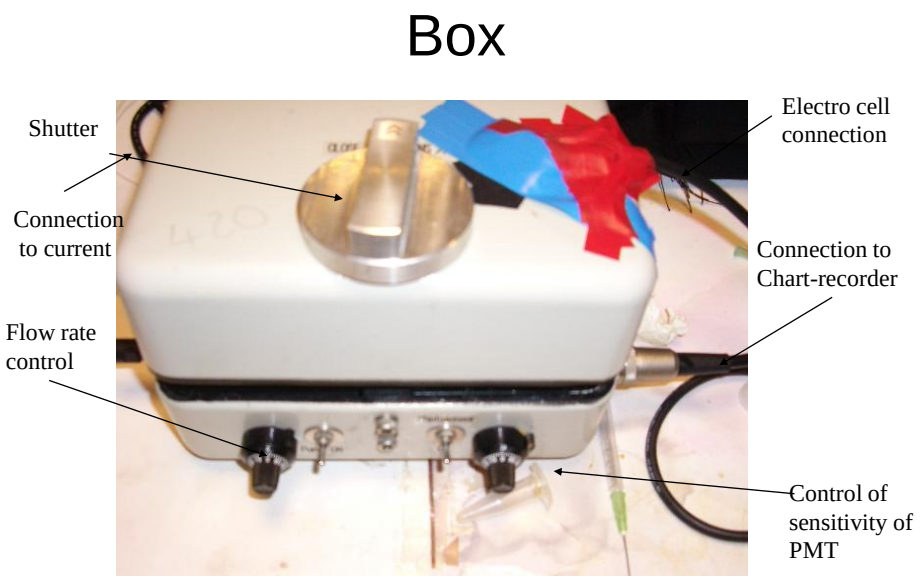

Figure 1.5: Chemiluminescence detector.

Glassy carbon with TOA/CH_2Cl_2

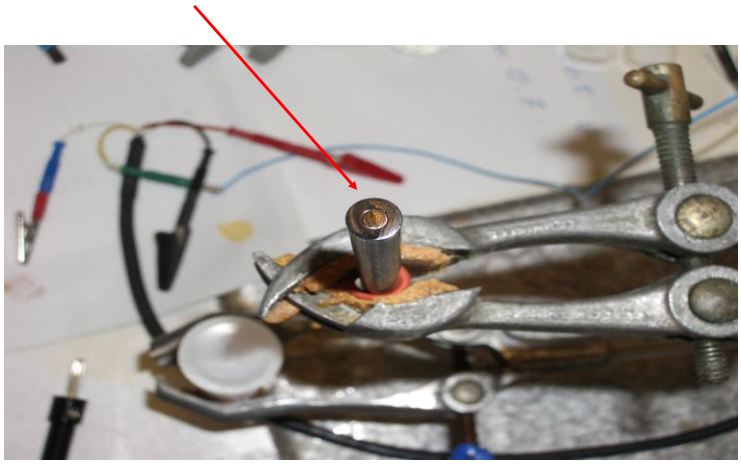

Figure 1.6: Glassy carbon electrode coated with TOA/CH_2Cl_2.

Appendix II